Republic of Iraq

Ministry of Higher Education and

Scientific Research

Babylon University

College of Engineering

Characterization of Carbon Nanotube for Electronic Stretchable Nano Devices Design

A thesis

Submitted to the College of Engineering\ University of

Babylon as Partial Fulfillment of the Requirements for the

Degree of Master's in Engineering /Electrical Engineering/ Indusdtial Electronic

By

Zahraa Eisa Mohammed

Supervised

Asst. Prof. Dr. Haider Al-Mumen

2023 A.D ***1445 A.H***

بسم الله الرحمن الرحيم

وَأَنْ لَيْسَ لِلْإِنسَانِ إِلَّا مَا سَعَى (39) وَأَنَّ سَعْيَهُ سَوْفَ يُرَى (40) ثُمَّ يُجْزَاهُ الْجَزَاءَ الْأَوْفَى (41) وَأَنَّ إِلَى رَبِّكَ الْمُنتَهَى (42)

صدق الله العلي العظيم

سورة النجم/ الآيات من (39-42)

Acknowledgments

First and foremost, I praise and thank my God "ALLAH", the Almighty, for blessing me to complete this work successfully despite all the difficulties.

I would like to give a strong thanks to my parents, for supporting me spiritually throughout my life, sister, and brothers who along the way believed in me.

I would like to express my deepest sincere gratitude to my advisor Dr. Haider Al-Mumen for the continuous support of my thesis, their sharp and quick understanding of the issues, and their advice which made me learn much. in addition, their patience, enthusiasm, motivation, and guidance helped me in all the time of this thesis also they have taught me the methodology to present this thesis as clearly as possible.

My thanks also go to all the people who work within the Department of Electrical Engineering /College of Engineering/University of Babylon/Iraq for their help in many matters.

Zahraa Eisa Mohammed

Abstract

Carbon nanotubes (CNTs) have witnessed great importance due to their electronic and mechanical properties. CNTs have excellent electrical conductivity and can be used to create high-performance transistors for electronic devices. CNT represents a potential material for future microelectronic devices. This thesis enhanced the design and simulation of CNT using COMSOL Multiphysics 6.0. The CNT was not included in the material library of COMSOL, its electrical and mechanical parameters were added, including relative permittivity, band gap, electron affinity, the effective density of states in the valence and conduction band, electron and hole mobility, Density, Young's modulus, and Poisson's ratio.

Design and simulation of the single-walled carbon nanotube-based field effect transistor with a back gate was presented. This model utilized the zig-zag chirality to obtain semiconductor properties for the CNT material. The chirality of the carbon nanotube must be considered when altering the carbon nanotube diameter. The diameter values of carbon nanotubes range from 1nm to 4.5nm. Also, the band gap of CNTs is affected by changing the diameter of CNTs. It was found that increasing the diameter range resulted in decreasing bandgap. In addition, the impact of varying silicon dioxide thickness (gate thickness) on the drain current was studied. As a result, that is found the drain current decreases with increasing gate oxide thickness. Additionally, the achieved resonance frequency for the designed CNTFET is equal to 50GHz, and the bandwidth is equal to 30GHz.

As well as this research discussed; the design and simulation of a single and multi-walled carbon nanotube-based piezoresistive pressure sensor. This sensor operates by sensing the change in resistance across the tubes due to applied pressure. The effect of changing diameter on the resistance of CNT and the energy bandgap was discussed. In the current design picked, the diameter limits from 1nm to 4nm. It was found that raising the diameter reduced the energy bandgap and

decreased the resistance. The suggested model of a piezoresistive pressure sensor was analyzed by calculating several factors, including substrate deflection, current, von Mises stress changes, sensitivity, time response, and frequency responses, using a single CNT and an array of CNTs.

Moreover, the sensitivity of SWCNTs and MWCNTs was calculated respectively, it was found the sensitivity of SWCNTs is better than the sensitivity of MWCNTs. due to the surface area of SWCNTs being higher than that of MWCNTs. The length and diameter of the carbon nanotube also affect the sensitivity of the sensor. SWCNTs are usually longer and narrower than MWCNTs, which may enhance their sensitivity. The time response of the device was determined at a pressure range from 100kPa to 250kPa and the corresponding rise time is 0.18s to 0.23s. The achieved response frequency of the CNT piezoresistive pressure sensor is 60Hz in the range from 0 to 200Hz. In addition, the linear characteristic of the sensor makes it promising for practical applications.

LIST OF CONTENTS

List of Figures

List of Tables

List of Abbreviations

Abbreviation	Definition
CNT	Carbon Nanotube
CNTFET	Carbon Nanotube Field Effect Transistor
CVD	Chemical Vapour Deposition
LOD	Limit of Detection
MEMS	Micro-Electromechanical Systems
MOSFETs	Metal Oxide Semiconductor Field Effect Transistors
MWCNT	Multi-Walled Carbon Nanotube
SB	Schottky-Barrier
SOI	Silicon on Insulation
SWCNT	Single-Walled Carbon Nanotube

List of Symbols

Symbol	Description
A	The cross-sectional area of the piezoresistive fabric
A_i	The graphene lattice unit vector length
a_{cc}	The length of the carbon-carbon bond
C	The length of the chiral vector
C_h	Chiral vector
c_o	Capacitance
Cg	The gate capacitance
D	Diameter
d_o	The distance between two parallel diaphragms
E_F	Fermi energy
E_g	The energy band gap
E	Young's modulus
E°	Energy
E_c	Conduction band level
E_v	Valence band level
E	The charge of an electron
G	Quantum conductance
g_m	The transconductance
H	Plank's constant
l_m	The mean free path
L	The length of the piezoresistive material
m_h	Effective mass of a hole
m_e	The effective mass of an electron
N_c	The effective density of states in the conduction band
N_d	Donor Concentration

N_v	Effective density of states in the valence band
n_i	The electron concentration
P	The label's nanotube family
p_i	Hole Concentration
R°	Resistance
R_Q	The quantum resistance
R_s	The contact resistance
r_0	The radius of the circular diaphragm
T	The transmission coefficient
T	Absolute temperature
V_{th}	Threshold voltage
ε_r	Dielectric constant
$\varepsilon_\circ$	Relative permittivity of free space
ρ	The material's resistivity
θ	Chiral angle
γ	Tight binding-overlap integral
ε	Strain
μ	Electron mobility
v	Poisson’s ratio
k	Boltzmann’s constant
μ1, μ2	Potential energy

Chapter One

Introduction

Chapter One

Introduction

1.1 Overview

Carbon nanotubes (CNTs) are carbon atoms bonded together in a hexagonal lattice like a honeycomb. Each carbon atom is covalently bonded via sp^2 molecular orbitals. The structure of CNTs consists of hollow tubes one-dimensional, made by rolling up a single layer of graphene. [1]. They are classified into two types single-walled and multi-walled carbon nanotubes [2]. There are three types of single-wall carbon nanotubes, depending on the method of folding: Zigzag, Armchair, and Chiral. They typically have lengths of several micrometers and a diameter of a nanometer [3]. CNTs are highly promising materials with a different of technical uses due to their tiny size, low mass, powerful mechanical strength, and excellent electrical and thermal conductivity [4,5].

1.2 The Carbon Nanotubes

There are two types of CNTs: single-walled (SWCNTs) and multi-walled (MWCNTs) [6]. SWCNTs are more flexible than their multi-walled counterparts because of their structural difference. MWCNT is formed of many concentric cylinders of SWCNT. Single-walled nanotubes are generally less thick than multi-walled ones [7].

1.2.1. Single-Walled Carbon Nanotube

SWCNT is composed of one layer of graphene rolled up into a cylindrical shape, as shown in Figure1.1. Individual tubes are twisted and looped instead of straight and have minimal diameters usually 1nm. Single-walled carbon nanotubes (SWCNTs) have garnered much attention due to their exceptional structure-dependent (chirality) properties, giving them

massive potential in various applications such as medicine, batteries, energy storage and transistor. SWNTs can be employed as an antenna in electromagnetic devices due to their strength, lightweight, and ability to operate as a good conductor [8]. Single-walled carbon nanotubes (SWNTs) are a novel class of materials for basic one-dimensional (1D) physics research and nanoelectronics and molecular electronics exploration.

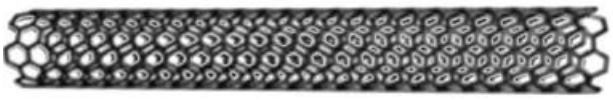

Figure 1.1. The Single-walled carbon nanotube [9]

1.2.2. Multi -Walled Carbon Nanotube

MWCNT is made up of more than two layers of graphite sheet, as presented in Figure 1.2. MWCNTs structures may be described using two different models that are the Russian Doll and Parchment model. The first model consists of multi concentrical cylinders made of graphite sheets, such as a single-walled nanotube (SWNT). The other model resembles a parchment scroll or a rolled newspaper which is made using a one layer of graphite that is tightly wound around itself [10]. Individual carbon nanotubes are nested closely together to form a multi-walled nanotube (MWNT). The interactions between adjoining cylindrical layers in MWCNTs, which cause them to be less flexible and to have more structural flaws, are caused by the sp^2 hybridization in MWCNTs [11].

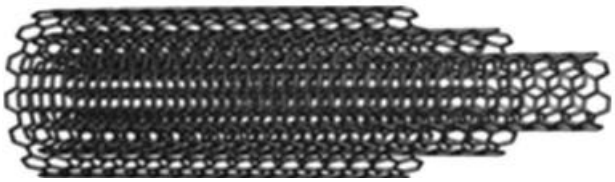

Figure 1.2. The Multi-walled carbon nanotube [9]

1.3 Synthes of Carbon Nanotubes, an Overview

The production of carbon nanotubes is usually achieved using three significant approaches: Arc-discharge, laser ablation, and chemical vapour deposition (CVD) technique [12]. One of the most influential and oldest techniques for making high-quality CNT is the Arc discharge. This method is based on the deposition of CNTs on the cathode of graphite while being subjected to current in a vacuum reactor [13]. The anode is the thin graphite rod, while the cathode is the thick graphite rod, the space between a graphite electrode and the other should be kept within 1 mm to maintain the arc [14]. The vacuum reactor is partially filled with inert gases like helium or argon for preventing the CNTs oxidation [15]. Another technique, laser ablation, is a straightforward and efficient modern technique [16]. The first step involves placing a piece of graphite in a vacuum furnace with some inert gas (such as helium) and high temperature. An instantaneous high temperature will then be produced by irradiating the metal catalyst and carbon atoms of the required graphite with an elevated-energy laser beam, leading to their immediate evaporation. Then, the carbon molecules and catalyst particles will be transported to the zone with high temperature by the carrier gas. Lastly, the deposition of the carbon atom clusters on the collector resulting in the CNTs generation. The importance of laser ablation represents in high purity and low defect rate of the generated CNTs [17]. Additionally, the CVD technique is widely utilized for generating CNTs [18]. The CVD process generally is happened in the furnace chamber. The chamber should be empty of gases by expelling them to prevent oxidation that could occur due to the sparking of oxygen-containing gases in the surrounding atmosphere. Then the carbon precursor gases, especially the hydrocarbons, are conducted into the chamber alongside an inactive gas such as argon or helium. The furnace is heated to evaporate and decompose the gases. The reaction between the reactive species from the gases and the catalyst causes carbon deposition on the substrate. The

vaporized hydrocarbons should interact with the metal catalyst to split into hydrogen and carbon. The metal will absorb carbon, while hydrogen will end up with evaporation. CVD is the most extensively utilized technology because of its affordability, high production, scalability, and simplicity of management. This process is used to generate a lot of nanotubes [19,20].

1.4 Literature Review

R. Jakati et al. 2016 [21] explain, comparing, and analyzing different pressure sensor mechanisms: Piezoresistive, capacitive, and piezoelectric pressure sensors. When comparing piezoresistive pressure sensors to capacitive and piezoelectric pressure sensors, piezoresistive pressure sensors attain higher linearity and better sensitivity.

T. Dinh et al. 2017 [22] effectively explained a technique for building a flexible pressure sensor. The sensor used acrylic elastomer as a flexible and stretchable substrate. The sensor has a high sensitivity of up to -0.86 Ω/kPa, with a 100 ms response time. The sensor could recognize finger pressing in real time.

S. Pyo et al. 2017 [23] an extremely sensitive pressure sensor has been developed using polyester fabric covered with carbon nanotubes (CNT). The material was produced using a quick and inexpensive "dipping and drying" process, and the dipping number was easily adjusted to control the fabric's characteristics. The fabric also showed excellent mechanical flexibility and durability against bending; the highest sensitivity of the sensor achieved 10.63%/kPa for pressure up to 10kPa, and it was noted that the resistance of the manufactured sensor decreased when exposed to external pressure.

A. Sanli et al. 2018 [24] described a piezoresistive pressure sensor that is simple to build using nanocomposites made of MWCNTs and epoxy. Display excellent durability, low hysteresis over 100 cycles.

K. Balavalad et al. 2018 [25] has developed and evaluated a tiny piezoresistive pressure sensors utilizing Si, SOI, and CNT. They demonstrated that the sensitivity of the CNT piezo resistor-based micro pressure sensor is higher than that of silicon and SOI-based sensors. The SOI-based sensors showed a low displacement in comparison to Si and CNT-based sensors, which showed a similar displacement.

R. Shaik et al. 2018 [26] designed and simulated a Polydimethylsiloxane (PDMS) and Multi-Wall Carbon (MWCNT) nanocomposite material as a piezoresistive pressure sensor. Simulation results are plotted for three varied concentrations of nanomaterial filler, which were 25% wt, 18% wt, and 4% wt, observing the maximum resistance change for 18% wt. Hence full conduction and lowest alteration in resistance are found for filler with concentration of 25%wt.

K. Park et al. 2019 [27] developed a flexible sensor based on MWCNT/PDMS has been developed and used in two medical applications. tactile sensing with touch sensors for rehabilitation activities, and a needle with strain sensors for in-situ tissue characterization. The characterization of MWCNT/PDMS elastomers and MWCNT dispersion techniques in PDMS are examined to determine the best manufacturing procedure. It has been shown that manufactured MWCNT/PDMS elastomers feature piezoresistivity, which is sensitive to mechanical strain, and a very flexible structure that permits 40–50% strain, enhancing the sensitivity of the sensors.

T. Kumpika et al. 2020 [28] discussed the manufacturing and properties of stretchy strain and pressure sensors made from a carbon nanotube and

graphene composite are discussed using the polymer's diffusion through nanostructured materials. The manufacturing method was easy, cheap, and highly sensitive. The strain sensor was durable (over 1000 cycles) and had a high GF (10.9). The pressure sensor remained steady even under elevated pressure (50 kg cm^2). The sensors' flexible strain and pressure sensing capabilities were put to the test for gait analysis applications. The sensors could measure high knee sagittal angles and forces during walking.

A. Soares et al. 2021 [29] designed and simulated a quantum carbon nanotube field-effect transistors based on top-gated to get excellent electrical characteristics for sub 5nm technologies.

T. Rijk et al. 2022 [30] presented a new pressure sensor that directly incorporates multi-walled carbon nanotubes (CNTs) into the polyimide sheet. The sensor is robust and can withstand pressures as high as the highest tested level of 55N. According to the primary findings, a linear pressure extent of up to 40N is measurable. Periodic pressure response tests demonstrate the sensor's recurrently and steady mechanical nature because of its robust polyimide foundation.

M. Zamzami 2022[31] discussed the fabrication of carbon nanotubes filed-effect transistor sensor and its characterization. The fabrication of CNT-FETs performed by following conventional photolithography method and lift-off techniques. It was found that 87% of the fabricated CNT-FETs were stable and functional.

G. Fedorov 2023 [32] investigated the effect of metal deformations on the gate voltage dependence of the conductance of metallic armchairs and zigzag CNT FETs. Was employed Density Functional Theory (DFT) calculations of deformed CNTs. It was found, in the case of armchair CNT, that the gate-voltage dependence of the conductance shows an ON/OFF ratio of about a factor of two, nearly independent of temperature.

C. Wang 2023 [33] a novel flexible sensor based on the carbon nanotube paper film (CNTF)and stress-induced square frustum structure (SSFS) was proposed. to develop an ultra-sensitive and wide-range flexible CNTF/SSFS pressure sensor. which exhibited an ultra-high sensitivity of 2027.5kPa^{-1} in the range of 0 to 20kPaa.

1.5 Problem Statement

The main problem that faces the use of most electronic devices is their size. Most electronic devices are large. CNT can be used to miniaturize electronic devices besides an efficient performance. This can lead to smaller, more compact, and more energy-efficient electronics.

1.6 Aim of Thesis

The thesis aims to:

- The modelling of CNT which was added to COMSOL Multiphysics as a new material.
- The design and simulation of field effect transistors based on carbon nanotubes modeling of single-walled carbon nanotube.
- The design and simulation of single and multi-walled CNTs piezoresistive pressure sensors then determine its sensitivity, time response, and frequency response.

1.7 Thesis Outline

Chapter 1: This chapter explains the introduction of the thesis.

Chapter 2: This chapter illustrates the theory of Carbon nanotube devices.

Chapter 3: This chapter provides the model design of CNTFETs and CNTs- based piezoresistive pressure sensors.

Chapter 4: This chapter provides the simulation results of CNTFETs and CNTs- based piezoresistive pressure sensors.

Chapter 5: This chapter contains the conclusion and future work of this thesis.

Chapter Two

Theory of CNTs Devices

Chapter Two

Theory of Carbon Nanotube Devices

2.1. Introduction

Carbon nanotube (CNT) has gained much attention due to its unique electrical and mechanical characteristics.

This chapter discusses the theory of nanomaterial devices which are CNTs based on field effect transistors and piezoresistive pressure sensors.

2.2. Nanomaterial (Carbon Nanomaterial)

Nanomaterials are materials with structures or features that have at least one dimension in the nanometer scale, typically ranging from 1 to 100 nanometers [6]. Nanomaterials can be categorized into various types based on their dimensions, composition, and properties. The properties of nanomaterials are influenced by increased surface area, and changes in electronic structure compared to bulk materials. These unique properties make nanomaterials valuable for a wide range of applications, including electronics, medicine, energy, catalysis, and materials science. Nanomaterial devices can be found in various fields, including electronics, medicine, energy, and materials science. Devices in the field of nanoelectronics utilize nanomaterials for the fabrication of components such as transistors, sensors, and memory devices. Nanotubes are common types of nanomaterials. CNTs are a type of allotrope of carbon, like graphene, and fullerenes. Nanotubes are hollow cylinders with diameters in the nanoscale [8]. CNTs can be used in the development of smaller and more efficient electronic devices, such as transistors and interconnects, due to their excellent electrical properties.

2.2.1. Properties of Carbon Nanotubes

CNTs exhibit a range of remarkable properties, making them a subject of extensive scientific research and exploration. Carbon nanotubes exhibit excellent electrical conductivity. They can conduct electricity as well as or even better than some metals. This property makes them suitable for applications in electronic devices. Additionally, carbon nanotubes are known for their exceptional mechanical properties. Theoretical models predict high tensile strength and stiffness. The strength arises from the strong covalent bonds within the graphene lattice, and the cylindrical structure enhances these mechanical properties. Then carbon nanotubes can be very small in diameter, on the order of nanometers. This small size allows for the development of nanoscale devices and components, which is challenging with traditional silicon-based technologies. Therefore, theoretical studies have explored the thermal conductivity of carbon nanotubes. Due to their one-dimensional structure and strong carbon-carbon bonds, nanotubes can exhibit high thermal conductivity, making them valuable for applications in thermal management. However, CNTs can exhibit ballistic conductance, allowing electrons to flow through them with minimal scattering, making them promise for use in high-performance electronic devices. Thus, CNTs are extremely lightweight, contributing to their use in lightweight and strong composite materials [9].

2.2.2. Application of Carbon Nanotube

CNTs have a lot of potential uses because of their exceptional properties, including electronic [34], optical [35], thermal [26], chemical, and mechanical properties [37, 38]. CNTs possess exceptional electrical characteristics because of their unique electronic structure and graphite's one-dimensional nature. Nevertheless, in CNTs, electrons are difficult to scatter [39]. CNT electronics have the potential to make the evolution of electronics extremely understandable and overcome the size limitations of circuits. It could have potential applications in energy conservation and integrated circuits. CNT-electronics can enhance current devices together with biotechnology and artificial intelligence [40]. Such advancements might be exploited when solving previously unsolvable issues. Reported articles have demonstrated that field-effect transistors can operate effectively in single-wall carbon nanotubes with a diameter of less than 1 nm. However, their versatility and potential for implementation in upcoming nanometer-scale circuits have steadily improved. Some potential applications based on carbon nanotubes include CNT based Field-Effect Transistors, Diodes, and Logic Circuits. SWNTs are promising for application in producing high-performance diodes due to their current-carrying capability [41]. Furthermore, Carbon nanotubes are the most powerful and stiffest materials regarding tensile strength and elastic modulus. This strength is a result of the covalent sp^2 bonds that have been created between the individual carbon atoms. Individual nanotubes' tensile strength may be 1000GPa, and their elastic modulus is in the tera-pascal range [42, 43].

2.2.3. Physical Structure of Carbon Nanotube

The SWCNT is a graphene sheet wrapped in a cylindrical form with axial symmetry, displaying a spiral structure called chirality. The way the graphene sheet is wrapped is represented by a pair of indices (n, m) called the chiral vector. Two atoms in a planar graphene sheet are chosen, and one is used as the origin. The chiral vector C_h is pointed from the first atom toward the second one and is defined by the relation [8]:

$$C_h = n \cdot a_1 + m \cdot a_2 \quad \ldots\ldots\ldots\ldots\ldots\ldots\ldots\ldots\ldots \text{(2.1)}$$

Where, n and m are integers denote the number of unit vectors along two directions in the honeycomb crystal lattice of graphene, and a1 and a2 are the graphene lattice vectors, as presented in Figure 2.1. The chiral vector length c equals the circumference of the CNT and is determined by the related equation:

$$c = |C| = a\sqrt{(n^2 + nm + m^2)} \quad \ldots\ldots\ldots\ldots\ldots\ldots\ldots \text{(2.2)}$$

The value $\boldsymbol{a}$ represents the unit cell vector length $\boldsymbol{a_1 or\ a_2}$. This length is linked to the length of the carbon-carbon bond $a_{cc}$by the relation.

$$a = |a_1| = |a_2| = a_{cc}\sqrt{3} \quad \ldots\ldots\ldots\ldots\ldots\ldots\ldots\ldots \text{(2.3)}$$

The carbon–carbon bond length is a_{cc} = 0.144 nm. The lattice basis vectors a_1 and a_2 are combined linearly to form the chiral vector Ch. The chiral indices are vectors with positive integers n and m. Basically, chiral indices are used to calculate the diameter and bandgap of SWCNT [8], The diameter is derived by,

$$d = \frac{\sqrt{3}\, a_{cc}}{\pi} \sqrt{n^2 + m^2 + 2nm} \quad \ldots\ldots\ldots\ldots\ldots\ldots \text{(2.4)}$$

The threshold voltage depends on the diameter of CNT, and can be calculated by the following equation:

$$V_{th} = \frac{aV_{\pi}}{\sqrt{3}e\, d_{CNT}} \quad \ldots\ldots\ldots\ldots\ldots\ldots\ldots\ldots\ldots\ldots \text{(2.5)}$$

The angle between the chiral vector and zig-zag nanotube axis is the chiral angle. This angle is denoted by:

$$\theta_t = \tan^{-1}(m\sqrt{3})/(m + 2n) \quad \text{.....(2.6)}$$

The chirality separates carbon nanotubes into three kinds, distinguished by their electronic characteristics. The three major structural kinds of single-walled carbon nanotubes identified are the armchair, zigzag, and chiral [6]. These different kinds of carbon nanotubes are made differently depending on how graphite is "rolled up" during manufacturing; they may be demonstrated by a vector, referred to as a chiral vector [44]. The chiral vector is the line connected by two crystallographically equivalently sites. The representation of the chiral vector is based on two indices, n, and m. The different types of structures are associated with (n, m and θ); as following [6]:

- Armchair (n = m, θ = 30˚).
- Zigzag (m = 0, n > 0, θ = 0˚).
- Chiral (m≠ n, 0 < θ < 30˚).

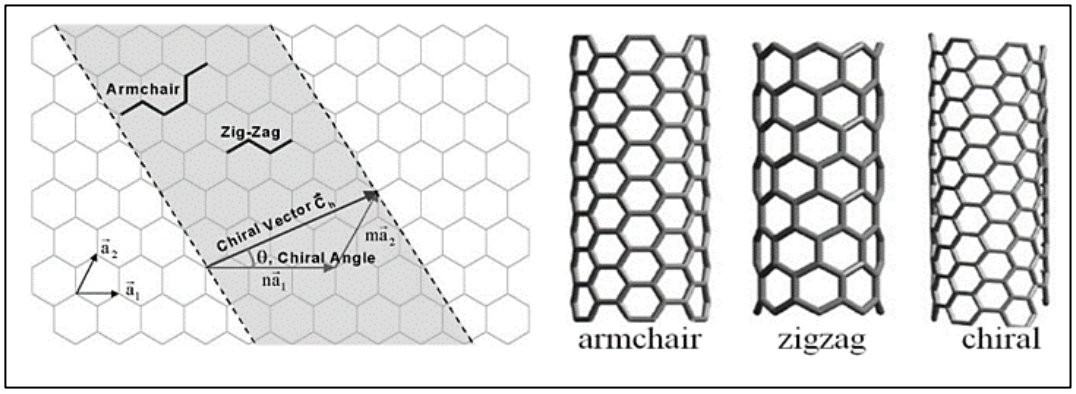

Figure 2.1. Schematic diagram showing how a hexagonal sheet of graphite is 'rolled' to form a carbon nanotube [44].

2.3. Carbon Nanotube-Based Field Effect Transistor

Carbon nanotube field-effect transistors have gained significant importance recently because of their superior electrical, mechanical, and thermal feature [45-47]. The development of single-walled CNTFETs has made tremendous progress (SWCNTFET) due to their unique properties, where it bows elastically (rather than fracture) under enormous bending or compressive forces. Many technologies are being considered to aid in miniaturizing transistors; carbon nanotubes have the potential to help [48, 49].

The CNTFET was designed to provide high-performance electronic devices. SWCNT field-effect transistors (FETs) differ from traditional semiconductor transistors in several significant ways, making them unique and intriguing: The one-dimensional CNT reduces scattering potential [42]. Consequently, the gadgets may operate quite quickly. The bonds at the surface are steady and saturated, so it is suitable for conduction occurrence. Therefore, there is no need for passivation in the boundary between the gate dielectric and the nanotube channel. The demand for tiny devices with more incredible operating speeds has arisen because of technological advancements in all sectors of life. Silicon scaling should be altered, so silicon MOSFET has been gradually replaced by carbon nanotube field-effect transistors (CNTFET). CNTFETs could widely be applied in almost all disciplines; digital logic circuits play an important role in producing semiconductor devices. When designing these circuits, the most important factors are speed, area, power consumption, and cost. CNTFETs have outstanding electrical characteristics, such as a carrier velocity and mobility, which can be utilized in various electrical usages.

2.3.1. Types of CNTFETs Based on the Geometry

Carbon Nanotube Field-Effect Transistors (CNTFETs) can be classified based on the geometry of the carbon nanotube used in their construction which includes Back Gate CNTFETs [50, 51], Top Gate CNTFETs [52], Warp Gate CNTFETs [53], and Suspended CNTFETs [54]. The geometry of the carbon nanotube primarily refers to its structure, specifically whether it is a metallic or semiconducting nanotube. The classification based on the geometry (metallic or semiconducting) is crucial in determining the electrical properties and potential applications of CNTFETs.

2.3.1.1. Back Gate CNTFETs

The elementary demonstration of CNTFET was made by Tans et al. in 1998 [26]. In the proposed design, a single-walled carbon nanotube connected two metal electrodes constructed on a silicon substrate. The metal electrodes are the source and drain, while the SWCNT is the channel. A metal contact is connected at the back, acting as the gate terminal [50]. Figure 2.1 demonstrates a graphical schema of back gate CNTFET. The purpose of the back gate is to provide an additional means of controlling the flow of current through the carbon nanotube channel. By applying a voltage to the back gate, you can modulate the electrostatic environment of the CNT and influence its electrical properties. The back gate can help improve the ON/OFF ratio of the CNTFET and Enhanced Control over Threshold Voltage. CNTFETs with back gates can be optimized for specific performance metrics, such as speed, power consumption, and noise margins.

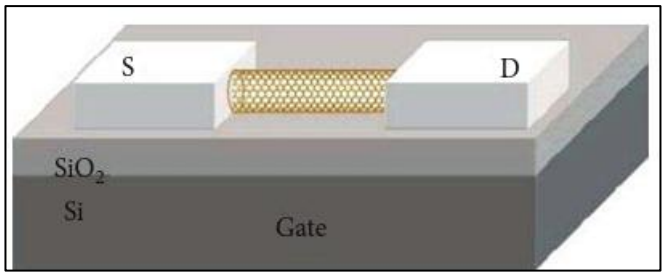

Figure 2.2. The Back Gate CNTFETs [50].

2.3.2. Operation of BG-CNTFETs

The CNTFETs operate on the same fundamental concept as MOSFETs. The source terminal supplies electrons, and the drain terminal collects them. The current transference is from the drain to the source terminal passing through the transistor channel, and its intensity is controlled by the gate terminal. The transistor is in an off state whenever no gate voltage is applied. The primary distinction between CNFETs and MOSFETs is that carbon nanotubes are utilized as the channel in CNFETS, whereas MOSFETs are composed of severely doped silicon. The SWCNTs may be metallic or semiconducting, based on their chirality and diameter. In a conventional CNTFET, the current is injected to a metal source and collected from drain electrodes, and they are connected to a semiconducting SWNT. A third gate controls the current flow between the source and the drain, which is coupled through an insolation sheet. carriers and conductance decrease in a positive gate voltage comparing to negative gate voltage causes carriers to accumulate and increases conductance. CNTFETs may successfully replace MOSFETs in nanoscale electronics. They are also highly promising regarding their I-V and transfer properties. The operation of two different structures is discussed. The first structure is Schottky-barrier CNFET, and the other is MOSFET-like CNFET.

2.3.2.1. Schottky Barrier of CNTFETs

A potential barrier is called the Schottky barrier (SB) at every point where a metal and a semiconductor contact occur. The rising of the barrier depends on the filling of metal-induced gap states. The SB is quite sensitive to changes in the immediate surroundings at the point of touch [55]. The SB-CNFET operates based on immediately transferring over the Schottky barrier at the source-channel junction. The system transconductance depends on the gate voltage, which regulates barrier width. A significant barrier restricts the channel's current at low gate bias. Increased gate bias narrows the barrier, improving quantum mechanical tunneling and boosting the transistor channel's current flow. The SB-CNTFET operates through adjusting the device's transport coefficient. The SB-CNFET exhibits robust ambipolar conduction, especially when the gate oxide thickness decreases [56]; until when the Schottky barrier is zero.

2.3.2.2. MOSFET- like CNTFETs

This device's structure differs somewhat from the SB-CNFET due to the use of doped terminals rather than metal. That kind of device was designed to resolve the issues of SB-CNFET by functioning as a standard MOSFET. This kind of transistor provides several benefits compared to SB-CNFET. This device may prevent ambipolar conduction. It also offers a higher channel length limit due to the greatly decreased density of metal-induced gap states. This kind of transistor provides several benefits when compared to the SB-CNFET. This device may prevent ambipolar conduction in SB-CNFET. It also offers a higher channel length limit due to the substantially lower density of metal-induced gap states.

The parasitic capacitance between the gate and the source terminal is significantly lowered, enabling the transistor to operate more quickly. One of the primary differences between CNTFETs and MOSFETs is using Carbon nanotubes (CNTs) as the channel material instead of silicon, which allows for a greater drive current density owing to the higher carrier mobility of CNTs as compared to bulk silicon [57].

2.3.3. Ballistic Transport

Ballistic transport occurs when the mean free path (l_m) longer than the travel length carriers. The mean free path is the average of a carrier travelling length that must be traveled before a carrier encountering a scattering phenomenon. Numerous sources must scatter the carrier, including lattice-vibrating acoustic and optical phonons, ionized impurities, defects, interfaces, and other carriers. At the low voltage and presuming ideal contact, it has been discovered that metallic nanotubes have (l_m) at least 1m at standard conditions. Additionally, the mean free path is inversely proportional to temperature. Landauer equation helps in understanding the carbon nanotubes transport characteristics, which explains quantum conductance of a quasi-1D conductor [6].

$$G = e^2/h \cdot \sum_{i=1}^{M} t_i (E_F) \quad \ldots\ldots\ldots\ldots\ldots\ldots\ldots\ldots\ldots\ldots\ldots\ldots\ldots\ldots \quad (2.7)$$

Where,

e^2/h is the quantum resistance (contact resistance),

t_i is transmission of a contributing conduction channel,

$E_F$is the Fermi energy.

Carbone nanotube follows the ballistic transportation, which means that the electron energy does not been scattered in the phonons form. The quantum resistance (contact resistance) of ballistic transport is given by the following equation [6]:

$$R_Q = \frac{h}{e^2} = 26\ K\Omega \quad \ldots\ldots\ldots\ldots\ldots\ldots\ldots\ldots\ldots\ldots\ldots\ldots\ldots\ldots\ldots\ldots \quad (2.8)$$

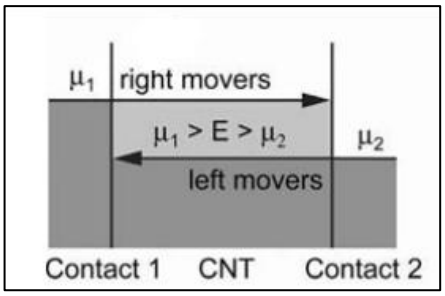

Figure 2.3. Illustration of ballistic transport in a system [17].

Carriers with energies up to μ1 and μ2 are inserted into the CNT from contacts 1 and 2, respectively, as shown in figure 2.5. Since the CNT does not scatter, carriers injected at a given energy E˚ go down the tube without losing energy. Carrier particles travelling from contact 1 to contact 2 with energies between μ1and μ2 carry the net currently. Scattering in the conduction channel could be included in the Landauer formula by incorporating an (momentum scattering length l_m):

$$R = R_Q \cdot L/l_m \quad \text{(2.9)}$$

Where,

R is the resistance of ballistic conductor.

L is the length of the conductor,

l_m is the mean free path.

R_Q is the quantum resistance.

2.3.4. Mathematical Model of CNTFETs

The electron mobility describes the movement of electrons through a semiconductor or a metal. Mobility is the rate at which charge carriers react to an external electric field. The equation (2.10) estimates the CNT electron mobility μ[72]:

$$\mu = \frac{L_{cnt}^2 \, g_m}{C_g \, V_d} \quad \text{(2.10)}$$

Where,

L is the length of CNTs,

$g_m$is the transconductance,

V_d is the drain voltage,

Cg is the gate capacitance that can be calculated by:

$$Cg = 2\pi L_{cnt}\varepsilon_r\varepsilon_\circ/\ln(2t_i/r) \quad \text{(2.11)}$$

Where,

ε_r is the dielectric constant of silicon dioxide,

t_i is thickness of silicon dioxide,

r is the radius of CNTs,

$\varepsilon_\circ$ is the relative permittivity of free space (8.8542×10^{-12} Fm^{-1})

The electron concentration in the conduction band is defined by this equation [50]:

$$n_i = N_c e\left[\frac{-(E_c-E_F)}{KT}\right] \quad \text{(2.12)}$$

Where,

$$N_c = (2\pi m_e kT/h^2)^{3/2} \quad \text{(2.13)}$$

N_c is the effect density of state in conduction band,

m_e is the effective mass of an electron,

k is Boltzmann constant,

T is temperature,

h is Planck constant equal 6.624 × 10−34 Js,

$$(E_c - E_F) = KT\ln\left(\frac{N_c}{N_d}\right) \quad \text{(2.14)}$$

E_F is the Fermi energy,

N_d is the donor concentration.

The electron in the valence band is defined by the hole concentration and is given by this equation [50]:

$$p_i = N_v e^{((E_v-E_F)/kT)} \quad \text{(2.15)}$$

Where,

$$N_v = 2(2\pi m_h kT/h^2)^{3/2} \quad \text{(2.16)}$$

N_v is the effect density of state in the valence band,

m_h is the effective mass of a hole,

k is Boltzmann constant,

T is Temperature,

h is Planck constant equal $6.624 \times 10{-}34$ Js.

2.4. Sensors Based-Carbon Nanotube

Sensors influence our daily lives significantly, and sensors measure or detect physical and chemical quantities, including temperature, pressure, sound, and concentration. Sensors are key in several scientific and technical applications, including controlling environment and chemical process, biomedical uses, and security. Enhancement of sensing materials and technologies has been extensively studied to accomplish the criteria of good sensors, like high sensitivity and reliability, quick response, low cost. Therefore, it becomes necessary to reduce sensors size because this could increase their performance and durability, allows integrating additional functionalities in a tiny package. The urgent need for smaller sensors led to the development new sensors that operate more effectively at the nanoscale, i.e., nano-sensors. It may all be accomplished using carbon-based nanomaterials, notably CNTs [60].

The basic idea behind a nano-sensor is to collect information at the atomic level and transmit it to the macroscopic realm as analyzable data. The purpose of the detecting mechanism is to precisely identify specific atoms or molecules by observing various in temperature, electricity, magnetic forces, volume, concentration, displacement, frequency, and velocity. Nano-sensors can be used for various purposes, such as early illness diagnosis, DNA sequencing, gene mutation detection, gas detection, monitoring blood sugar levels in diabetic patients, precise monitoring of material states, and more [28]. The manufacture of sensors is one of the

most important uses for functionalized CNTs nanotubes in various industries, including nanotechnology, medicine, industry, electronics, etc.

CNTs have the potential to revolutionize the sensor industry due to their intrinsic qualities, including tiny size, high strength, high electrical and thermal conductivity, and high specific surface area. Carbon nanotubes (CNTs) give many advantages as sense items, including a high surface area for electrical conductivity, cheap cost, low-temperature functioning, and the capacity to be functionalized with different polymers for greater sensitivity. The sensor should be able to respond quickly to external stimuli, detect analytes in proportions as small as feasible, recover quickly, identify the correct analyte, and be simple to use. Sensors are a group of devices that are significantly utilized, from the disclosure of gas molecules to the momentum monitoring of chemical signals in biological cells. Sensors are miniature devices used to collect qualitative and quantitative analytical data by continually monitoring a given analyte's physicochemical or biological characteristics.

CNT-based biosensors have several benefits, Compared to commercially available silicon- and metal-oxide-based biosensors. electronic goods and is crucial to new artificial intelligence applications. According to their features, there are several types of sensors, including gas, temperature, pressure, etc.

2.4.1. Pressure Sensor Based Carbon Nanotubes

Carbon nanotube pressure sensor is one of the favorable sensing components in sensing technology to transform a tactile input into electrical signals. SWCNTs and MWCNTs have been utilized as active sensing components in pressure sensors to create devices that are very sensitive to changes in pressure. Pressure sensors are highly important and utilized in many sectors, including aerospace, barometry, manufacturing, transportation, and medicine. Pressure sensitivity, pressure range, and the

capacity to detect and endure tiny and large pressures are important performance indicators defining pressure sensors. Several pressure sensing methods are utilized, such as piezoelectricity, piezo resistivity, and capacitive. Piezoresistive pressure sensors exceed the opposition in applications used in everyday life due to their easy device form, simple signal collecting, low cost, and simple fabrication process. However, the piezoelectric pressure sensor reacts to external pressure by creating immediate electrical signals. A piezoelectric pressure sensor responds to a change in electrical potential by sensing and detecting the pressure that has been applied. Piezoelectric sensors are often used to dynamically detect pressure and high-frequency vibration due to their great sensitivity and capacity for transient detection. Piezoelectric sensors are ineffective for sensing static pressure because their output voltage is pulsed. The detecting element is made of ceramic or quartz that has been metalized. Mechanical deformation is converted into an electrical signal (voltage) by a piezoelectric element via the creation of charge and an alteration in capacitance. A positive charge is formed when the crystal is stressed. The piezoelectric effect occurs when mechanical stress or pressures are enforced along certain planes to various crystal materials, producing an electric potential over the surface of those materials. An electric field is generated within a polarized crystal due to application of a stress to it and this is described as piezoelectricity. Surfaces of the crystal may differ because of this field, which could be measured. The use of piezoelectric sensors to monitor the structures health is an excellent illustration of this phenomenon. Additionally, the capacitive pressure sensor comprises two parallel plates that serve as capacitor electrodes and are spaced apart by an insulating medium (dielectric). Capacitive pressure sensors operate to measure the parallel plate capacitor's change in capacitance, which is described by the equation capacitance.

$$c_o = \varepsilon_r \varepsilon_\circ A \backslash d_o \quad \text{..... (2.17)}$$

Where,

$c_o$is a capacitance, $\varepsilon_\circ$ is relative permittivity of free space, ε_r is dielectric constant, A is the area of two plate, and d_o is a distance between two parallel diaphragms. The capacitance depends on the contact surface, plate distance, and effective dielectric constant influenced by pressure-induced deformation [70]. A capacitive pressure sensor determines the pressure's intensity by sensing a change in capacitance, which is occurred when the spacing between two electrodes changes under applied pressure. The most significant benefits of capacitive sensors are their consistent sensing capability, high dynamic response, and low power consumption.

2.4.1.1. Piezoresistive Pressure Sensor

The piezoresistive pressure sensor operates based on the piezoresistive effect. When the pressure sensor is put under mechanical strain, the mobility of the silicon carriers varies, which in turn affects the effective mass of silicon atoms, which influences the effective mass of silicon atoms, therefore changing the material resistance (R°) by the formula below:

$$R^\circ = \frac{\rho l}{A} \quad \text{..... (2.18)}$$

Where,

ρ is the material's resistivity,

A is the cross-sectional area of the piezoresistive fabric,

l is the length of the piezoresistive material.

There are several considerations should be taken to design a piezoresistive pressure sensor. The choice of piezoresistive materials is the first item to consider. Which is Silicon [65], Polysilicon, Silicon dioxide, Carbon nanotubes [66], and Graphene, all normally employed piezoresistive materials. As a result, the choice of material is essential as it influences the change in sensor output. The performance of piezoresistive pressure sensor depends on the material's features, the sensor's structure, the resistors' location, how big they are, how thick the diaphragm is, etc. Piezoresistive sensors have received significant research attention due to the simple, inexpensive, and simple fabricated they are. Piezoresistive sensors' resistance changes primarily result from the contact resistance between two conductive modules when subjected to external pressure, Figure 2.8 show that. The substrate and ingredient of a piezoresistive pressure sensor are considered two critical elements of it. Carbon nanotubes are widely used as a piezoresistive element in piezoresistive pressure sensors due to their unique mechanical, electrochemical, piezoresistive, and other physical qualities.

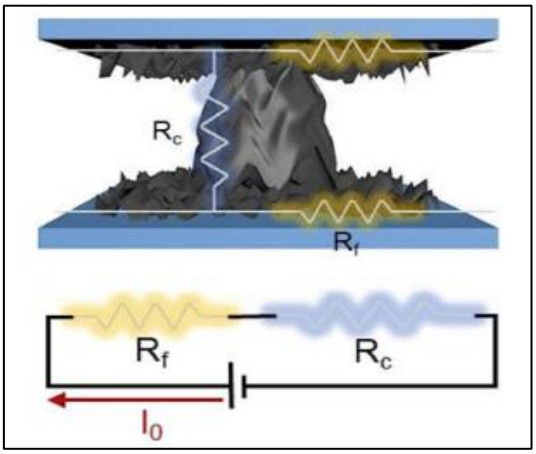

Figure 2.4. Schematic diagram and sensing mechanism of a piezoresistive pressure sensor [67]

The basic structure of a piezoresistive pressure sensor typically involves a diaphragm or a flexible membrane that deforms under the influence of pressure. This diaphragm is often made of a piezoresistive material, such

as silicon. When pressure is applied, the diaphragm flexes, causing a change in the electrical resistance of the piezoresistive material. The change in resistance is then converted into an electrical signal, usually in the form of a voltage or current, which can be measured and correlated with the applied pressure. This conversion is often achieved by incorporating a Wheatstone bridge circuit into the sensor design.

2.4.1.2. Application of CNT Pressure Sensor

In recent years, CNTs have provided distinctive properties to improve sensors that can make the devices smaller, more sensitive, have high accuracy, are less expensive, and have less power consumption. Pressure sensors may be successfully used in applications for personal electronics, artificial intelligence, and industrial production. Pressure sensors are utilized in mobile biomonitoring in medical diagnostics and healthcare. CNT-based pressure sensors are employed in renal dialysis equipment, breathing devices, and eye procedures [64]. To assess the effectiveness of a sensing device, it is necessary to know the essential variables of the pressure sensor. These essential variables include sensitivity, the limit of detection (LOD), linearity, response time, and stability.

The sensitivity of pressure sensors is one of the most essential parameters, as it determines the measurement accuracy and efficiency of the device. The pressure sensitivity is defined as $S = dX/dP$, where S represents the sensitivity, X represents the quantitative output signal, and P represents the applied pressure. Limit of detection (LOD) is a second important metric. It refers to the minimum pressure required to produce a noticeable signal change. Improving the LOD of pressure sensors is essential for creating highly efficient pressure sensors that operate at ultra-low and subtle levels. Usually, linearity is described as the degree to

which the current performance of a pressure sensor throughout a certain operating scale arrives at an upright line. In general, linearity is expressed as a percentage representing the drift from a linear regression line. Pressure sensor responses within the linear operating range are more precise and reliable. Therefore, these pressure sensors are highly sensitive and have a wide linear range for practical applications.

Response time is a significant factor in assessing the effectiveness of pressure-sensing devices. The response time refers to the duration it takes for a pressure sensor to generate a consistent signal output after receiving input pressure. Pressure sensors are excellent options for advancing science and technology in contemporary culture due to their extensive use in personal electronic devices and industrial monitoring [63].

Flexible and wearable electronics have recently attracted much scientific attention because of their potential use in wearable technology, energy storage materials, electronic skins, sensors, etc. Advanced technology for sensing pressure with flexibility significantly speeds up the advancement of electronic devices with touch sensitivity. Pressure sensors that are flexible are excellent options for electronic utilization that are practical because of their superior mechanical properties, as shown in Figure 2.7. Lately, scientists have started using elastic and adaptable electronic materials to develop pressure sensors that cover large areas and are inexpensive in response to the widespread interest in flexibility. Electronic products that are flexible and touch-sensitive are gaining interest for use in pertinent applications. Numerous varieties of flexible e-skins have been developed, and many of them possess exceptional sensory capabilities. Recently, products for monitoring health through wearables have garnered significant interest. Smart bracelets are an example of advanced technology used in health monitoring that provides real-time

data. Wearable health monitoring devices need sensitive organics pressure sensors that are lightweight, highly flexible, and portable.

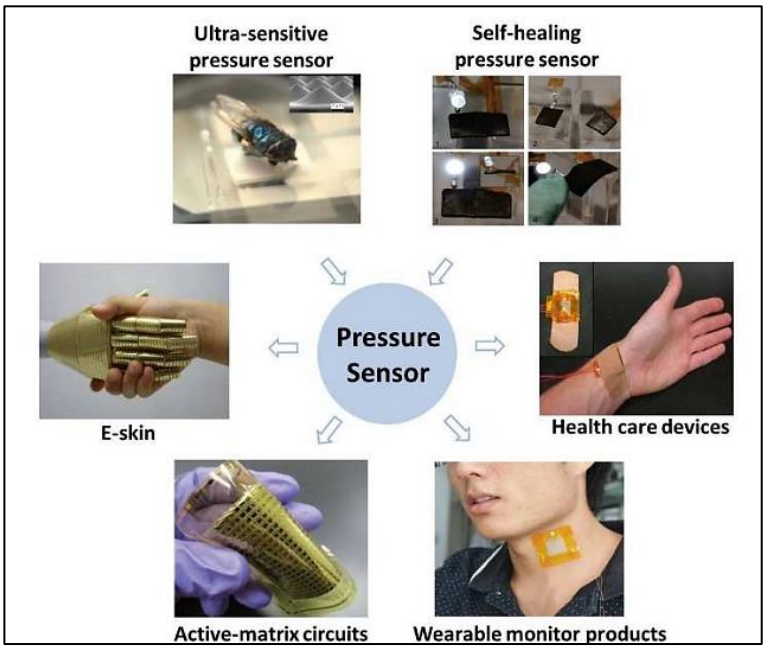

Figure 2.5. The promising applications of the pressure sensor [64]

2.4.2. Mathematical Model of CNT Pressure Sensor

The Carbon nanotube resistance based on its energy band gap, and it is expressed by the following equation [69]:

$$R_{tot}(\varepsilon) = R_s + \frac{1}{t^2}\frac{h}{8e^2}\left[1 + \exp(\frac{E_g}{kT})\right] \quad \text{.....(2.19)}$$

Where,

R_s is the contact resistance,

t is the transmission coefficient,

h is Plank's constant,

e is the charge of an electron,

E_g is the energy band gap,

T is absolute temperature, and

k is Boltzmann's constant.

The energy band gap of CNTs is dependent on its diameter estimated by the following equation [70]:

$$E_g = E_g^{\circ} + \frac{dE_g}{d\varepsilon}\varepsilon \quad \text{.....(2.20)}$$

Where,

$$E_g^{\circ} = \frac{|P|2\gamma a}{\sqrt{3}d} \quad \text{.....(2.21)}$$

And

$$\frac{dE_g}{d\varepsilon} = \text{sign}\,(2p+1)3\gamma[(1+v)\cos 3\theta_t] \text{.....(2.22)}$$

Where,

ε is applied strain,

γ =2.6 eV is a tight binding-overlap integral,

a= 0.249nm is the graphene lattice unite vector length,

d is the diameter of CNTs,

v is a Poisson ratio of CNTs,

θ is a chiral angle.

p=0,∓1 is the label's nanotube family is given by the chiral index (n, m) to determine p from n-m=3q+p, where q is an integer.

Additionally, the equation (2.15) describes radial and tangential strains at the substrate center [71]:

$$\varepsilon = \frac{3P\, r_0^2(1-v^2)}{8\, h_2^2\, E} \quad \text{..... (2.23)}$$

Where,

P is the pressure applied on the circular diaphragm,

r_0 is the radius of the circular diaphragm,

E is young's modulus of SiO2,

$h_2$is the thickness of SiO2,

v is the Poisson's ratio of SiO2.

Chapter Three
Methodology

Chapter Three

Modelling

3.1. Introduction

This chapter explains the methodology of work. In the first, the CNT was added as a new material to COMSOL Multiphysics. Then two models were built in several steps. The first model was CNT-FETs, and the second was a CNT-based piezoresistive pressure sensor. Then the design was built based on specified geometry. Where the geometry is designed based on dimensions such as length, width, CNT diameter, CNT thickness, height, and rotation angle and specified the unit scale.

The material selection utilized in the design, includes carbon nanotube, silicon, gold, and silicon dioxide. The properties of this material such as band gap, electron mobility, hole mobility, electron affinity, the effective density of the state conduction band, the effective density of the state valence band, density, Poisson's ratio, and Young's modulus are added after choosing the material.

After specifying the material properties for this model, the next step would be to define the physics of design. In the first model, the semiconductor physics was used. This physics lets us define the CNT properties and specify the source, drain, and gate connections. Another physics was the analytic doping model to set the donor or acceptor concentration in the CNT. Furthermore, the trap-assisted recombination another physics was selected to set the electron and hole lifetime. In the second model, the piezoresistive material physics, boundary load (pressure), fixed constrained, and current voltage terminal was selected. The mesh was utilized for the model geometry to know how the

geometry is split. Finally, the study step was built according to the model required to generate the plot curve of the design.

3.2. Material Selection and Physics

The selection of materials has an essential step in building the model. The model has some layers, as each layer in the design has a material that differs from the others. The material was selected from the library of materials, specified the domain for this material, and material properties. The substrate layer is silicon, the insulation layer is silicon dioxide, the metal contact is gold, and the channel between the metal contact is a carbon nanotube.

As the CNT was not included in the material library of COMSOL, was added the CNT as new material. This is done by adding full properties of CNT, including relative permittivity, band gap, electron affinity, the effective density of states in the valence and conduction band, and electron and hole mobility in the material properties. Other materials, silicon, silicon dioxide, and gold, were added from the material library. The thermal conductivity of silicon is greater than that of silicon dioxide. Furthermore, silicon's relative permittivity is higher than silicon dioxides.

The main justifications for utilizing gold are it raises the conductivity and accuracy of semiconductors and enhances the flow of electrons and holes. Silicon is the finest material, providing a minimal flow of electricity when acting as a semiconductor. The silicon dioxide increases the dielectric strength and functions as an exceptional insulator.

The physics utilized in this model of CNT-FET are the semiconductor material model, analytical doping model, metal contact, and trap-assisted recombination. The CNT behaves similarly

to a model of semiconductor material so that needed to specify the properties. The trapping-assisted model is the Shockley-Read-Hall-Recombination was used to set the electron lifetime and hole lifetime. The analytic doping model physics was used to specify the impurity type (donor concentration or acceptor concentration). The CNT behaves as an n-type doped semiconductor with donor concentration. The metal contact physics was used to specify the source, drain, and gate.

3.2.1. The Addition of Carbon Nanotube Model

Carbon nanotubes (CNTs) have been included in the material library of COMSOL Multiphysics following the next steps: In the beginning opening of the model or application where CNT material is required to be used in the COMSOL Multiphysics software. After that defining a new material in the material browser, which is usually present on the screen left side of the Model Builder window. Additionally, entering the properties of CNTs in the Material Settings dialog box; including electrical conductivity, thermal conductivity, band gap, electron mobility, hole mobility, electron affinity, the effective density of the state conduction band, the effective density of the state valence band, density, Poisson’s ratio, and Young’s modulus. Then specifying the parameters of CNTs that describe the behavior of CNTs. These parameters may include electrical conductivity, thermal conductivity, Young's modulus, Poisson's ratio, etc. After defining the material properties, saving the new material to the library. This allows us to reuse it in other simulations or models.

Table 3.1. The parameter of CNT utilizing
in COMSOL Multiphysics [71,73].

Parameter	Value
Young modulus	1000GPa
Poisson's ratio	0.2
Thickness of SiO2	1.5 µm
Temperature	293.15K
Transmission coefficient	0.5
Relative permittivity	237.4
Electrical conductivity	150 S/m
Density	2100[kg/m^3]
Effective density of state in the conduction band	8.88e20
Effective density of state in the valence band	7.36e20
Electron affinity	3.2eV

The parameter utilized in MWCNTs is 1.99MPa, 0.19 of Poisson's ratio and Young modulus, respectively [36].

3.2.2. Analytical Model of CNT

The essential parameters utilized in this model are diameter, threshold voltage, chiral angle, energy bandgap. These parameters are dependent on the chirality of the carbon nanotube. The zig-zag type of chirality was used. In the zig-zag type, the chiral index m=0 and n>0, so the CNT is a semiconductor material.

3.2.2.1. Chirality (13, 0)

Chirality is ascribed to the coordinate system in graphite sheets given by the two numbers (n, m), which denote the direction in which the sheet is rolled and the diameter of the CNTs.

A. Diameter of Chirality (13,0)

The diameter of CNTs is dependent on the chirality and is given by the equation (2.4):

a_{cc}=0.144nm

$$d = \frac{\sqrt{3} \times 0.144nm}{\pi} \sqrt{13^2 + 0^2 + 2 \times 13 \times 0}$$

$$d = 1\text{nm}$$

B. Threshold Voltage of Chirality (13,0)

The threshold voltage depends on the diameter of CNT, and can be calculated by (2.5):

Where,

a=0.249nm, V_π=3.033eV, e=1.6021×10^{-19} coulomb

Sub in equ (2.5)

$$V_{th} = \frac{0.249\text{nm} \times 3.033\text{eV}}{\sqrt{3} \times 1.6021 \times 10^{-19}\text{coulomb} \times 1\text{nm}}$$

$$V_{th} = \frac{0.436\text{V}}{1} = 0.436\text{V}$$

C. Chiral Angle of Chirality (13,0)

From equation (2.6) the chiral angle

$$\theta_t = \tan^{-1}\left(\frac{0 \times \sqrt{3}}{0 + 2 \times 13}\right) = zero$$

D. Energy Band Gap of Chirality (13,0)

The semiconductor band gap is given by this equation (2.21):

Where,

$\gamma = 2.6\text{eV}, a_\circ = 0.249\text{nm}, p = +1$

Sub in equ (2.21)

$$E_g^\circ = \frac{|1| \times 2 \times 2.6 \times 0.249}{\sqrt{3} \times 1} = 0.747\text{eV}$$

The change in bandgap energy with respect to strain is given by the equation (2.22):

$$\frac{dE_g}{d\varepsilon} = \text{sign}\,(2p+1)3\gamma[(1+v)\cos 3\theta_t]$$

Where,

v=0.2, $\theta_t = 0°, p = +1$

$$\frac{dE_g}{d\varepsilon} = \text{sign}\,(2\times 1+1)3\times 2.6\text{eV}[(1+0.2)\cos(3\times 0)]$$

$$\frac{dE_g}{d\varepsilon} = 9.36\text{eV}$$

The energy band gap of carbon nanotube estimated by the equation (2.20):

$$E_{g=}E_g^{\circ} + \frac{dE_g}{d\varepsilon}\varepsilon$$

Where, $\varepsilon = 0$

$$E_g = 0.747\text{eV} + 9.36\text{eV}\times 0 = 0.747\text{eV}$$

At $\varepsilon = 0.01$

$$E_{g=}0.747\text{eV} + 9.36\text{eV}\times 0.01 = 0.8406\text{eV}$$

At $\varepsilon = 0.02$

$$E_{g=}0.747\text{eV} + 9.36\text{eV}\times 0.02 = 0.9342\text{eV}$$

At $\varepsilon = 0.03$

$$E_{g=}0.747\text{eV} + 9.36\text{eV}\times 0.03 = 1.0278\text{eV}$$

At $\varepsilon = 0.04$

$$E_{g=}0.747\text{eV} + 9.36\text{eV}\times 0.04 = 1.1214\text{eV}$$

3.2.2.2. Chirality (26, 0)

Chirality is given by two number (n, m)

A. Diameter of Chirality (26,0)

From equation (2.4)

a_{cc} = 0.144 nm

$$d = \frac{\sqrt{3} \times 0.144nm}{\pi} \sqrt{26^2 + 0^2 + 2 \times 26 \times 0}$$

$$d = 2nm$$

B. Threshold Voltage of Chirality (26,0)

From equation (2.5)

Where,

a=0.249nm, V_π=3.033eV, e=1.6021×10^{-19} coulomb

$$V_{th} = \frac{0.249nm \times 3.033eV}{\sqrt{3} \times e\ 1.6021 \times 10^{-19} coulomb \times 2nm}$$

$$V_{th} = \frac{0.436V}{2} = 0.218V$$

C. Chiral Angle of Chirality (26,0)

From equation (2.6)

$$\theta_t = \tan^{-1}\left(\frac{0 \times \sqrt{3}}{0 + 2 \times 26}\right) = zero$$

D. Energy Band Gap of Chirality (26,0)

From equation (2.21)

Where,

$$\gamma = 2.6eV, a_\circ = 0.249nm, p = +1$$

$$E_g^\circ = \frac{|1| \times 2 \times 2.6 \times 0.249}{\sqrt{3} \times 2} = 0.373eV$$

The change in bandgap energy with respect to strain is calculated by equation (2.22):

Where,

v=0.2, $\theta_t = 0°, p = +1$ sub in equ (2.22)

$$\frac{dE_g}{d\varepsilon} = \text{sign}\,(2\times 1+1)3\times 2.6\text{eV}[(1+0.2)\cos(3\times 0)]$$

$$\frac{dE_g}{d\varepsilon} = 9.36\text{Ev}$$

The energy band gap of carbon nanotube is derived by (2.20):

Where, $\varepsilon = 0$

$$E_g = 0.373\text{eV} + 9.36\times 0 = 0.373\text{eV}$$

At $\varepsilon = 0.01$

$$E_{g=}0.373\text{eV} + 9.36\text{eV}\times 0.01 = 0.4666\text{eV}$$

At $\varepsilon = 0.02$

$$E_{g=}0.373\text{eV} + 9.36\text{eV}\times 0.02 = 0.5602\text{eV}$$

At $\varepsilon = 0.03$

$$E_{g=}0.373\text{eV} + 9.36\text{eV}\times 0.03 = 0.6538\text{eV}$$

At $\varepsilon = 0.04$

$$E_{g=}0.373\text{eV} + 9.36\text{eV}\times 0.04 = 0.7474\text{eV}$$

3.2.2.3. Chirality (39,0)

A. Diameter of Chirality (39,0)

From equation (2.4)

a_{cc} = 0.144 nm

$$d = \frac{\sqrt{3}\times 0.144nm}{\pi}\sqrt{39^2+0^2+2\times 39\times 0}$$

$$d = 3\text{nm}$$

B. Threshold Voltage of Chirality (39,0)

From equation (2.5)

Where,

a=0.249nm, V_π=3.033eV, e=1.6021×10^{-19} coulomb

$$V_{th} = \frac{0.249nm \times 3.033eV}{\sqrt{3} \times e\ 1.6021 \times 10^{-19} coulomb \times 3nm}$$

$$V_{th} = \frac{0.436V}{3} = 0.145V$$

C. Chiral Angle of Chirality (39,0)

From equ (2.6)

$$\theta_t = \tan^{-1}\left(\frac{0 \times \sqrt{3}}{0+2\times 39}\right) = \text{zero}$$

D. Energy Band Gap of Chirality (39,0)

The semiconductor band gap is derived by equ (2.21):

Where,

$$\gamma = 2.6eV, a_\circ = 0.249nm, p = +1$$

$$E_g^\circ = \frac{|1| \times 2 \times 2.6 \times 0.249}{\sqrt{3} \times 3} = 0.249eV$$

The change in bandgap energy with respect to strain sub in equ (2.22):

Where,

v=0.2, $\theta_t = 0°, p = +1$

$$\frac{dE_g}{d\varepsilon} = \text{sign}\,(2 \times 1 + 1)3 \times 2.6eV[(1 + 0.2)\cos(3 \times 0)]$$

$$\frac{dE_g}{d\varepsilon} = 9.36Ev$$

The energy band gap of carbon nanotube is derived by equ (2.20)

Where, $\varepsilon = 0$

$$E_g = 0.249eV + 9.36 \times 0 = 0.249eV$$

At $\varepsilon = 0.01$

$$E_{g=} 0.249eV + 9.36eV \times 0.01 = 0.3426eV$$

At $\varepsilon = 0.02$

$E_{g=}0.249eV + 9.36eV \times 0.02 = 0.4362eV$

At $\varepsilon = 0.03$

$E_{g=}0.249eV. + 9.36eV \times 0.03 = 0.5298eV$

At $\varepsilon = 0.04$

$E_{g=}0.249eV + 9.36eV \times 0.04 = 0.6234eV$

3.2.2.4. Chirality (51,0)

A. Diameter of Chirality (51,0)

From equ (2.4)

a_{cc} = 0.144 nm

$$d = \frac{\sqrt{3} \times 0.144nm}{\pi} \sqrt{51^2 + 0^2 + 2 \times 51 \times 0}$$

$d = 4nm$

B. Threshold Voltage of Chirality (51,0)

To find threshold voltage of chirality (51,0) estimated by equ (2.5)

Where,

a=0.249nm, V_π=3.033eV, e=1.6021×10^{-19} coulomb

$$V_{th} = \frac{0.249nm \times 3.033eV}{\sqrt{3} \times e\ 1.6021 \times 10^{-19} coulomb \times 4nm}$$

$$V_{th} = \frac{0.436V}{4} = 0.109V$$

C. Chiral Angle of Chirality (51,0)

From equ (2.6)

$$\theta_t = \tan^{-1}\left(\frac{0 \times \sqrt{3}}{0 + 2 \times 51}\right) = zero$$

D. Energy Band Gap of Chirality (51,0)

The semiconductor band gap was defined by equ (2.21):

Where,

$\gamma = 2.6eV, a_{\circ} = 0.249nm,\ p = +1$

$\mathrm{E_g^{\circ}} = \frac{|1|\times 2\times 2.6\times 0.249}{\sqrt{3}\times 4} = 0.1868\mathrm{eV}$

The change in bandgap energy with respect to strain in equ(2.22):

Where,

v=0.2, $\theta_t = 0°, p = +1$

$\frac{dE_g}{d\varepsilon} = \text{sign}\,(2\times 1+1)3\times 2.6\mathrm{eV}[(1+0.2)\cos(3\times 0)]$

$\frac{dE_g}{d\varepsilon} = 9.36\mathrm{eV}$

The energy band gap of carbon nanotube calculated by (2.20):

where, $\varepsilon = 0$

$\mathrm{E_g} = 0.1868\mathrm{eV} + 9.36\times 0 = 0.1868\mathrm{eV}$

At $\varepsilon = 0.01$

$\mathrm{E_{g=}} 0.1868\mathrm{eV} + 9.36\mathrm{eV}\times 0.01 = 0.2804\mathrm{eV}$

At $\varepsilon = 0.02$

$\mathrm{E_{g=}} 0.1868\mathrm{eV} + 9.36\mathrm{eV}\times 0.02 = 0.374\mathrm{eV}$

At $\varepsilon = 0.03$

$\mathrm{E_{g=}} 0.1868\mathrm{eV} + 9.36\mathrm{eV}\times 0.03 = 0.4676\mathrm{eV}$

At $\varepsilon = 0.04$

$\mathrm{E_{g=}} 0.1868\mathrm{eV} + 9.36\mathrm{eV}\times 0.04 = 0.5612\mathrm{eV}$

3.3. Designing of CNTFETs

COMSOL Multiphysics is utilized to design an SWCNT- FET with a back gate. Figure 3.1 (a) describes the back gate schematic of SWCNT-FET. In this research, an SWCNT is formed by rolling up a single graphene layer (hollow cylindrical). The source and drain electrodes, which are metal, are connected by the CNT. The CNT physical dimensions are designed with thickness of 0.345nm, length of 3.5µm, and diameter 1nm. The thickness of CNT is the difference between the outer and inner radius. Figure 3.1(b) illustrate the dimension of SWCNTs. Gold was utilized for fabricating the metal contact source and drain with a length and thickness of about 1650nm and 50nm; respectively. This structure was insulated by a silicon dioxide layer 300nmover a substrate of silicon 2µm and 6800nm length. An n-type Silicon substrate was obtained by doping substrate of silicon using Boron. Table 3.2 represents the parameters used in the current design.

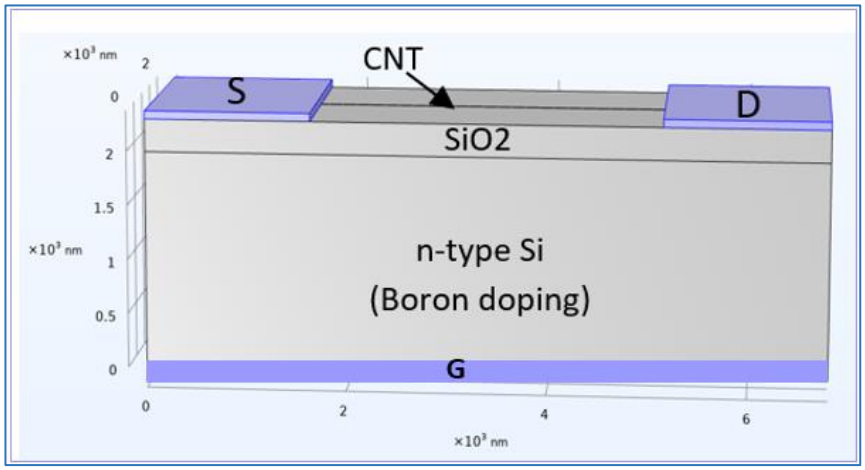

(a)

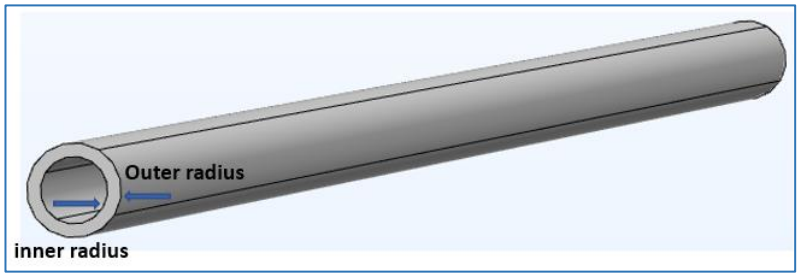

(b)

Figure 3.1. (a) Schematic of CNTFET in COMSOL Multiphysics

(b) Schematic of SWCNT

Table 3.2 The parameters of SWCNT transistor used in COMSOL Multiphysics

Parameters	Value
Thickness of CNT	0.345nm
Diameter of CNT	1nm
Thickness of Silicon dioxide	300nm
Thickness of gold contact	50nm
Thickness of silicon	2000nm
Length of CNT	3500nm
Width of silicon	6800nm
Hole effective mass	$0.5m_o$
Electron effective mass	$0.5m_o$
Temperature	293.15K
Electron affinity of CNT	3.2eV
mobility of CNT	$0.0025m^2$/V. s
Relative permittivity of SiO2	3.9
Relative permittivity of CNT	11
Effective density of state in the conduction band	$4.282e^{24}$ $1/m^3$
Effective density of state in the valence band	$8.556e^{24}$ $1/m^3$
Donor concentration	$1.5e^{24}$
Drain contact type	Ideal ohmic
Source contact type	Ideal ohmic

3.3.1. Analytical Model of CNT-FETs

3.3.1.1. Electron Concentration

The conduction band equation presents the number of electrons. The intrinsic concentration is computed for both n-type and p-type transistors, as depicted below:

$$m_e = 0.5m_\circ = 0.5 \times 9.11 \times 10^{-31}\text{kg}$$

$$m_e = 4.55 \times 10^{-31}\text{kg}$$

Sub in equ (2.13)

$$N_c = \left(\frac{2\pi \times 4.55\times10^{-31}\text{kg} \times 4.05\times10^{-21}\text{J}}{(6.626\times10^{-34}Js)^2}\right)^{\frac{3}{2}}$$

$$N_c = 4.2826\ \text{e24}\ 1/\text{m}^3 \text{ sub in (2.12)}$$

$$n_i = 4.2826\ \text{e24}\ 1/\text{m}^3 \times e\left[\frac{-(E_c - E_F)}{KT}\right]$$

$$(E_c - E_F) = \text{KTln}\left(\frac{N_c}{N_d}\right)$$

$$(E_c - E_F) = 4.047 \times 10^{-21}\ln\left(\frac{4.2826e24}{1.5e24}\right)$$

$$(E_c - E_F) = 4.245 \times 10^{-21}J$$

$$n_i = 4.2826\ \text{e24}\ 1/\text{m}^3 \times e\left[\frac{-(E_c - E_F)}{KT}\right]$$

$$n_i = 1.5014\ \text{e24}\ 1/\text{m}^3$$

3.3.1.2. Hole Concentration

The number of electrons in the valence band which is define by the equation (2.16).

$$m_h = m_e = 0.5m_\circ = 0.5 \times 9.11 \times 10^{-31}\text{kg}$$

$$m_h = 4.55 \times 10^{-31}\text{kg}$$

Sub in equ (2.16)

$$N_v = 2\left(\frac{2\pi \times 4.55\times10^{-31}\text{kg} \times 4.047\times10^{-21}\text{J}}{(6.626\times10^{-34}\text{Js})^2}\right)^{\frac{3}{2}}$$

$N_v = 8.556\ e^{24} 1/m^3$ sub in (2.15)

$$(E_v - E_F) = 4.047 \times 10^{-21} J \times \ln\left(\frac{8.556e24}{1.5e24}\right)$$

$$(E_v - E_F) = 7.051 \times 10^{-21} J$$

$$p_i = N_v e\left(\frac{E_v - E_F}{KT}\right)$$

$$p_i = 8.556 \times 10^{24} e\left(\frac{7.051 \times 10^{-21}}{4.047 \times 10^{-21}}\right)$$

$$p_i = 14.90\ e24\ 1/m^3$$

3.3.1.3. Electron Mobility of CNTs

Electron mobility in semiconductors is essential for understanding the performance of any electric device. Electron mobility is utilized to characterize the passage of electrons through a semiconductor material.

From equ (2.10) and equ (2.11) estimated electron mobility:

Where,

$L_{cnt} = 3500nm$, $\varepsilon_r = 3.9$, $\varepsilon_\circ = 8.854 \times 10^{-12}$, $t = 300nm$, r=0.5nm sub in equ (2.11)

$$Cg = \frac{2\pi \times 3500nm \times 3.9 \times 8.854 \times 10^{-12} F/m}{\ln\left(\frac{2 \times 300nm}{0.5nm}\right)}$$

$Cg = 1.07e^{-7} nF$ sub in equ (2.10)

$$g_m = \left(\frac{\partial I_d}{\partial V_g}\middle| V_{d=1V}\right)$$

$g_m = 1.6\mu A/V$ sub in equ (2.10)

$$\mu = \frac{(3500nm)^2 \times 1.6\mu A/V}{1.07 \times 10^{-7} \times 1V}$$

$$\mu = 4.77 \times 10^{-26} cm^2 v^{-1} s^{-1}$$

3.4. Designing of CNT- Based Piezoresistive Pressure Sensor

The carbon nanotube-based piezoresistive pressure sensor is designed in this section, as depicted in Figure 3.2. In this design, SWCNT

and MWCNT were used. The SWCNTs have one layer consisting of an inner radius of r_1 and an outer radius of r_2. While the MWCNTs have four layers consisting of an r_1 to r_8. The distance between layers necessitates being convergent as shows in Figure 3.3. The CNTs are placed between two metals on top of the substrate (Si/SiO2). The CNTs act as a piezoresistive pressure sensor component to detect changes in pressure. The pressure applied at the backside of the circular substrate is 300kPa. The substrate will become bent due to the applied pressure so the CNT will become bending. As a result, CNT's resistance will alter. The basic simulation procedures include the following:

- Modeling (building geometry),
- Material selection, (Si, SiO2, Gold, CNT)
- Boundary condition setting (boundary load and fixed constraint), The fixed edge of the circular diaphragm is one of the pressure sensor's boundary conditions.
- Initial condition,
- Meshing,
- Running the model,
- Viewing the results.

The model construction consists of various procedures. Firstly, building the design of 3D geometry according to the measured dimensions are length, width, and thickness. Another important component is selecting the material type of design. The materials utilized are n-type silicon, silicon dioxide, CNT, and Gold. Each material has properties, including relative permittivity, Young's modulus, Poisson's ratio, electrical conductivity, and density, which are summarized in Table 3.3. The boundary load and fixed constraint were chosen in the solid

mechanic's physics. The load type is a pressure that applies at a substrate's lower surface.

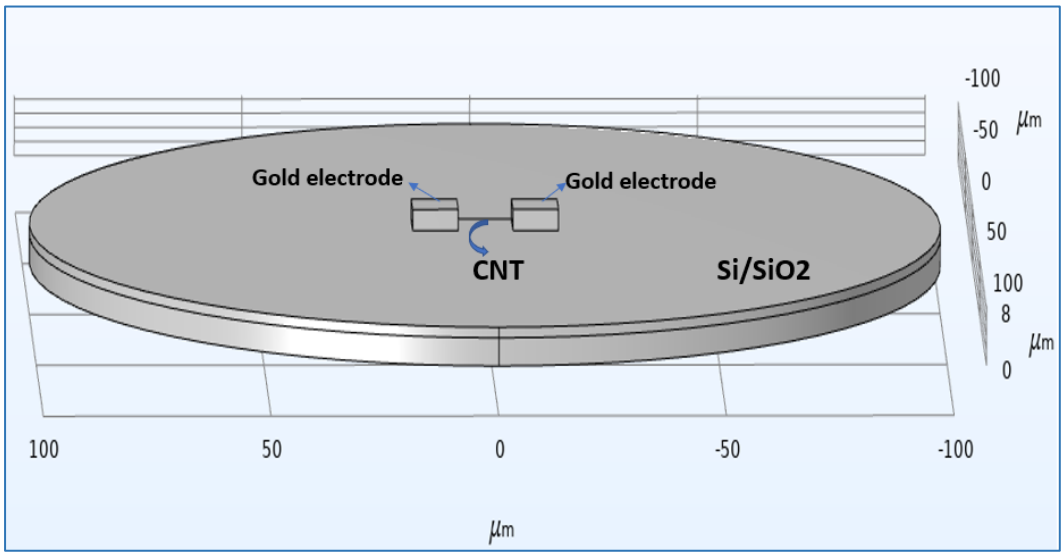

Figure 3.2. Geometry of CNT Piezoresistive Pressure Sensor

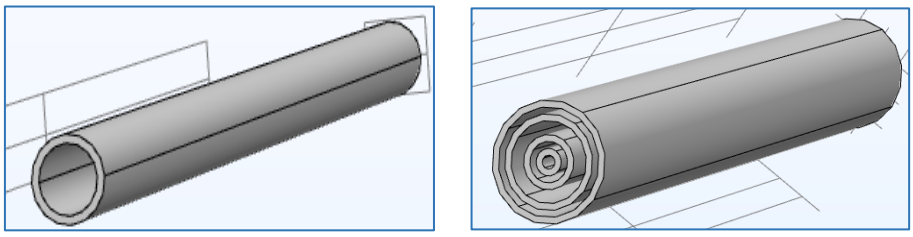

(a) **(b)**

Figure 3.3. Schematics of CNTs (a) SWCNTs. (b) MWCNTs

In this model, n-type silicon is the substrate, CNT is the sensing element, and the insulation layer is silicon dioxide. The substrate was utilized in the model is circular. The circular substrate of 100μm radius to silicon/ silicon dioxide, and the silicon has a thickness of 4 μm, whereas the silicon dioxide thickness is 1.5 μm. The dimension of metal contact (gold) is 10μm×10μm, and 3μm is thickness. The CNT has Poisson's ratio of 0.2, Young's modulus 1000GPa, a relative permittivity of 237.4, an electrical conductivity of 150 S/m, and a 2100kg/m^3 density. The parameters used in this design as shown in Table 3.3.

Table 3.3. The parameter of CNT pressure sensor utilizing in COMSOL Multiphysics [71].

Parameter	Value
Young modulus	1000GPa
Poisson's ratio	0.2
Radius of diaphragm	100 µm
Thickness of SiO2	1.5 µm
Length of CNTs	14.99 µm
Temperature	293.15K
Transmission coefficient	0.5
Relative permittivity	237.4
Electrical conductivity	150 S/m
Density	2100[kg/m^3]

3.4.1. The SWCNTs Pressure Sensor

The CNT was placed on top of silicon dioxide and was a suspending, and Figure 3.4 illustrate the model's design. The SWCNT dimension includes length, diameter, and thickness; measurements are 14.99 µm, 4nm, and 2nm, respectively. Two metals made from gold electrodes are used to contact the CNT.

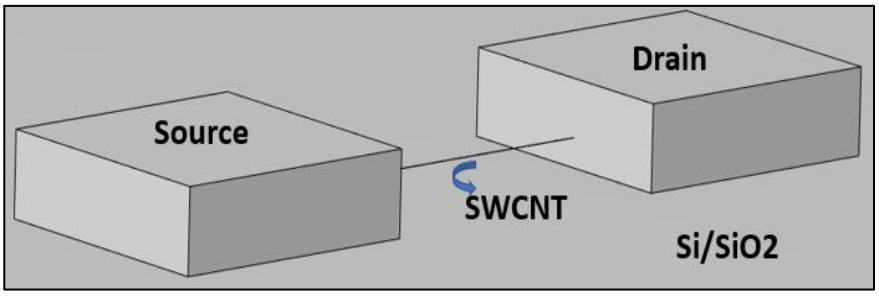

Figure 3.4. Geometry of single walled CNT in COMSOL Multiphysics

3.4.1.1. Array of Two SWCNTs Pressure Sensor

In this section, was increase the number of single-walled Carbon nanotubes with the same structure at 100 μm radius of silicon /SiO2 and 4 μm thickness of silicon and 1.5 μm thickness of silicon dioxide, as shown in Figure 3.5. At the same time, the dimensions of the metal contact are 10×10×3 μm, as length, width, and thickness, respectively. The outer radius of CNTs is 4nm, the inner radius is 2nm, and the thickness is 2nm. The distance between CNT is 1nm, at length is 14.99 μm.

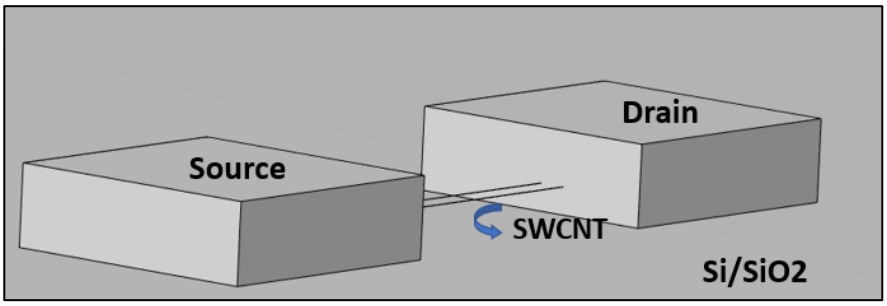

Figure 3.5. Geometry of two single walled CNT in COMSOL Multiphysics

3.4.1.2. Array of SWCNTs Pressure Sensor

Figure 3.6 illustrates the fabricated array of SWCNTs-based pressure sensors. The design included a layer of silicon dioxide with a silicon layer 4μm thick and single-walled carbon nanotubes suspended between two metal electrodes. The geometric of this model dimensions are length, radius, and thickness. Starting from a silicon substrate with a radius 100 μm and a silicon dioxide insulation layer at 1.5 thickness and 100 μm radius to the Carbon nanotube at 14.99 μm length and 2nm thickness and electrode of gold with dimensions are 10×10×3 μm, length, width, and thickness. The array type is linear, and the displacement between these is one. The number of nanotubes is four; all nanotubes have the same dimensions.

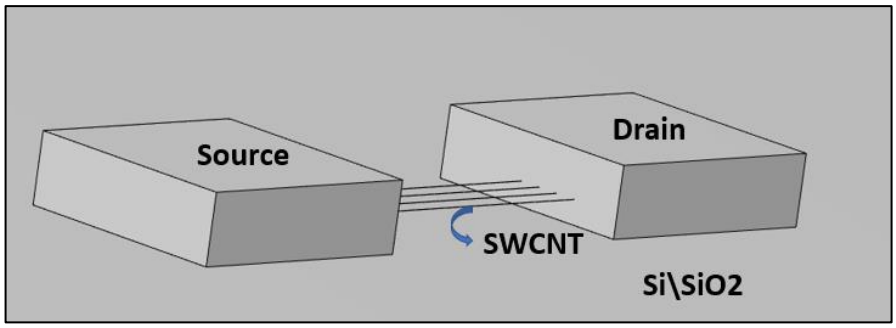

Figure 3.6. Geometry of Array single walled CNTs

3.4.2. The Single MWCNT Pressure Sensor

In this model, the MWCNTs are taken as a piezoresistive pressure sensor connected between two gold electrodes on the silicon dioxide. The MWCNTs have four layers, each with two radiuses (inner and outer radius), illustrated in Figure3.7. For this design, the dimensions that were taken into consideration are r_1=2nm; r_2=4nm; r_3=6nm; r_4=8nm; r_5=10nm; r_6=12nm; r_7= 14nm; r_8=16nm; Figure 3.8 show schematics layer of MWCNTs. In the first layer, the inner radius is 2nm, but the outer radius equals 4nm. In addition, the inner radius in the second layer equals 6nm, but the outer equals 8nm. Besides, in the third layer, the inner radius is 10nm, but the outer radius equals 12nm. Finally, the fourth layer contains an inner radius equal to 14nm and an outer radius equal to 16nm. Consequently, the thickness at one-layer equals 0.345nm, and the distance between layers equals 2nm.

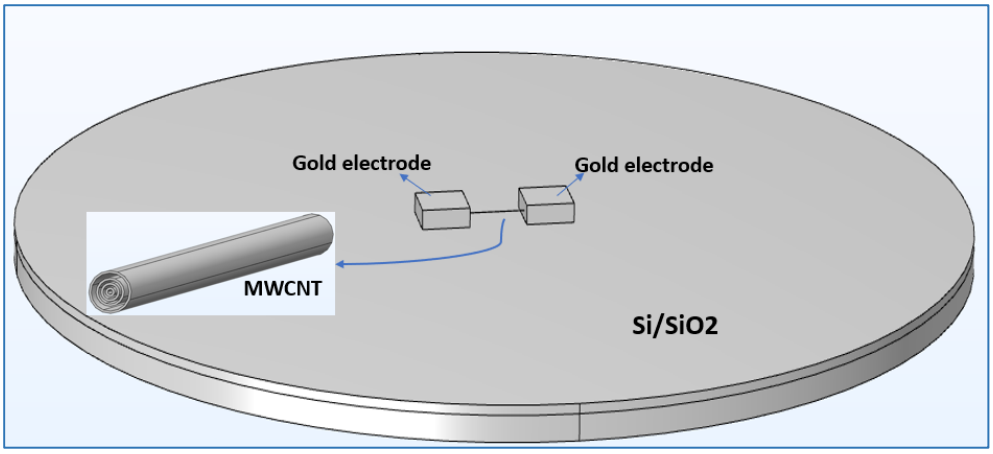

Figure 3.7 Geometry of MWCNTs piezoresistive pressure sensor

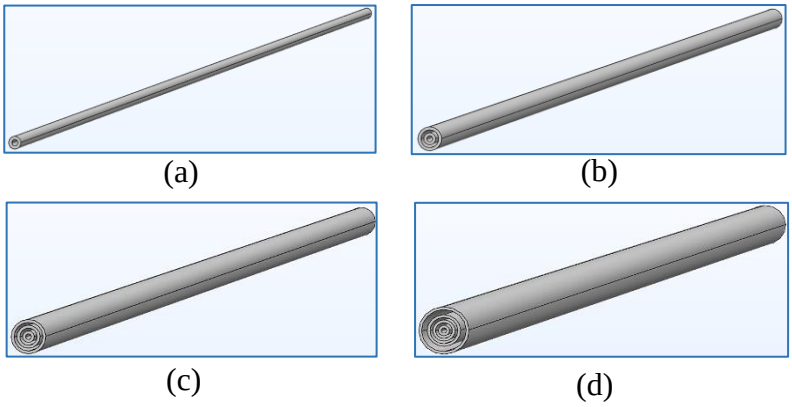

Figure 3.8. Schematics layer of MWCNTs (a) First layer (SWCNT) (b) Second layer (DWCNT) (c) Third layer (TWCNT) (d) Fourth layer (MWCNT).

3.4.2.1. Array of Two MWCNT Pressure Sensor

In this design, was utilized two multi-walled carbon nanotubes. The nanotubes have 14.99μm lengths with different radiuses starting from 2nm to 16nm; the two nanotubes have the same dimensions, and the displacement between the two nanotubes is 1 μm. The two nanotubes are connected between gold electrodes to flow electric current. Then, the nanotube was placed on the silicon dioxide layer and under this layer is the silicon substrate; its radius is 100 μm, and its thickness is 4 μm. Figure 3.9 illustrates the design.

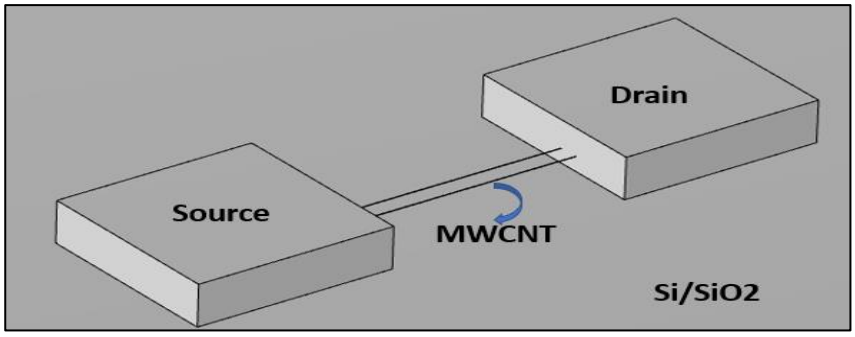

Figure 3.9. Schematics geometry of two array multi-walled CNT

3.4.2.2. Array of MWCNT Pressure Sensor

The design adopted in this section is the same as CNT-FETs, consisting of a circular substrate with a radius100 and thickness of 4μm, and above it is an insulation layer of silicon dioxide with a thick 1.5 μm. In this model, was used an array of CNTs; this array of CNT exists between two electrodes of gold to pass electric current from source to drain. The number of CNT utilized is four, as shown in the Figure 3.10. The displacement between each nanotube is 1 μm, with a length of 14.99 μm and different radii.

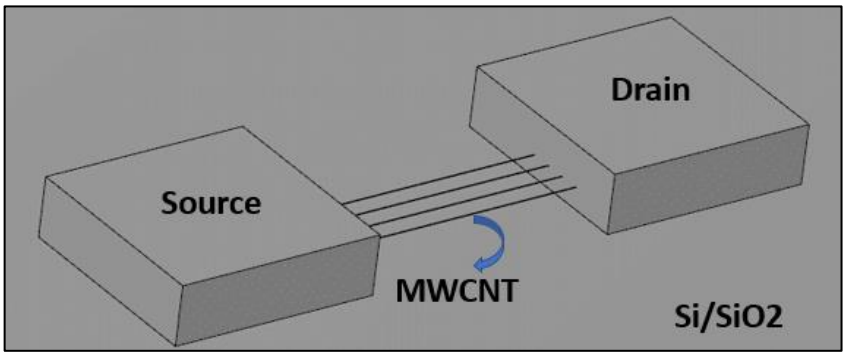

Figure 3.10. Schematics geometry of array multi-wall CNT

3.4.3. Analytical Model of CNTs Pressure Sensor

3.4.3.1. Resistance of Chirality (13,0)

The resistance of carbon nanotube dependent on energy band gap and is given by equation (2.19):

$$R_{tot} = R_s + \frac{1}{t^2}\frac{h}{8e^2}\left[1 + \exp\left(\frac{E_g}{kT}\right)\right]$$

Where,

$R_s = 13k\Omega$, $t = 0.5$,

$h = 6.626 \times 10^{-34}$,

$e = 1.602 \times 10^{-19}$,

$k = 1.38 \times 10^{-23}$J/k, T=293.15k

$$R_{tot} = 13k\Omega + \frac{1}{(0.5)^2}\frac{6.626\times10^{-34}}{8\times(1.602\times10^{-19})^2}\left[1 + \exp\left(\frac{E_g}{1.38\times10^{-23}\times1.38\times10^{-23}}\right)\right]$$

$$R_{tot} = 13k\Omega + 0.05 \times 10^8[E_g]$$

At $E_{g=}0.747eV \longrightarrow R_{tot} = 3748k\Omega$

At $E_{g=}0.8406eV \longrightarrow R_{tot} = 4216k\Omega$

At $E_{g=}0.9342eV \longrightarrow R_{tot} = 4684k\Omega$

At $E_{g=}1.0278eV \longrightarrow R_{tot} = 5152k\Omega$

At $E_{g=}1.1214eV \longrightarrow R_{tot} = 5620k\Omega$

3.4.3.2. Resistance of Chirality (26,0)

The resistance of CNTs dependent on the energy bandgap:

From equation (2.19)

$$R_{tot} = R_s + \frac{1}{t^2}\frac{h}{8e^2}\left[1 + \exp\left(\frac{E_g}{kT}\right)\right]$$

Where,

$R_s = 13k\Omega$,

$T = 0.5, h = 6.626 \times 10^{-34}$,

$e = 1.602 \times 10^{-19}$,

$k = 1.38 \times 10^{-23}$J/k, T=293.15k

$$R_{tot} = 13k\Omega + \frac{1}{(0.5)^2}\frac{6.626\times10^{-34}}{8\times(1.602\times10^{-19})^2}\left[1 + \exp\left(\frac{E_g}{1.38\times10^{-23}\times1.38\times10^{-23}}\right)\right]$$

$$R_{tot} = 13k\Omega + 0.05 \times 10^8[E_g]$$

At $E_{g=}0.373eV \longrightarrow R_{tot} = 1878k\Omega$

At $E_{g=}0.4666eV \longrightarrow R_{tot} = 2346k\Omega$

At $E_{g=}0.5602eV \longrightarrow R_{tot} = 2814k\Omega$

At $E_{g=}0.6538eV \longrightarrow R_{tot} = 3282k\Omega$

At $E_{g=}0.7474eV \longrightarrow R_{tot} = 3750k\Omega$

3.4.3.3. Resistance of Chirality (39,0)

From equ (2.19)

Where,

$R_s = 13k\Omega$, $t = 0.5$,

$h = 6.626 \times 10^{-34}$,

$e = 1.602 \times 10^{-19}$,

$k = 1.38 \times 10^{-23}$J/k,

T=293.15k

$$R_{tot} = 13k\Omega + \frac{1}{(0.5)^2}\frac{6.626\times10^{-34}}{8\times(1.602\times10^{-19})^2}\left[1 + \exp\left(\frac{E_g}{1.38\times10^{-23}\times1.38\times10^{-23}}\right)\right]$$

$$R_{tot} = 13k\Omega + 0.05 \times 10^8[E_g]$$

At $E_g = 0.249eV \longrightarrow R_{tot} = 1258k\Omega$

At $E_g = 0.3426eV \longrightarrow R_{tot} = 1726k\Omega$

At $E_g = 0.5298eV \longrightarrow R_{tot} = 2662k\Omega$

At $E_g = 0.6538eV \longrightarrow R_{tot} = 3282k\Omega$

At $E_g = 0.6234eV \longrightarrow R_{tot} = 3130k\Omega$

3.4.3.4. Resistance of Chirality (51,0)

By equ (2.19):

Where,

$R_s = 13k\Omega$, $t = 0.5$

$h = 6.626 \times 10^{-34}$,

$e = 1.602 \times 10^{-19}$Coulomb,

$k = 1.38 \times 10^{-23}$J/k, T=293.15k

$$R_{tot} = 13k + \frac{1}{(0.5)^2}\frac{6.626\times10^{-34}}{8\times(1.602\times10^{-19})^2}\left[1 + \exp\left(\frac{E_g}{1.38\times10^{-23}\times1.38\times10^{-23}}\right)\right]$$

$$R_{tot} = 13k\Omega + 0.05 \times 10^8[E_g]$$

$$\text{At } E_g = 0.1868\text{eV} \longrightarrow R_{tot} = 947\text{k}\Omega$$

$$\text{At } E_g = 0.2804\text{eV} \longrightarrow R_{tot} = 1415\text{k}\Omega$$

$$\text{At } E_g = 0.374\text{eV} \longrightarrow R_{tot} = 1883\text{k}\Omega$$

$$\text{At } E_g = 0.4676\text{eV} \longrightarrow R_{tot} = 2351\text{k}\Omega$$

$$\text{At } E_g = 0.5612\text{eV} \longrightarrow R_{tot} = 2819\text{k}\Omega$$

Chapter Four

Simulation Results

Chapter Four

Simulation Results

4.1. Introduction

The design and performance of CNT utilizing circular substrate have been investigated. This chapter presents the results of the thesis, which will be divided into two steps. The first simulates a single-walled carbon nanotube field effect transistor, and the second simulates a CNTs-based piezoresistive pressure sensor.

In the first step, the current transport of CNTFETs, and the effect of changing parameters on the drain current were studied, including the effect of changing the diameter of CNTs, the effect of changing the thickness of silicon dioxide, and the effect of changing the length of CNTs. As well as the second step studied the effect of changing pressure on displacement, von Mises stress, and the current. Also, the effect of changing resistance of CNT after pressure is applied was studied.

The finite element method (FEM) is used as an evaluation method for the piezo resistance of semi-conducting CNTs. The finite element method (FEM) is functional minimization for resolving issues by partial differential equations, known as a numerical approach. In this thesis, COMSOL Multiphysics 6.0 was used to simulate a carbon nanotube.

4.2. Simulation of SWCNT-FET

The electronic properties of SWCNT are determined by chiral numbers (n, m). It can be either metallic or semiconductor, depending on its chirality. The carbon nanotube used for this simulation is a zig-zag nanotube with indices (n,0). The proposed method of finding the diameter depends on the chirality, where each diameter value has an exact chirality value. The bandgap and threshold voltage are inversely proportional to its diameter, as shown in Table 4.1.

Table 4.1. The SWCNT parameters at different chirality

Chirality	Diameter (nm)	Drain current (μA)	Bandgap (eV)	Threshold Voltage (V)
(13,0)	1	4.075	0.747	0.436
(19,0)	1.5	6.604	0.498	0.291
(26,0)	2	9.013	0.373	0.218
(32,0)	2.5	13.168	0.299	0.174
(39,0)	3	17.136	0.249	0.145
(45,0)	3.5	21.487	0.213	0.124
(52,0)	4	26.165	0.186	0.109
(58,0)	4.5	31.33	0.166	0.096

It can be seen from Table 4.1 that the increase in the diameter leads to a decrease in both bandgap and threshold voltage while the drain current increases. For example, increasing the carbon nanotube diameter from 1nm to 4.5nm leads to a decrease in the energy bandgap from0.747eV to 0.1 66eV, which is about (five times); this means that one can control the semiconductor properties of CNT by changing the diameter of CNT, illustrate in Figure 4.1.

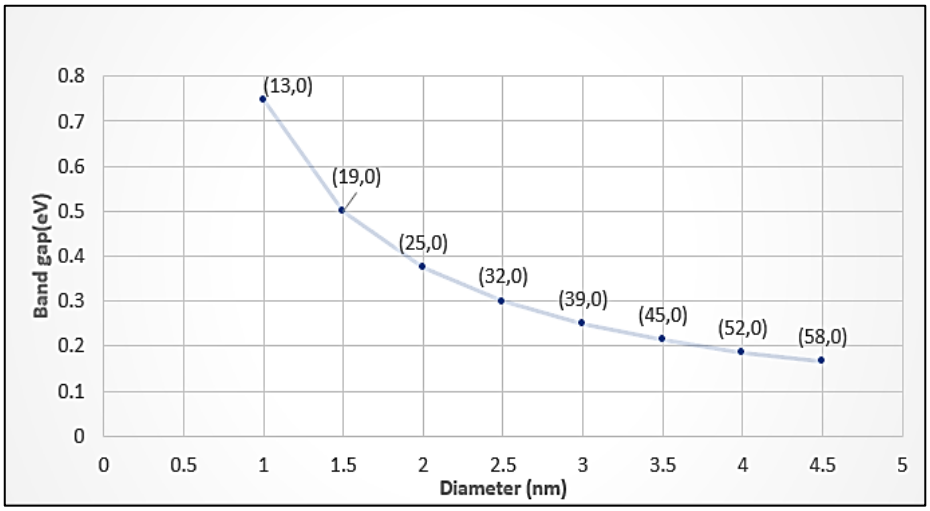

Figure 4.1. Diameter vs bandgap

The changing diameter was achieved in this work by rolling a single wall nanotube graphene layer. This system noticed that the drain current changed from 4.075µA to 31.33µA. The drain current increases as the diameter of the CNTs increases, as shown in the Figure 4.2.

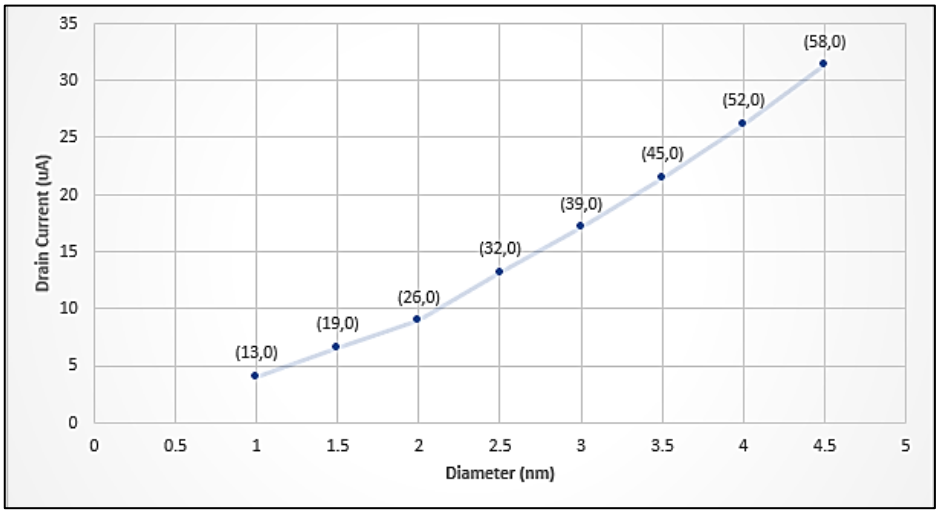

Figure 4.2. Diameter vs drain current.

The threshold voltage of the CNTFET may be controlled by altering the chirality vector or the diameter of the CNT. The threshold voltage is the voltage required to turn-on the transistor. Threshold voltage is inversely proportional to the diameter of carbon nanotube or chirality vector of CNT, as shown in Figure 4.3. The inverse relationship between the threshold voltage and the diameter (or

chirality) of a CNT is a result of the impact of these structural parameters on the electronic properties, particularly the bandgap. The CNT with smaller diameter and larger bandgaps generally requires higher threshold voltage for transistor operation, while the CNT with larger diameter and smaller band gap have lower threshold voltages. In this result, the threshold voltage decreased from 0.436V to 0.096V when the diameter increased from 1nm to 4.5nm utilizing the chirality from (13,0) to (58,0).

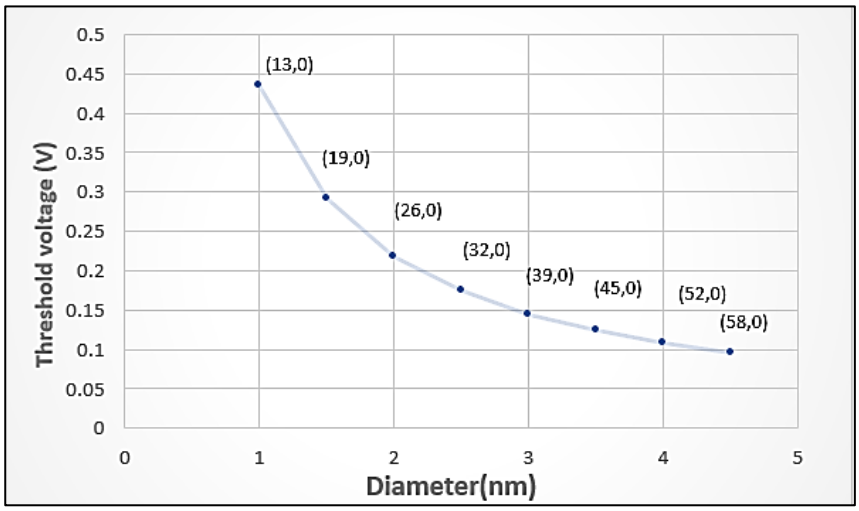

Figure 4.3. Diameter vs threshold voltage.

4.2.1. Current Transport of the Designed SWCNT-FETs

The Id-Vd characteristics of CNTFET are presented in Figure 4.4 and Figure 4.5 for various gate voltage values. Additionally, Figure 4.6 and Figure 4.7 shows the relationship between (Id-Vg) for different drain voltage values. The influence of changing drain and gate voltage on the drain current was studied. The CNT parameters used to determine the current transport are diameter equals 1nm, length equals 100nm, and chirality is (13,0). The thickness of the silicon dioxide is equal to 10nm. It was observed that the drain current increases with increasing of the drain voltage. Also, when reducing the values of gate voltage, the drain current decreases.

In these results, the threshold voltage equals 0.436V, the energy band gap equals 0.747eV, and the transconductance equals 10µA/V at drain voltage 1V.

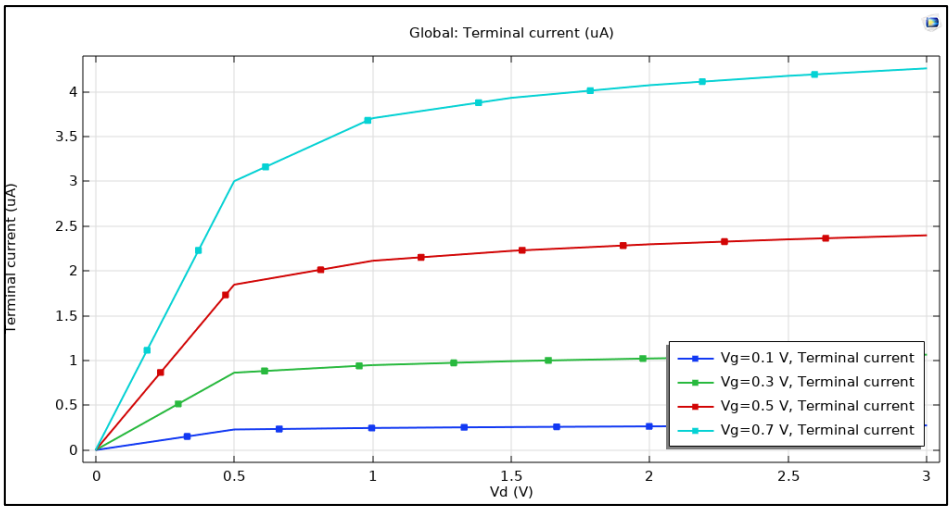

Figure 4.4. Current transport characteristics Id-Vd at gate voltage (0.1 ,0.3 ,0.5,0.7) V

The increase in drain current with an increase in gate voltage in CNT-based FETs is a result of the control of electron flow through the CNT channel by the electric field generated by the gate voltage.

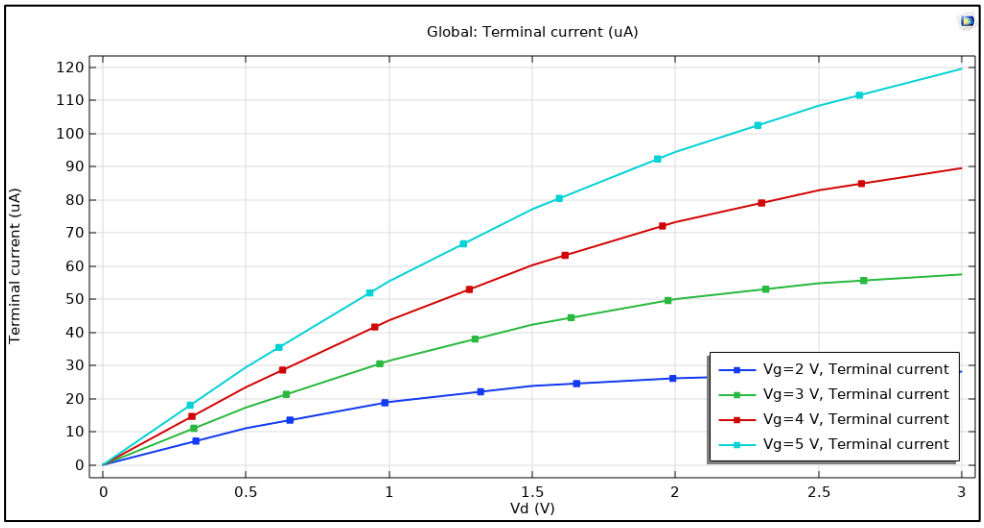

Figure 4.5. Current transport characteristics Id-Vd at gate voltage (2 ,3 ,4,5) V

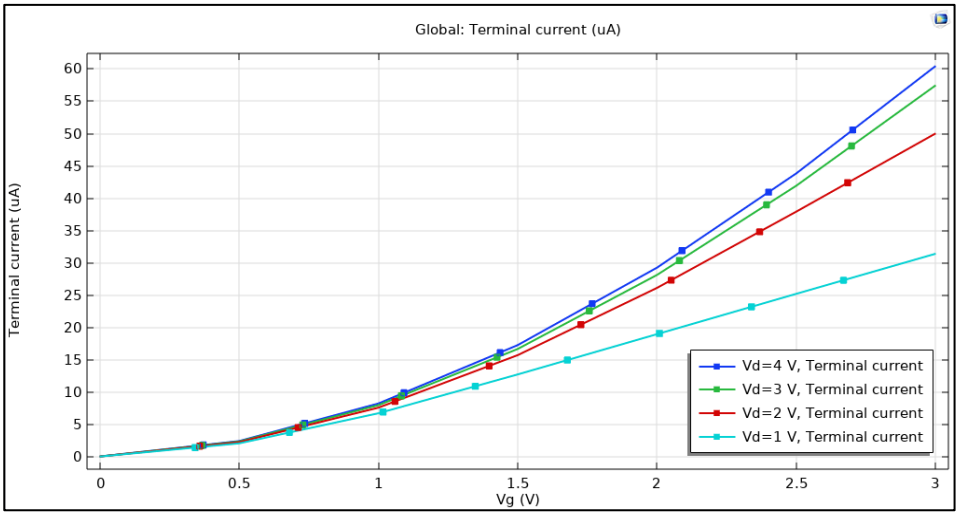

Figure 4.6. Current transport characteristics Id-Vg at drain voltage (1,2 ,3,4) V

The drain current typically increases with an increase in drain voltage due to the drain current being controlled by the voltage applied to the gate terminal. The gate voltage creates an electric field that influences the flow of charge carriers between the source and drain terminals. This increased of electric field can lead to a higher flow of charge carriers from the source to the drain. allowing for a greater flow of charge carriers, and consequently, an increase in the drain current in CNT-FETs.

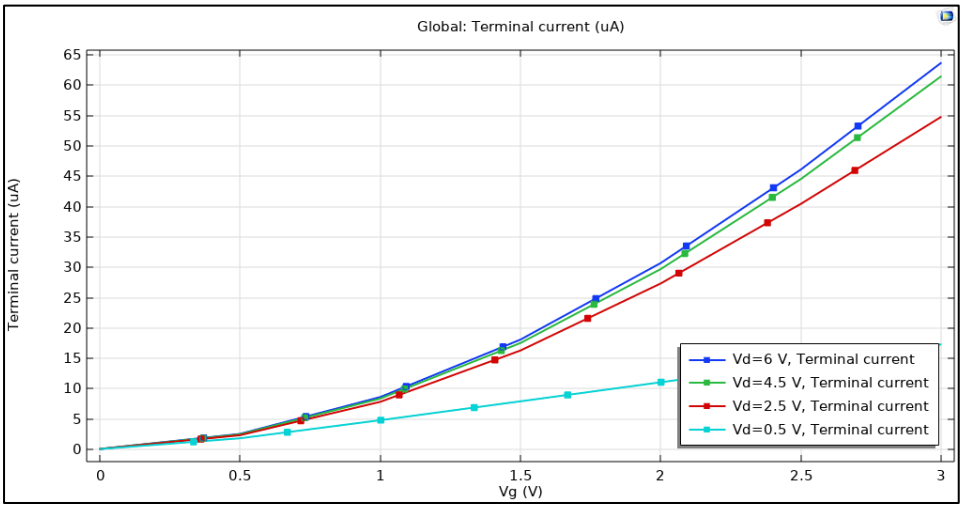

Figure 4.7. Current transport characteristics Id-Vg at drain voltage (0.5,2.5 ,4.5,6) V

4.2.2. The Effect of Altering Diameter of the SWCNT

In this section, the current-voltage relationship was determined for the range of the diameter length, 1nm to 4.5 nm, with a length of 3.5 µm. The thickness of the SiO2 is 300 nm. Figure 4.5 shows the Id vs. Vd at the gate voltage of 1.5 V. The results show that increasing the value of the carbon nanotube diameter leads to an elevation in the drain current, where the drain current increased from 4.5µA to 22µA when the diameter from 1nm to 4.5nm. Changing the diameter alters the electronic band structure and the density of states, affecting the availability of charge carriers. A larger diameter may provide a higher density of electronic states, allowing for more charge carriers and thus a higher current. A larger-diameter CNT may exhibit higher carrier mobility, leading to better charge transport and higher drain current. A larger diameter may result in a lower effective mass, which can enhance carrier mobility, consequently, increase the drain current.

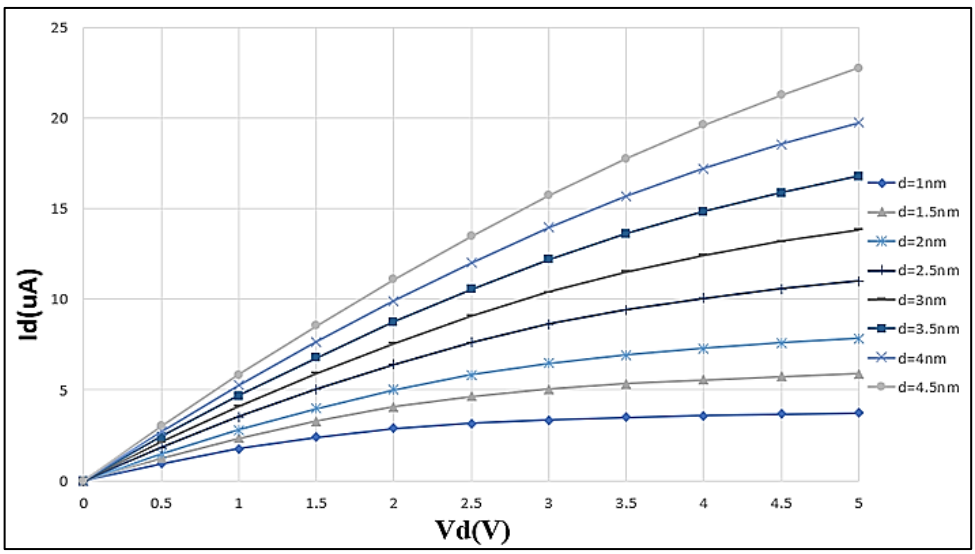

Figure 4.8. Drain current vs drain voltage at Vg=1.5V

4.2.3. The Effect of Altering Length of the SWCNT

To study the effect of changing carbon nanotube length on the drain current, a range of lengths from 32nm to 3500nm was selected, as illustrated

in Table 4.2. It was found that the drain current increased as the length of CNT decreased. Furthermore, the electron mobility is directly proportional to the length of CNT. Increasing the length of the CNT channel in a CNTFET leads to higher channel resistance and decrease in the drain current. That is this higher resistance impedes the flow of electrons from the source to the drain.

The measurement was done at a gate voltage of 1.5V, diameter of 1nm, energy band gap of 0.747eV and threshold voltage 0.436V. For more investigation of the property of CNT, the effect of the thickness of silicon dioxide on the current transport of CNT was studied. We figured out that the drain current elevated as silicon dioxide's thickness decreased. These results compared with previous studies that utilized a diameter of 1nm, chirality (13,0), band gap of 0.83eV, and channel length from 0 to 300nm. In our result, the drain current equals 8μA at a gate voltage of 0.1V, while in the previous study, the drain current was 6μA at a gate voltage of 0.6V.

Figure 4.9 shows the drain voltage relationship at several CNT lengths at an oxide thickness of 50nm; additionally, Figure 4.10 shows the relationship between drain voltage and drain current with different lengths of CNT at an oxide thickness of 300nm.

Table 4.2. Different lengths of CNT

Length of CNT (nm)	Drain current(µA)
32	1876.996
100	928.38
150	425.77
200	240.29
250	159.30
500	48.94
1000	18.35
1500	11.06
2000	7.8
2500	6.1
3000	4.9
3500	4.1

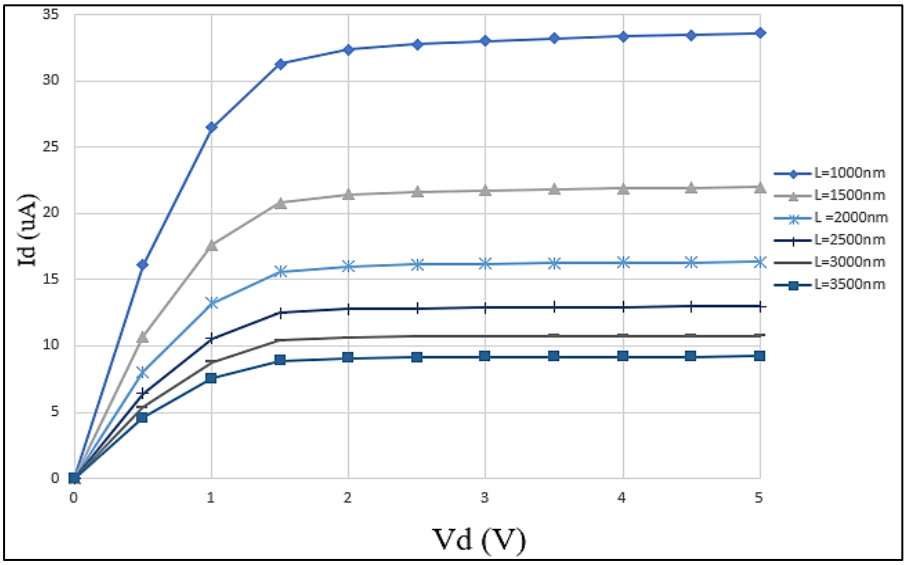

Figure 4.9. I-V characteristics of different lengths of carbon nanotube at oxide thickness is equal 50nm.

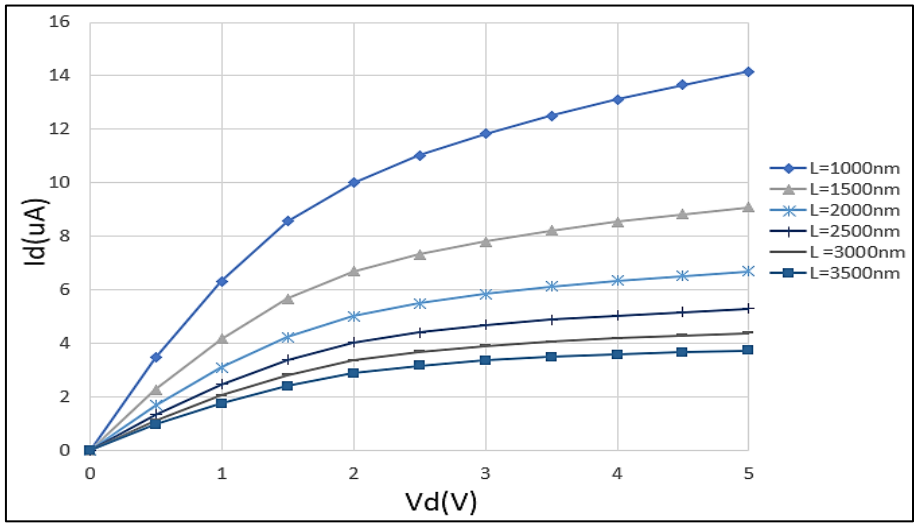

Figure 4.10. I-V characteristics of different lengths of carbon nanotube at oxide thickness is equal 300nm.

4.2.4. The Effect of Altering Thickness of Silicon Dioxide of SWCNT

In this section, current-voltage characteristics (Id-Vd) curves were plotted with various values of gate oxide thicknesses, from 1.5nm to 300nm at gate voltage equal to 3V and diameter of CNT of 1nm, as presented in Figure 4.11. The drain current decreases with increasing gate oxide thickness. The increase in gate oxide thickness generally results in a higher threshold voltage, reduced capacitance, lower electric field, and decreased carrier mobility. These factors collectively contribute to a decrease in the drain current. For example, when the gate oxide thickness increased from 1.5nm to 300nm, the drain current declined to about 53 times.

The drain current was obtained at various parameters at an energy band gap of 0.747eV, a channel length of 3500nm, and gate oxide thickness from 1.5nm to 300nm. The maximum drain current equals 250µA at 2.5nm gate oxide thickness. These results were compared with the previous research where the drain current equals 10µA at a channel

length of 15nm, the energy band gap of 0.61eV, chirality (16,0), and gate oxide thickness of 2.5nm.

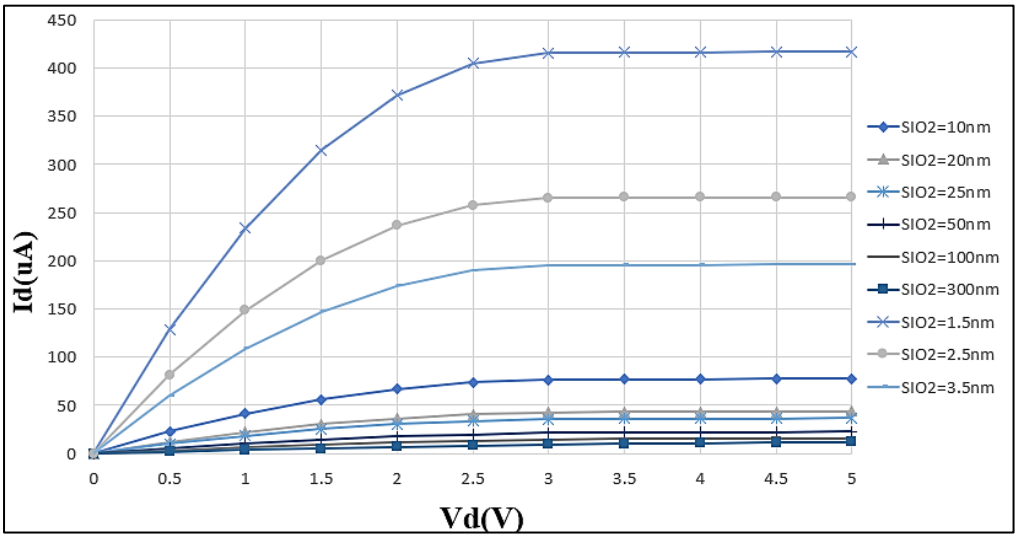

Figure 4.11. Id vs Vd at gate oxide thickness from (1.5nm to 300nm)

4.2.5. Frequency Response of SWCNT-FETs

The Performance of carbon nanotube Field -Effect transistors (CNTFETs) was characterized using frequency response to find its bandwidth and the resonance frequency. To estimate the bandwidth of CNTFETs, was utilized f-3dB as a realistic Figure 4.12 of merit. The frequency response of CNFETs influenced parasitic capacitances at gigahertz frequencies. Cutoff frequency was used to describe the high-frequency performance of the transistor. The intrinsic cutoff frequency is determined by $f_c = g_m/2\pi C_g$. Where gm is the transconductance, and Cg is the intrinsic gate capacitance. The cutoff frequency is directly proportional to the gm and inversely proportional to Cg. Based on this result, the resonance frequency for this designed CNTFET is equal to 50GHz, and the bandwidth is equal to 30GHz.

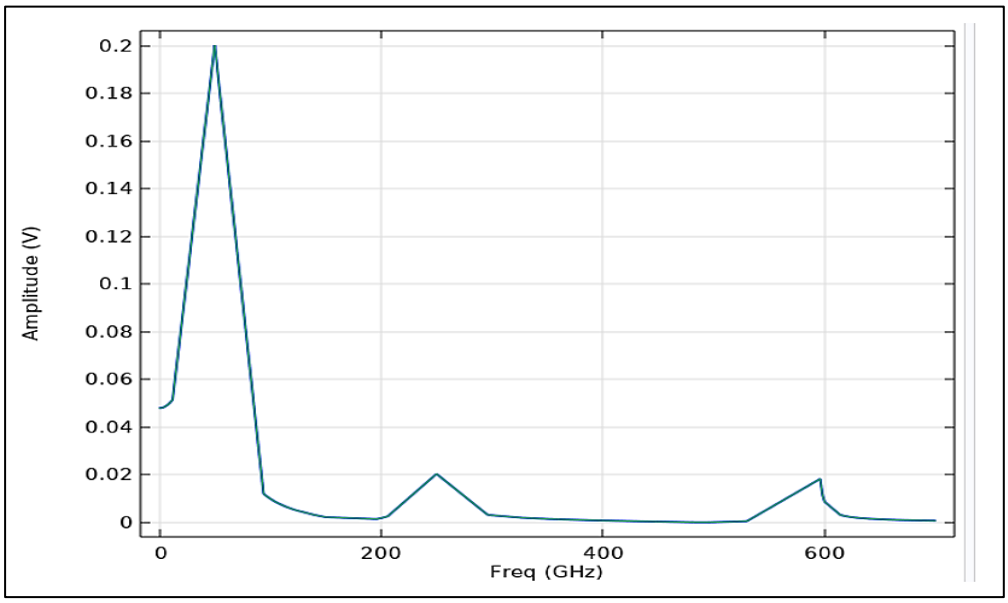

Figure 4.12. Frequency (GHz) vs Amplitude (V)

4.3. Mesh Convergence

The mesh convergence process may largely determine the precision of the solution achieved using numerical methods. The mesh parameters control the resolution of the discretized model's finite element mesh. The analysis area must be divided into smaller parts to use the finite element approach. The model in the finite element method is divided into tiny geometrical elements in simple shapes, tetrahedrons. The deformation of each tetrahedrons in three coordinates directions could be approximated using a group of polynomial functions. In our result, mesh convergence was used to find the accuracy of simulation results. For 3D meshing, a free set of tetrahedral meshing predefined as normal meshing was used. Figure 4.14 presents the mesh geometry of the CNTs pressure sensor. The mesh element parameters are set as follows: maximum element size is 5μm; minimum element size is 0.1μm; the maximum element growth rate is 1.4; and the resolution of the narrow region of 0.7 and factor of curvature is 0.4.

This mesh is then used to formulate the FEA structural mechanic model. The analysis of the solid structure in the FEM begins by dividing it into a finite number of elements, which are interconnected at the nodes, as shown in Figure 4.13.

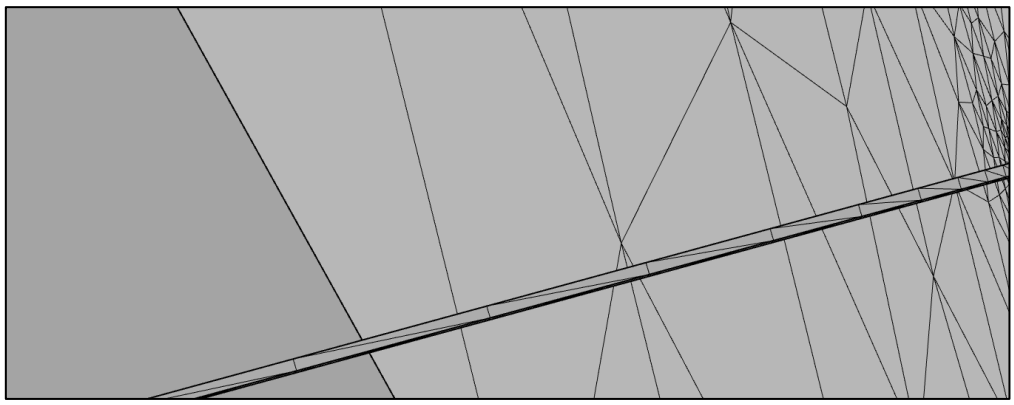

Figure 4.13. Mesh of SWCNTs between two metal contact

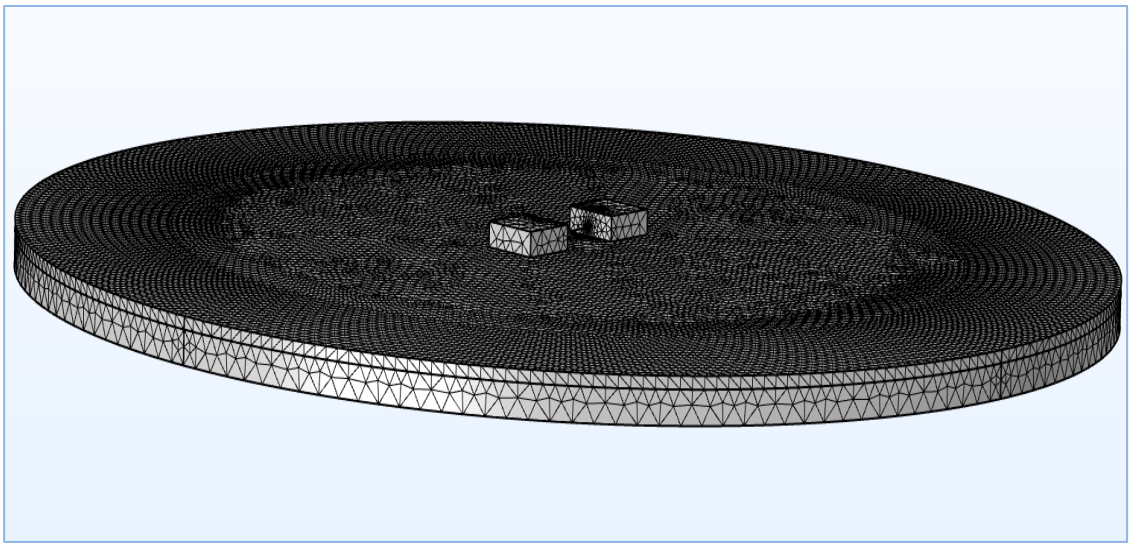

Figure 4.14. Mesh geometry of CNTs piezoresistive pressure sensor

Table 4.3. Comparison related work for CNT based field effect transistor.

Ref.	Year	Diameter	Threshold Voltage	Gate Voltage	Drain Current	Energy Band gap	Transconductance
[74]	2015	1nm	0.245V	0.6V	6.99µA	-	27µs
[75]	2015	1nm	-	1V	5.53 µA	-	13 µs
[76]	2017	-	-	0.7V	50 µA	-	63.21µs
[73]	2020	1nm	0.254V	0.8V	4.75×10^{-3} A	0.45eV	-
[77]	2021	3nm	0.34 V	0.8V	47.9 µA	-	-
This work	2023	1nm	0.436V	1.5V	4.075µA	0.49eV	1.25µs

Table 4.3. demonstrates that decreasing Vg resulted in massive increase in drain current and transconductance. While the band gab increased slightly with the high increment in the gate voltage. Although equation (4) was adopted to calculate threshold voltage in this research and studies [73] used another equation results were again for the same diameter (1nm).

4.4. Result Discussion of CNT-Based Piezoresistive Pressure Sensor

The resistance of the CNTs sensor varies depending on the applied pressure or strain. Additionally, whereas the diameter of CNTs is inversely proportional to the energy band gap, the resistance is directly related to the energy band gap. The proposed method of finding resistance and energy band gap was mathematically calculated using equations 2.19 and 2.20. Tables (4.4,4.5,4.6,4.7) explain the effect of changing strain on the energy band gap. At the same time, the energy bandgap is affected by the strain and the diameter of CNTs. At the same time, the resistance of CNT depends on the energy bandgap. When took specific values for the strain from 0 to 0.045, the energy bandgap was increased, and thus, the resistance increased.

Table 4.4. The SWCNTs results with different parameter at diameter =1nm

Strain	Energy band gap (eV)	Resistance (KΩ)
0	0.426	2143
0.005	0.4728	2377
0.01	0.5196	2611
0.015	0.5664	2845
0.02	0.6132	3079
0.025	0.660	3313
0.03	0.706	3547
0.035	0.753	3781
0.04	0.800	4015
0.045	0.847	4249

Table 4.5. The SWCNTs results with different parameter at diameter =2nm

Strain	Energy band gap (eV)	Resistance (KΩ)
0	0.213	1078
0.005	0.259	1312
0.01	0.306	1546
0.015	0.353	1780
0.02	0.400	2014
0.025	0.447	2248
0.03	0.493	2482
0.035	0.540	2716
0.04	0.587	2950
0.045	0.634	3184

Table 4.6. The SWCNTs results with different parameter at diameter =3nm

Strain	Energy band gap (eV)	Resistance (kΩ)
0	0.142	723
0.005	0.188	957
0.01	0.235	1191
0.015	0.282	1425
0.02	0.329	1659
0.025	0.376	1893
0.03	0.422	2127
0.035	0.469	2361
0.04	0.516	2595
0.045	0.563	2829

Table 4.7. The SWCNTs results with different parameter at diameter =4nm

Strain	Energy band gap (eV)	Resistance (kΩ)
0	0.106	543
0.005	0.152	777
0.01	0.199	1011
0.015	0.246	1245
0.02	0.293	1479
0.025	0.340	1713
0.03	0.386	1947
0.035	0.433	2181
0.04	0.480	2415
0.045	0.527	2649

The Tables (4.4,4.5,4.6,4.7) illustrate that the increasing diameter from 1nm to 4nm led to decrease in energy bandgap from 0.426eV to 0.106 eV and a reduction in the resistance from 2143kΩ to 543kΩ at zero strain. Rolling a single wall nanotube graphene sheet allowed to change the diameter in this study. The current system observed that the resistance and energy band gap changes from 543kΩ to 2143 kΩ and 0.106eV to 0.426eV, respectively. The resistance of CNTs is directly proportional to the energy bandgap, as shown in eq (2.19). As result, the resistance increased linearly with an energy band gap. The energy band gap is affected by the diameter. When increasing the diameter, the energy band gap decreases; Figure 4.15 presents that.

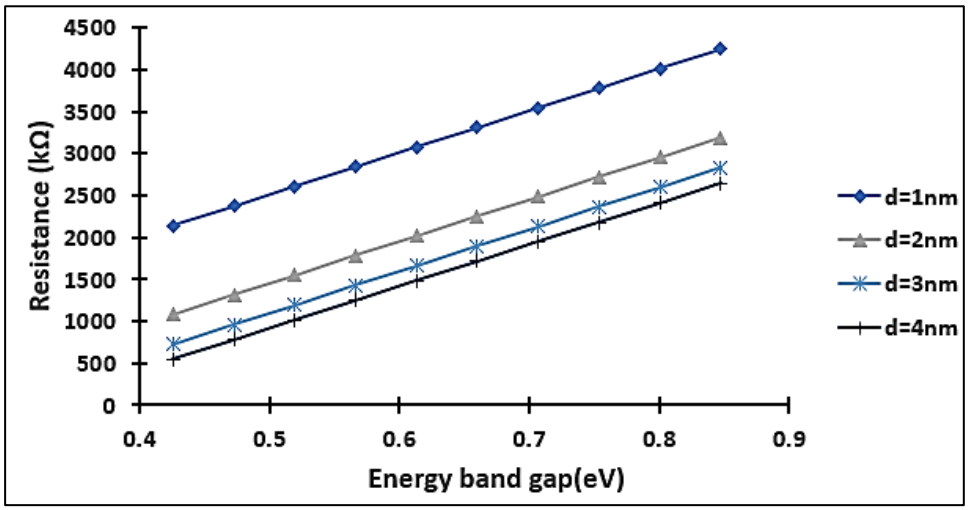

Figure 4.15. Resistance vs Energy Band gap

The resistance of CNTs was plotted versus strain for various diameter values, as illustrated in the Figure 4.16. The range of diameter is from 1nm to 4nm. The resistance decreases as the diameter increases because when the diameter of the CNT increases the cross-sectional area (A) will be increased which, according to the equ (2.10) decreases the resistance. When the diameter increases, the energy band gap decreases, and thus the resistance decreases.

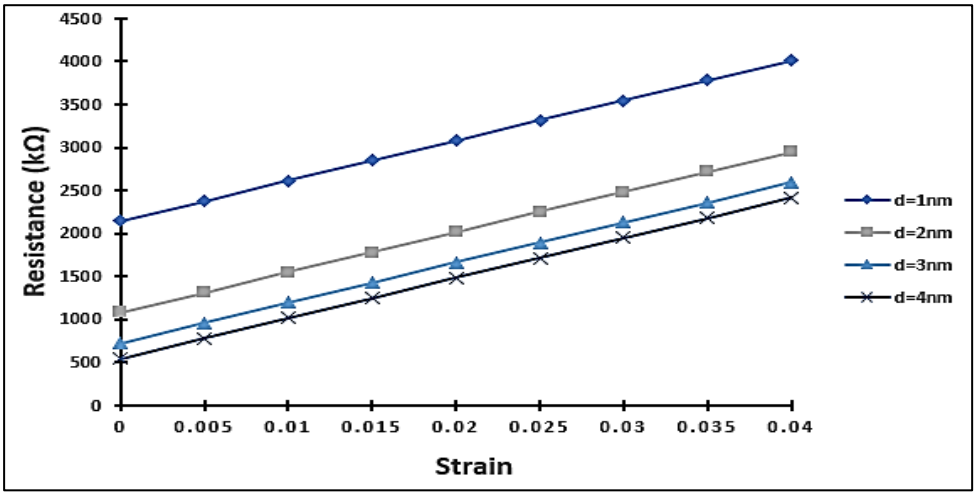

Figure 4.16. Strain vs Resistance

The relationship between strain vs energy band gap is shown in Figure 4.17 with different diameter values. These findings show that strain may be utilized to adjust a CNT's bandgap continually. The capability to control bandgap is crucial in enhancing our comprehension of transportation in CNTs.

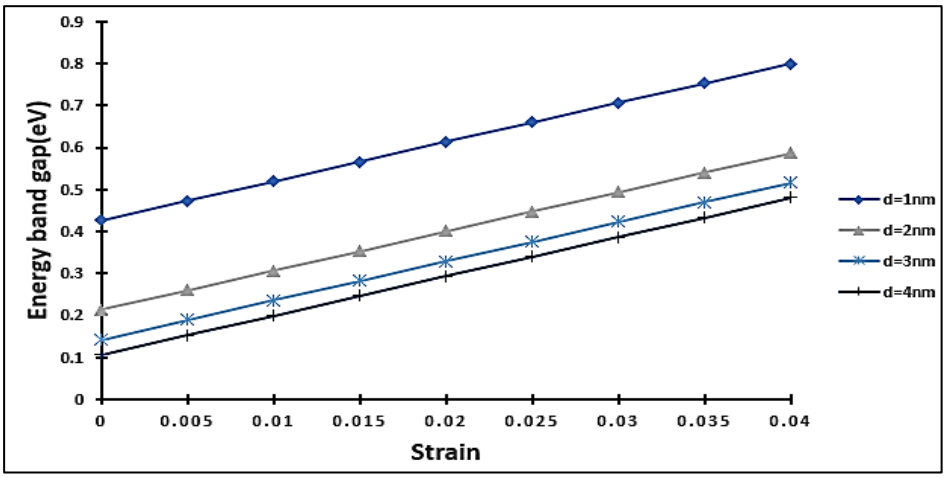

Figure 4.17. Strain vs Energy Band gap

4.4.1. The Effect of Pressure on Von-Mises Stress

This section shows the effect of changing pressure on von Mises's stress. Several single-walled and multi-walled CNT one, two, four walls were analyzed, and the relationship was plotted as shown in Figure 4.18. The applied pressure range was 0 to 300 kPa. The results show that von-mises stress is in a linear relationship with pressure. It was also observed that increasing the number of CNTs increases von-mises stress. Increase in the number of CNTs may lead to a more efficient load transfer in some cases, resulting in higher overall strength. Increasing the number of CNT can enhance its sensitivity and accuracy. High stress is usually not recommendable as it increases the chance of failure of the material. The diaphragm edge experiences more von-mises stress than the other geometry parts. These results show that the von Mises stress of 4SWCNTs is greater than 1SWCNTs. Figure 4.18 illustrates the linear relationship between the von Mises stresses and pressure.

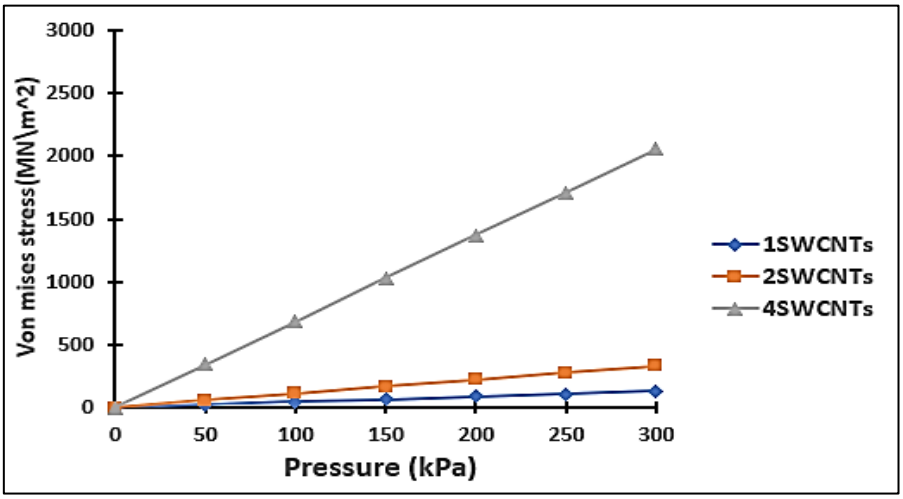

Figure 4.18. Effect different pressure on the von mises stress at single-walled CNT

It can be noticed from Figure 4.19 that the value of von Mises stress ranges between 6.51×10^{7} N/m^2 and 9.52×10^{-4} N/m^2. The maximum von-mises stress was at (anchors), which is signified as red color, as shown in Figure 4.20. That

means the endpoints have maximum chances of failure of the structure of nanotubes.

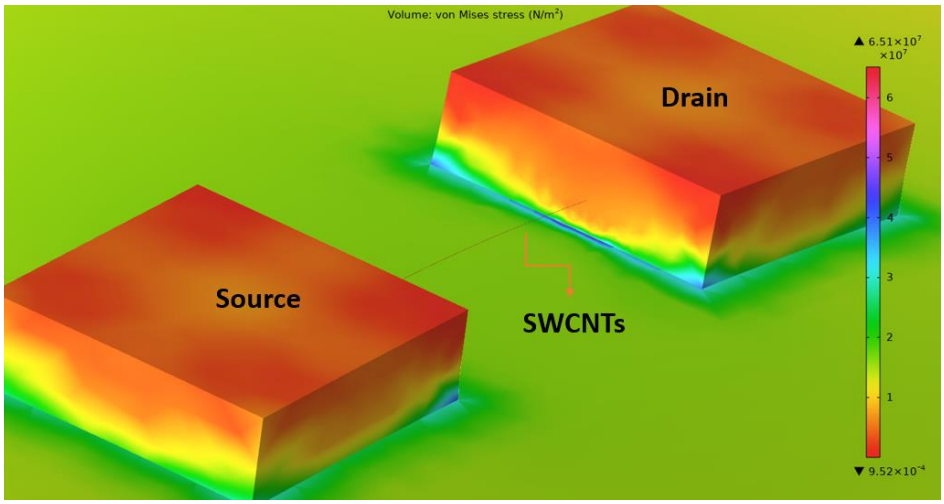

Figure 4.19. Effect the von mises stress on SWCNTs.

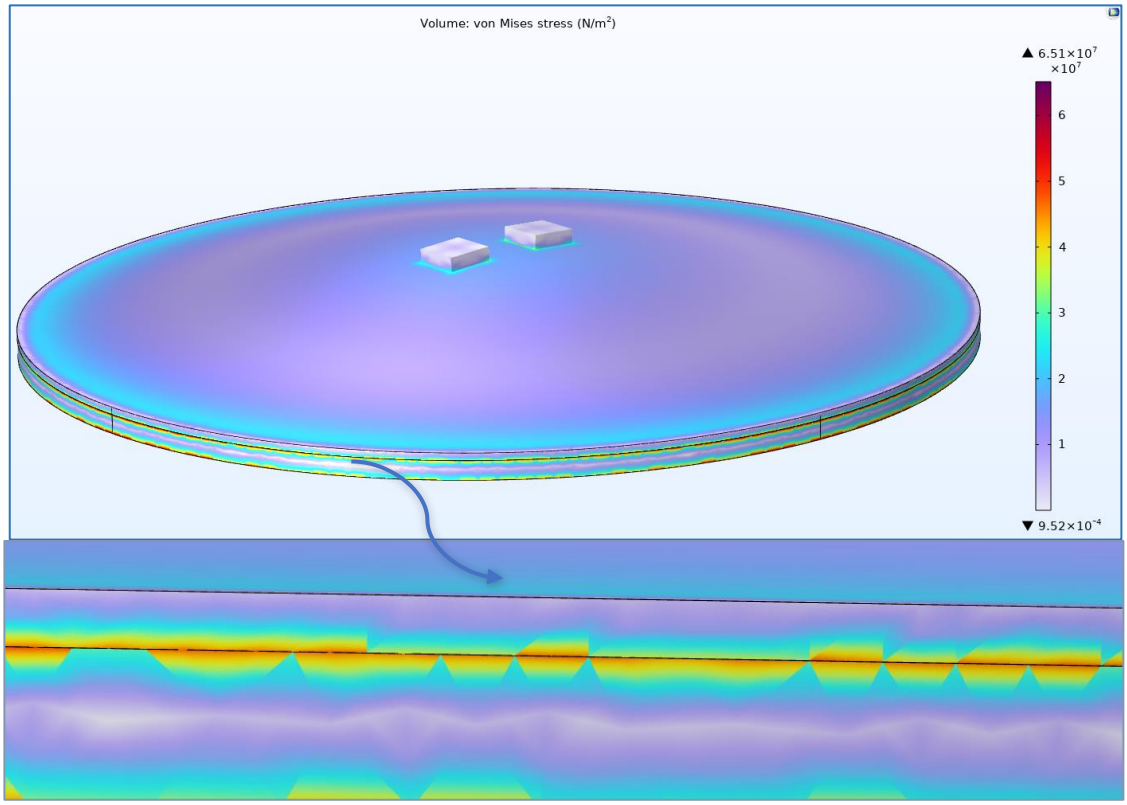

Figure 4.20. Simulation results of von mises stress of SWCNTs

For 2SWCNTs the maximum von Mises stress is 1.66×10^{8}N/m^2 while the minimum is 9.49×10^{-4} N/m^2. The von Mises stress increased when increasing the number of CNT, as illustrate in Figure 4.21.

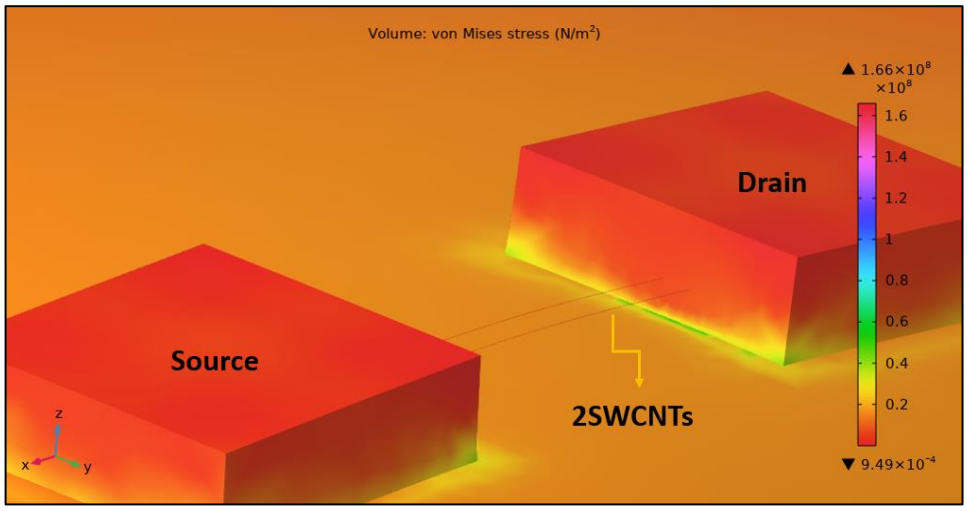

Figure 4.21. Effect the von mises stress on 2SWCNTs.

Figure 4.22 shows that the maximum von Mises stress for 4SWCNTs was $1.03\times10^{9}N/m^{2}$, while the minimum von Mises stress was $2.25\times10^{5}N/m^{2}$.

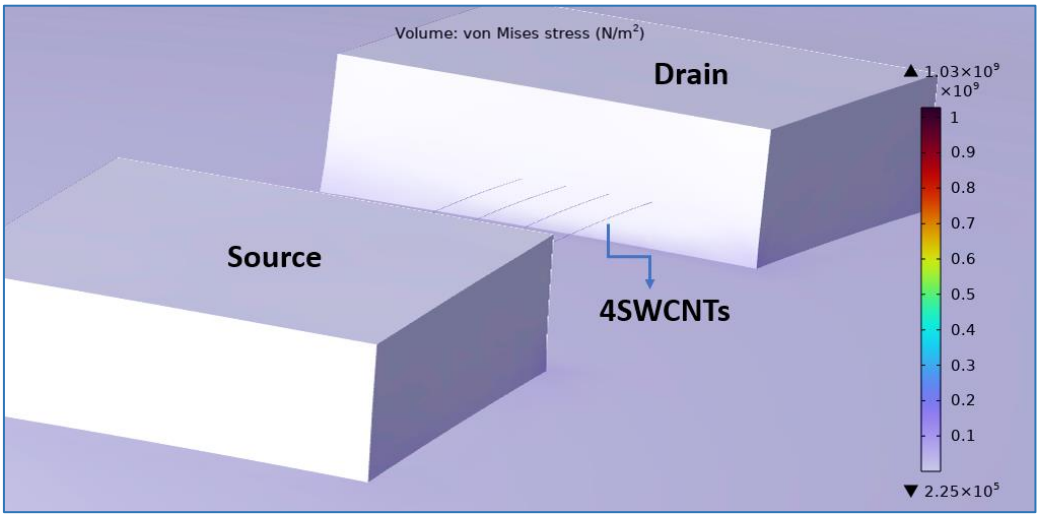

Figure 4.22. Effect the von mises stress on 4SWCNTs.

The von Mises stress for MWCNTs is presented in Figure 4.23. It was noticed that the von Mises stress is a linear relationship with pressure. The graph illustrates when increasing the number of MWCNTs, the von Mises stress will be increased.

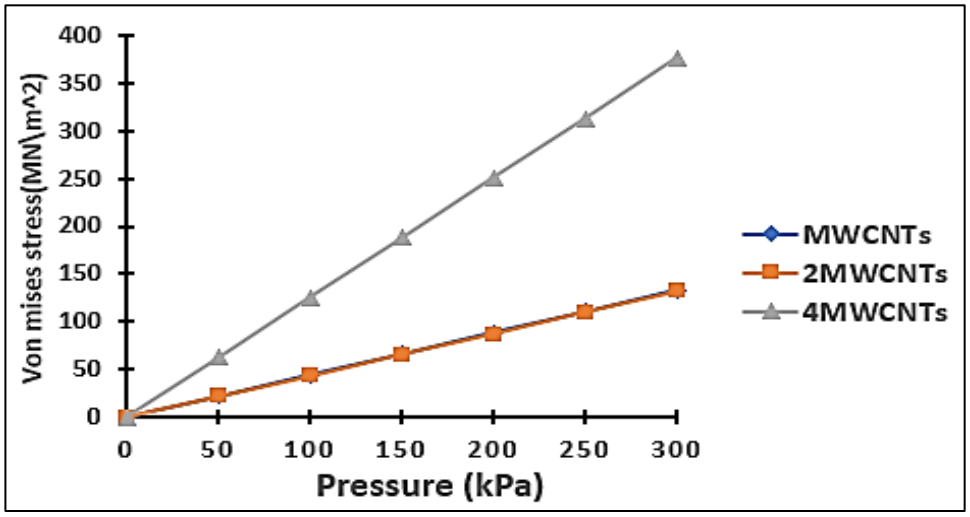

Figure 4.23. Pressure vs von mises stress at multi-walled CNT

Figure 4.24 shows that the maximum von Mises stress was at (anchors), which is highlighted as pink color. That means the endpoints have maximum chances of failure of the structure of nanotubes.

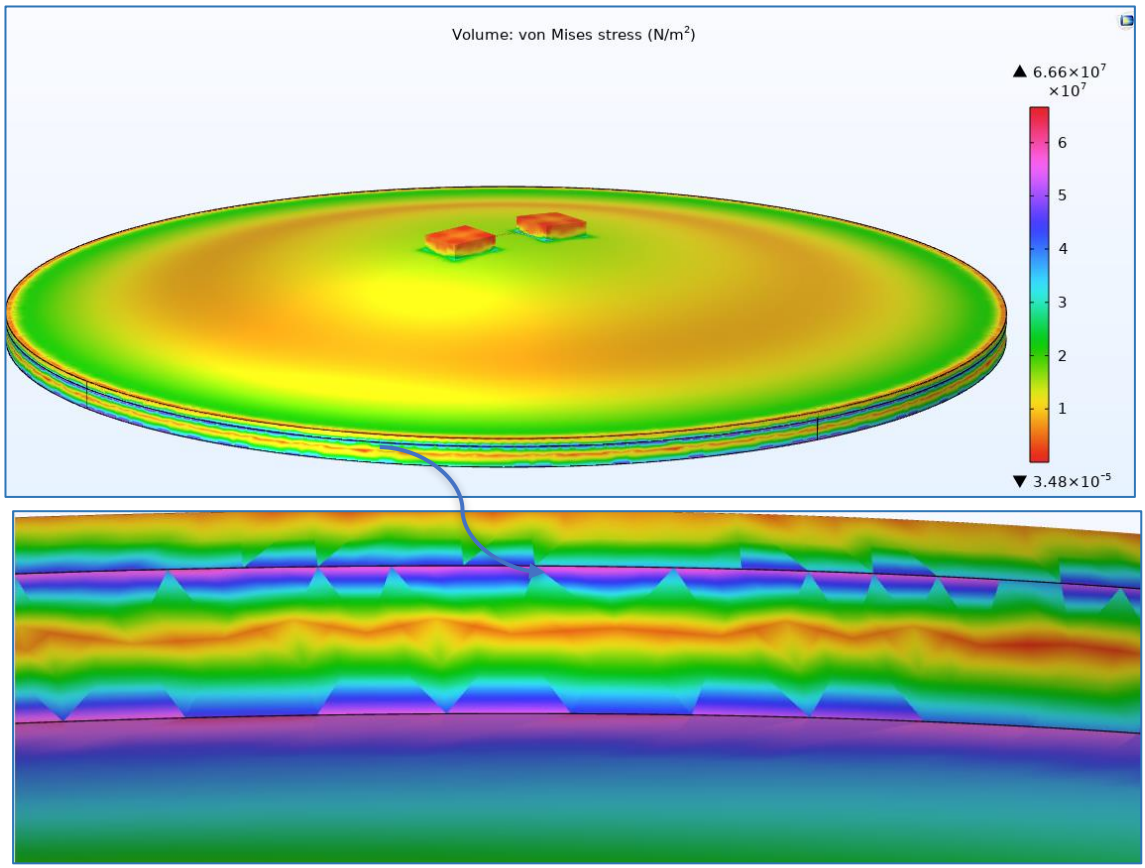

Figure 4.24. Simulation results of von mises stress of MWCNTs

For MWCNTs, the maximum von Mises stress is 6.66×10^{7} N/m^2, while the minimum is 3.48×10^{-5}N/m^2.When applying pressure to the MWCNTs, the deformation of the carbon nanotubes that have become bending was noticed. Figure 4.25 shows that.

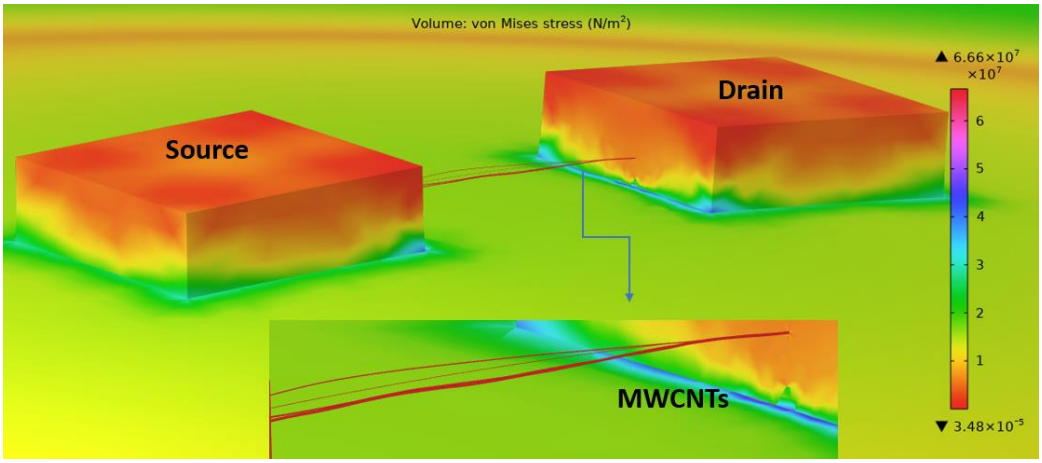

Figure 4.25. Effect the von mises stress on the MWCNTs.

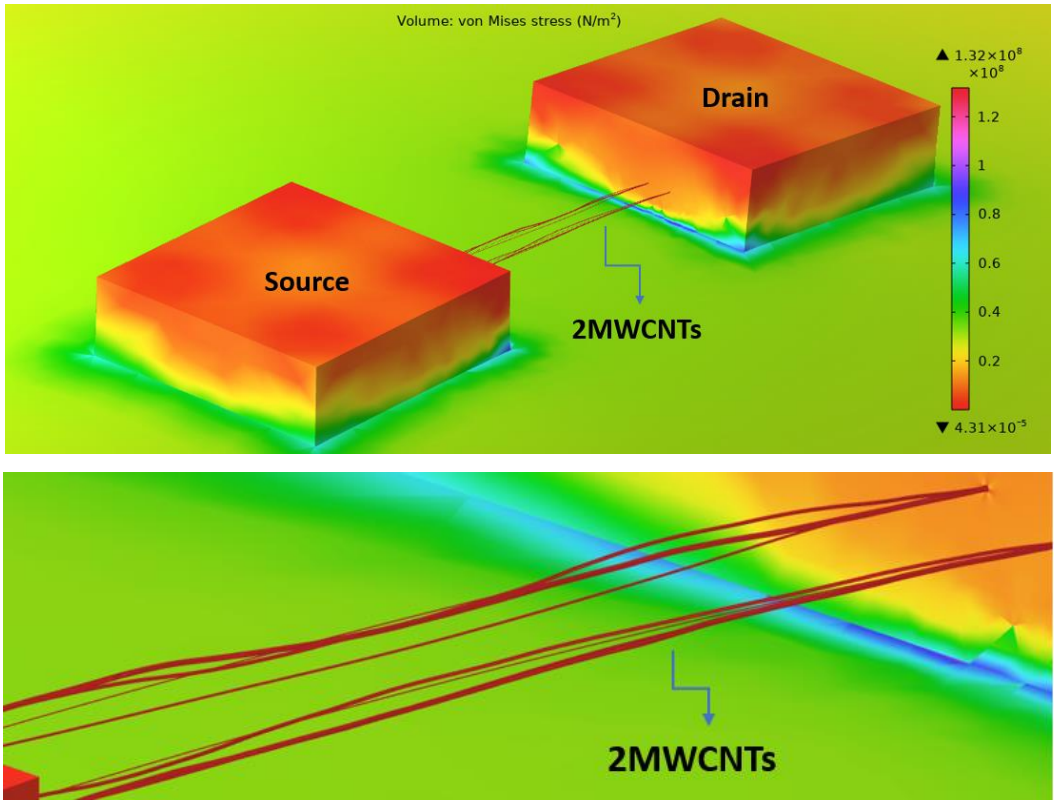

Figure 4.26. Effect the von mises stress on the two MWCNTs.

Figure 4.26 shows that the maximum von Mises stress for two MWCNTs is $1.32\times10^{8}N/m^{2}$, while the minimum is 4.31×10^{-5}. It was noticed distortion of 2MWCNTs was due to applied pressure at the bottom substrate of the CNTs, as indicated in the red colour. The minimum value of von Mises stress was observed in the metal contact region, which is highlighted in yellow. The fixed edge was denoted by the red and pink colour, which represents the greatest von Mises stress value.

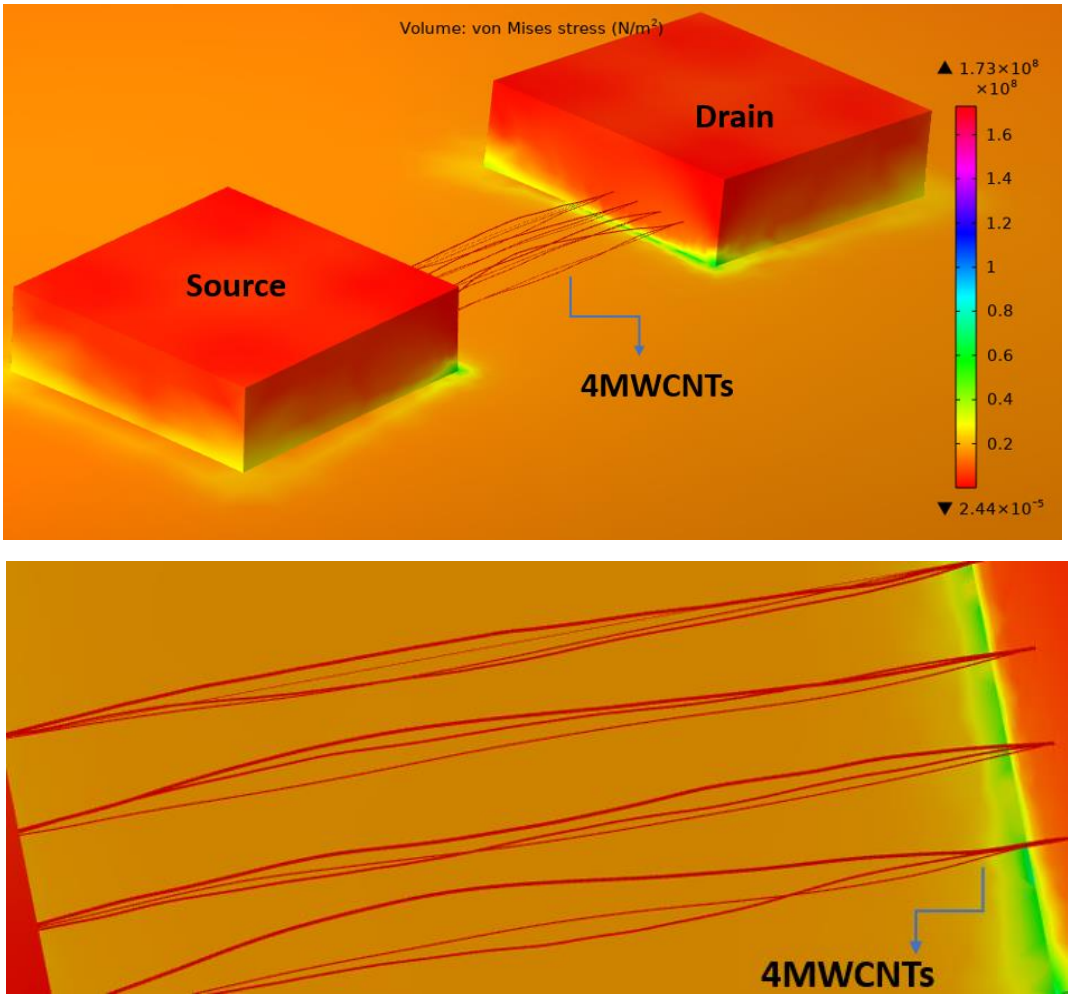

Figure 4.27. Effect the von mises stress on the four MWCNTs.

The von Mises stress of array MWCNTs is explained in this paragraph. The highest von Mises stress recorded is $1.73\times10^{8}N/m^{2}$, while the lowest is $2.44\times10^{-5}N/m^{2}$. The damage of CNTs is very clear in the four MWCNTs. It can be seen in

the middle region of CNTs, which is presented in Figure 4.27. The von Mises stress is highest at the circular substrate's fixed end.

4.4.2. The Effect of Pressure on Displacement of CNTs

The displacement is directly proportional to the applied pressure, as presented in Figure 4.28 and Figure 29, for several single-walled CNTs and multi-walled CNTs, respectively. The applied pressure increased from 0 to 350kPa, which increased the displacement from 0 to 0.5µm. These results showed that increasing the number of CNTs does not affect its displacement. The deviation of the displacement was minimal in both SWCNTs and MWCNTs. The specific behavior of CNTs under pressure can depend on various factors, including the type of CNT (single-walled or multi-walled), diameter, chirality, and the applied pressure conditions.

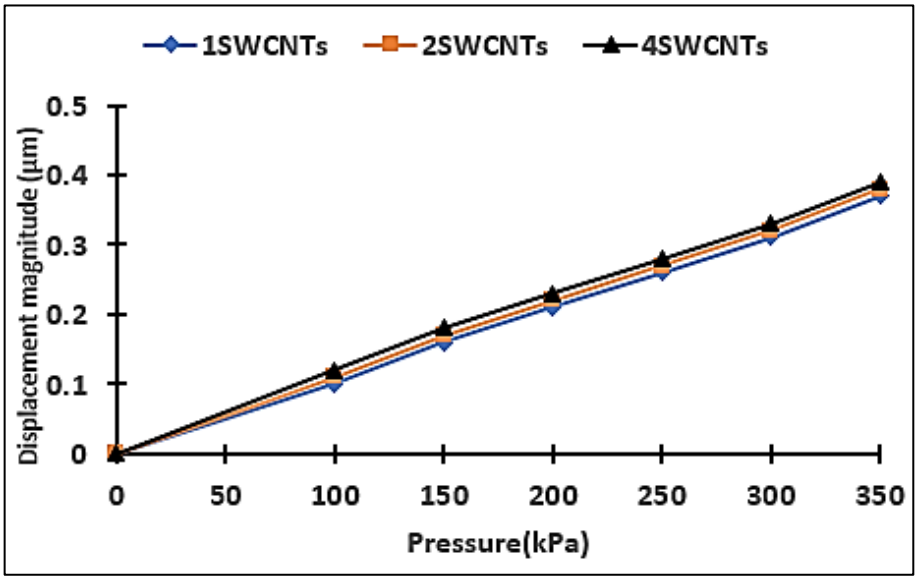

Figure 4.28. Pressure vs Displacement of SWCNTs

The maximum displacement in the MWCNTs was equal to 0.5µm at pressure 350kPa. It was observed the displacement increased linearly with pressure, as illustrated in Figure 4.29.

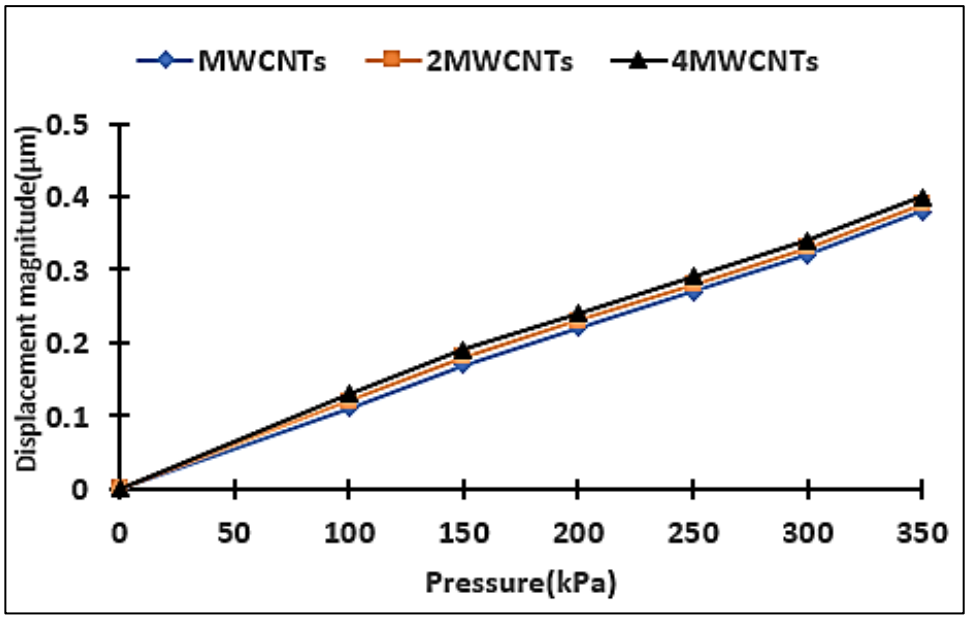

Figure 4.29. Pressure vs displacement of MWCNTs.

The maximum displacement occurs at the center of the substrate (diaphragm); the blue colour indicates zero displacements, while red was the maximum displacement, as depicted in Figure 4.30. The substrate membrane is deflected when pressure is applied underneath the sensor; this changes the carbon nanotube's resistance. For example, an applied pressure of 150kPa generates a displacement of 0.16 µm at the center of the diaphragm.

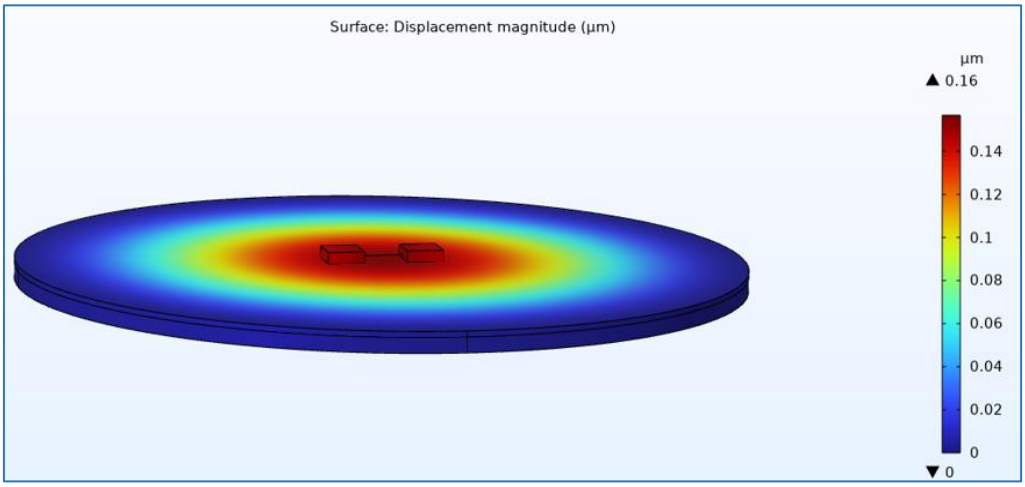

Figure 4.30. Displacement magnitude in COMSOL Multiphysics.

The mechanical sensitivity of SWCNTs is known as S=dX/dP, where X is the displacement, and P is the applied pressure. The mechanical sensitivity is 1.4×10^{-4}µm/Pa. Figure 4.31, illustrated the displacement field of CNTs. The direction of displacement is the upper surface. A process of assigning vectors to each point inside an area defined as displacement field arrow surface.

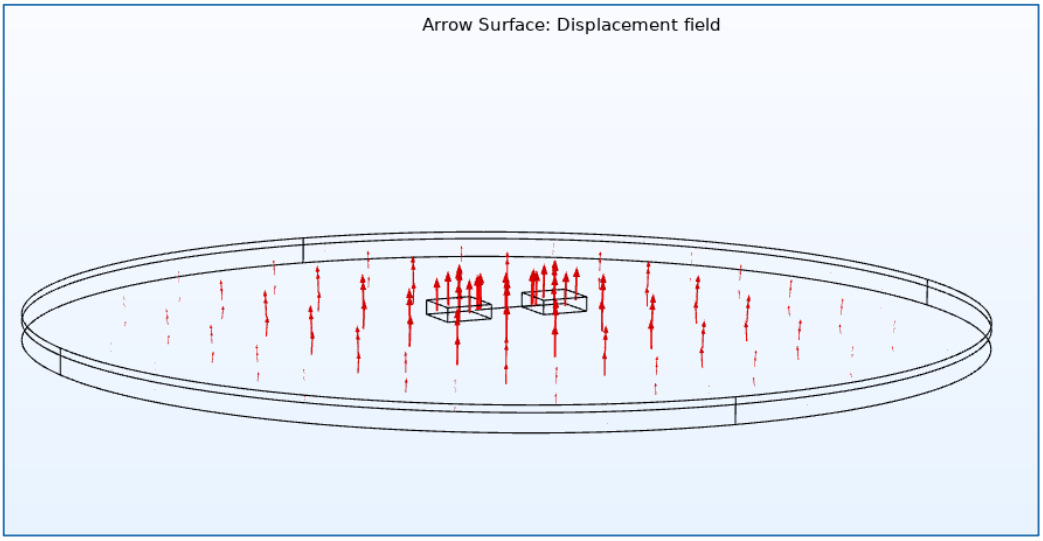

Figure 4.31. Displacement field of CNTs in COMSOL Multiphysics

4.4.3. The Effect of Pressure on Current

This section presents the effect of pressure changes on the current of carbon nanotubes. The results show the current increases linearly with increased pressure. The spacing between the particles decreases, and the particles become closer to each other due to the increasing pressure. When the cross-section area is small, it results in high current density; thus, the high current will be passed through the CNTs (hollow cylindrical).

The pressure ranges from zero to 16MPa, for one, two, and an array of SWCNTs. When increased the numbered of SWCNTs, the current will be increased. For example, the maximum current in 4SWCNTs equals 7×10^{-4}µA while the maximum current in 1SWCNTs equals 2.9×10^{-4}µA, as

illustrated in Figure 4.32. The sensitivity of SWCNTs equals 7.5×10^{-11}µA/Pa.

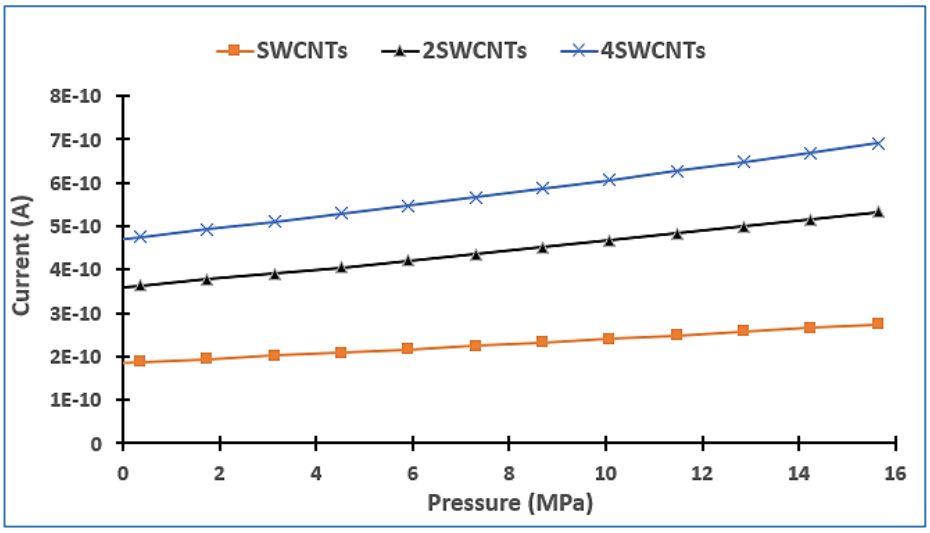

Figure 4.32. Graph of current against pressure of SWCNTs

The plot of the current with various arrays of MWCNTs for a pressure range of 0 to 16MPa is present in the Figure 4.33. The graph that has been plotted shows the current will increase with an increase in the number of multi-walled CNTs. The sensitivity of MWCNTs equal 1.5×10^{-12}µA\Pa.

The current of SWCNTs was equal to 2.8×10^{-10} at pressure 16MPa, while the current of MWCNTs was equal to 4.2×10^{-10} at the same pressure. At the same time, the current of 4SWCNTs equal 7×10^{-10}A, while 1.6×10^{-9}A of the 4MWCNTs. It was noticed the current of MWCNTs is greater than the SWCNTs. Additionally, the sensitivity of MWCNTs is larger than that of SWCNTs due to the diameter of MWCNTs being higher of SWCNTs which results in a large cross-section area, thus increasing the current of MWCNTs.

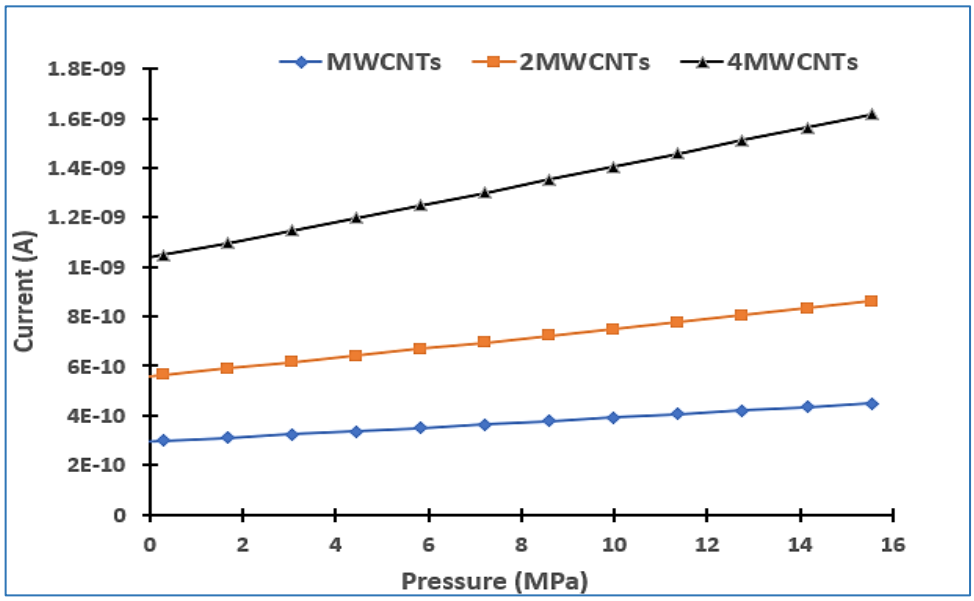

Figure 4.33. Graph of current against pressure of MWCNTs

4.4.4. Arc Length vs von Mises stress

The highest tensile stress occurs at the edge of the substrate, while the highest compressive stress occurs at the center of the substrate, at the centerline of substrate. This occurred due to the silicon substrate constricting in the middle and expanding outwards at the edges when pressure was applied evenly from the bottom. This graph displays the von Mises stress impact throughout the carbon nanotubes' length. Results show that the stress initially increases, becomes stable, and rises again at the second end. The total length of CNT is 14.99µm; the von Mises stress only fluctuates at the endpoints and remains constant in the middle section of the carbon nanotube, as shown in Figure 4.34. For example, the von Mises stress equals 1.11kN/m^2 at the Arc length 3µm.This Means von Mises's stress is in control and will not be led to the failure of stress in this selected range of applied pressure.

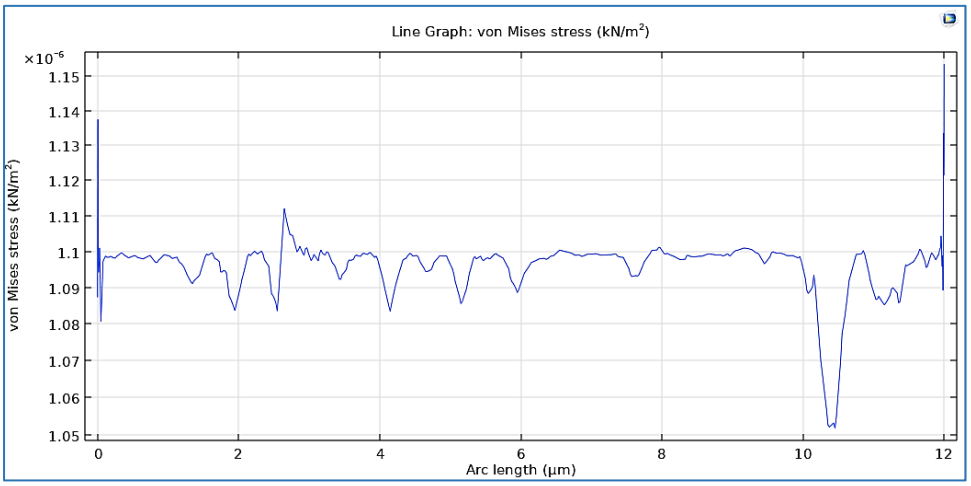

Figure 4.34. Graph of arc length vs von mises stress at pressure=150kPa

The von Mises stress against Arc length for SWCNTs with various pressures from 100kPa to 250kPa, as depicted in Figure 4.35. For instance, initially, the von Mises stress equal to 7.25×10^{-7}kN/m^2, 1.09×10^{-6}kN/m^2,1.45×10^{-6}kN/m^2, and 1.81×10^{-6}kN/m^2, for applied pressures are 100kPa,150kPa, 200kPa, and 250kPa, respectively. When the arc length arrived at the 12µm, the von Mises stresses rose to 7.69×10^{-7}kN/m^2 at the 100kPa pressure, 1.15×10^{-6}kN/m^2 at the pressure 150kPa, 1.54×10^{-6}kN/m^2 at the pressure 200kPa, and 1.92×10^{-6}kN/m^2 at the pressure 250kPa. As a result, the von Mises stresses increased by increasing the pressure and arc length.

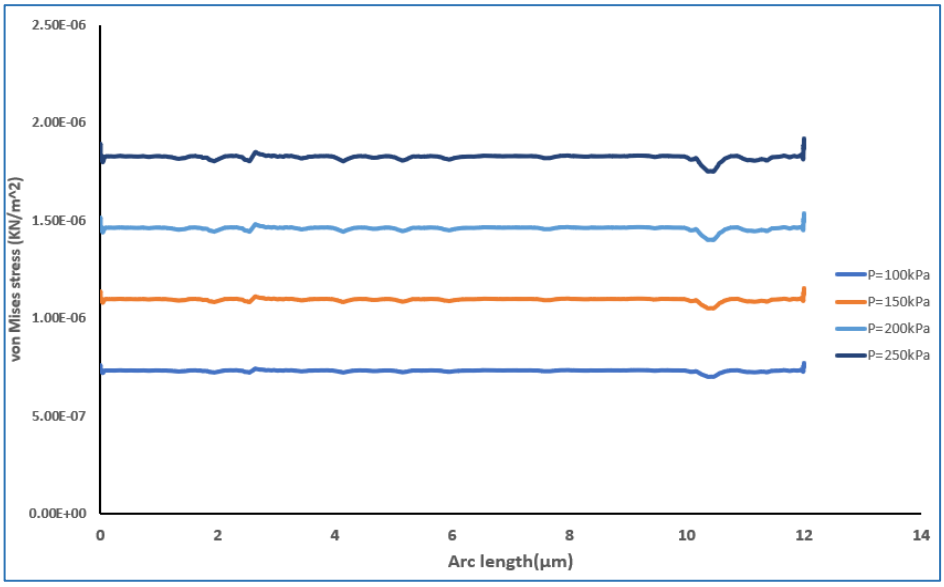

Figure 4.35. Arc length vs von mises stress of SWCNTs at different pressure.

The von Mises stress curve for MWCNTs with a maximum of $200\times10^{-7}kN/m^2$ at the initial point of the Arc length, After that, the von Mises stress remains unstable in a state of increase and decrease, as the highest value of von Mises stress is $20\times10^{-7}kN/m^2$ at the arc length from 0.5µm to 10.5µm; when the arc length reaches a 12µm, the value of von Mises is equal to $500\times10^{-7}kN/m^2$, as presented in the Figure 4.36. This line graph of von Mises stress at the pressure of 150kPa.

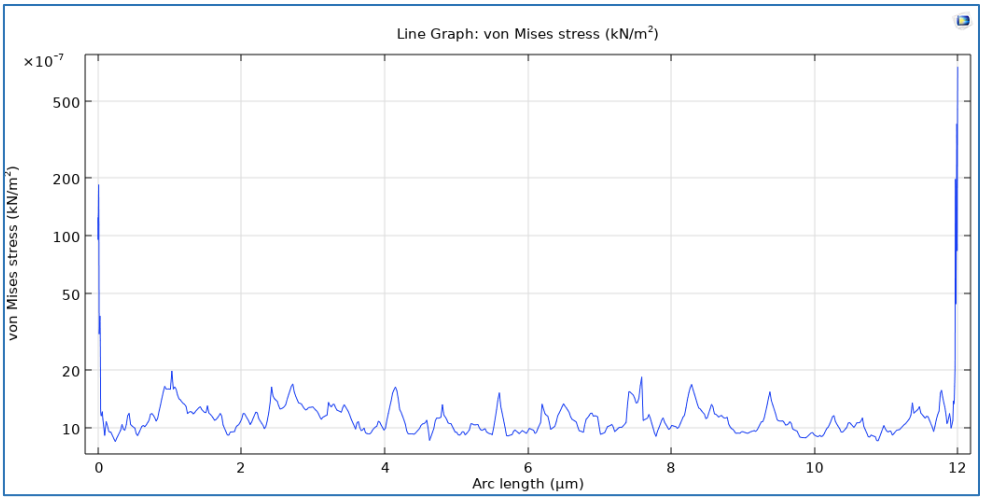

Figure 4.36. Arc length vs von Mises stress of MWCNTs at pressure 150kPa

The line graph of von Mises stresses for MWCNTs of different applied pressure range from 100kPa to 250kPa, as depreciated in Figure 4.37. In our model, the length of CNTs equal 14.99µm. Thus, the von Mises stress in carbon nanotubes varies based on the length of the arc and the amount of pressure applied to them. For example, firstly, when the arc length equals 0um, the von Mises stress equal 8.3×10^{-9} for 100kPa pressure, 1.25×10^{-8} for pressure150kPa,1.66×10^{-8} for pressure 200kPa and 2.08×10^{-8} for Pressure 250kPa. When arc length arrived at the 2µm, the von Mises stress increased to 5.04×10^{-8}kN/m^2 at pressure 100kPa, while at pressure 150kPa, the von Mises stress of 7.57×10^{-8}kN/m^2, the von Mises stress of 1.01×10^{-7}kN/m^2 and the von Mises stress equal 1.26×10^{-7}kN/m^2. The increase in pressure and arc length resulted in a noticeable rise in von Mises stress.

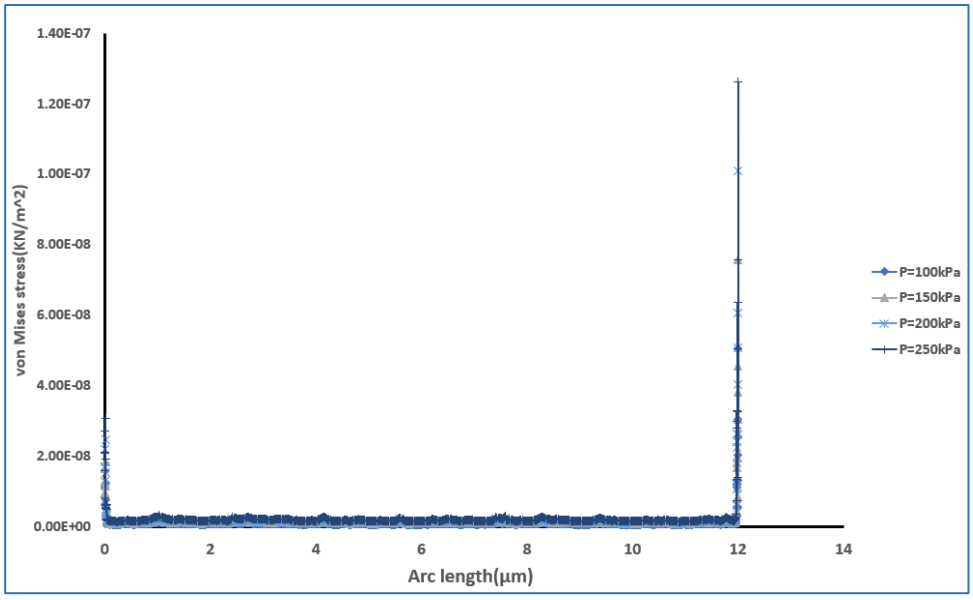

Figure 4.37. Arc length vs von Mises stress of MWCNTs at different pressure.

The comparison of the simulation results of von Mises stresses between SWCNTs and MWCNTs at the same pressure of 150kPa with an arc length of 0µm and 12µm. The von Mises stress equals 1.15×10^{-6} kN/m^2 at arc length 12 µm for SWCNTs, while the von Mises stress equals 7.57×10^{-8} at arc length 12µm

for MWCNTs. The von Mises stresses of SWCNTs were observed to be greater than those of MWCNTs.

4.5. Time Response

The response time is the amount of time electrons need to move spatially within the sensor. There are two components to the time response transient state and steady state. As a result, a transient response is what the control system's response is known as during the transient condition. The rise time is needed to accomplish between 10% and 90% of the overall displacement change. Once an input is applied to the control system, the output requires a specific amount of time to attain a steady state. Transient behavior ends when the displacement achieves its ultimate steady-state value within the specified resolution. This model was designed with dimensions 14.99mm and 2nm of the length of SWCNTs and diameter of SWCNTs.

The time response curve of four pressure sensors from 100kPa to 250kPa is illustrated in Figure 4.38. In the applied pressure 250kPa, the maximum displacement equal 1.6×10^{2}μm at the time 0.2ms; when the time arrived at 0.8ms (steady state), the displacement equals 1.4×10^{2}μm. It was observed the displacement reduced when the time increased. While the maximum displacement equal 6×10^{-1}μm at time 0.2ms and 5.8×10^{-1}μm at time 0.8ms when the applied pressure is 100kPa. A time range from 0 to 1ms with step 0.2ms using time dependent in COMSOL Multiphysics. The maximum overshoot was 0.31μm at pressure range 100 to 250kPa. The rise time equal 0.18ms at pressure 100kPa, and at pressure 150kP, the rise time equal 0.2ms, while the rising time equals 0.21ms, 0.23ms at pressure 200kPa, and 250kPa, respectively.

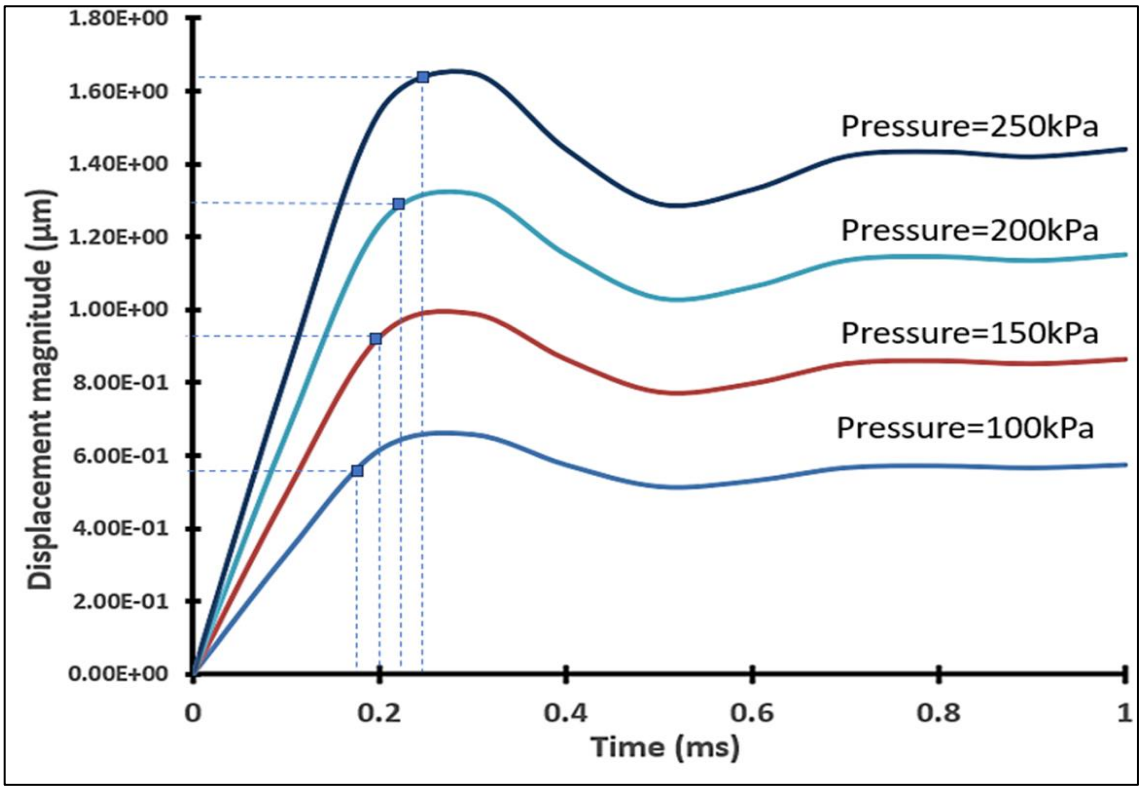

Figure 4.38. The time-displacement curve for pressure ranges from 100kPa to 250kPa

4.6. Frequency Response

The displacement frequency response of the array's piezoresistive sensors is evaluated using COMSOL in the intended resonance mode to ascertain the functional frequency range of the suggested sensor. Fig 4.39 illustrates the displacement frequency response of the CNTs sensor. In the current model, the dimension of SWCNTs used is 14.99µm, 2nm, length, and diameter, respectively. The total applied force is from 50N to 250N. The frequency range is set at 0 Hz to 200 Hz. The frequency step size is 20Hz. In these results, the maximum displacement equal to 600µm at force applied is 250N at resonance frequency equals 60Hz while the displacement equal to 350µm when the applied load equal 150N, the displacement reduced to 50N at the same resonance frequency 60Hz.

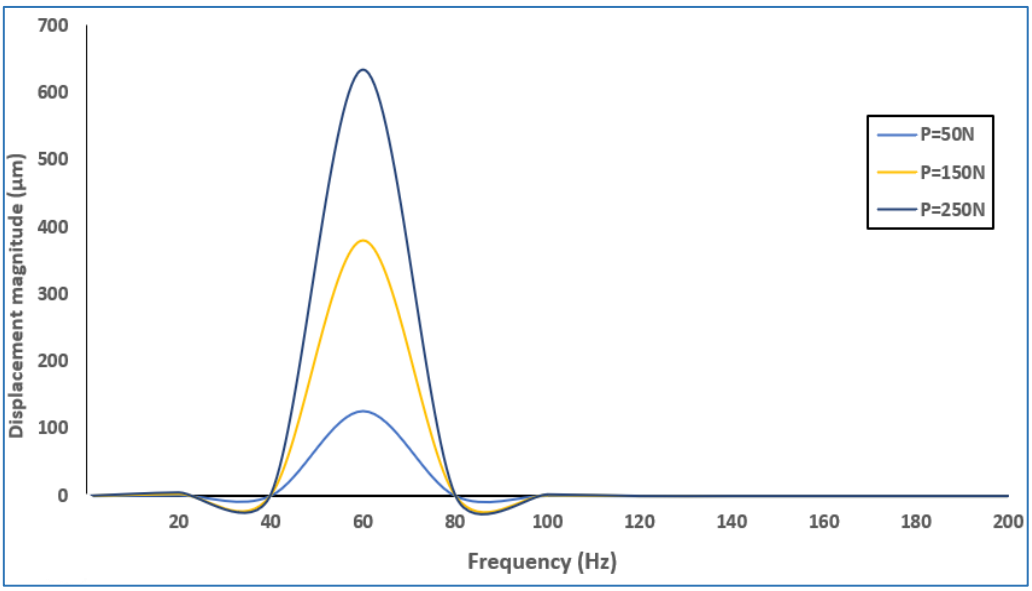

Figure 4.39. Frequency response of CNTs pressure sensor

Table 4.8. Comparison related work for CNT based piezoresistive pressure sensor.

Ref.	Year	Device size (µm×µm)	Pressure range	Displacement	Sensitivity
[74]	2011	1× 250	1kPa to 500kPa	9.89µm	1500 Ω/Pa
[71]	2013	0.01×0.1	0Pa to 1000Pa	6 µm	0.145mV/V/kPa
[78]	2015	1×10	0kPa to 100kPa	4.7µm	1.1 x10^{-1} V/Pa/V
[79]	2018	1×10	0kN/m^2 to 0.2kN/m^2	-	4.37 m^2/kN
[35]	2018	400×400	0MPa to 1MPa	2.55µm	308.7mV/MPa
[80]	2019	50 × 10	0kPa to 1000kPa	6 µm	0.145mV/V/kPa
This work	2023	4×100	0kPa to 350kPa	0.16 µm	7.5×10^{-11}µA/Pa

Chapter Five
Conclusion
and
Future work

Chapter Five

Conclusion

5.1. Conclusion

The proposed method in this work is the modelling of CNT to control the characteristics and specifications of single-walled carbon nanotube field effect transistors. The specification of carbon nanotubes was investigated in terms of changing their diameter, length, and thickness of silicon dioxide. To improve simulation result it was increasing the diameter, the drain current was increased. A larger-diameter CNT may exhibit higher carrier mobility, leading to better charge transport and higher drain current. In addition, it was found that the drain current increased as the length of CNT decreased. Increasing the length of the CNT channel in a CNTFET leads to higher channel resistance and decrease in the drain current. The drain current decreases with increasing gate oxide thickness. Furthermore, the increase in gate oxide thickness generally results in a higher threshold voltage, reduced capacitance, lower electric field, and decreased carrier mobility.

Additionally, this research discussed the design and simulation of single and multi-walled CNTs piezoresistive pressure sensors. The sensitivity, time response, and frequency response were determined. It was observing the sensitivity of MWCNTs (1.5×10^{-12}μA/Pa) is greater than SWCNTs (7.5×10^{-11}μA/Pa). The SWCNTs typically have a higher surface area per unit mass compared to MWCNTs. This increased surface area provides more active sites for interactions with target molecules in sensing applications. As a result, SWCNT-based sensors may exhibit higher sensitivity. Furthermore, the rise time is 0.188ms as the pressure ranges from 100kPa to 250kPa, and the resonance frequency is 60Hz.

5.2. Future Work

The suggested work for the future includes:

- Design and simulation CNTs of the digital circuit such as logic gates circuit.
- Designing CNT-based pressure sensors with low power consumption, making them suitable for battery-operated devices and energy-efficient applications.
- Future work may involve addressing challenges related to large-scale manufacturing, cost reduction, and integration into mainstream semiconductor fabrication processes.

Reference

Reference

[1] N. Gupta, S. M. Gupta, and S. Sharma, "Carbon nanotubes: Synthesis, properties and engineering applications," *Carbon Letters,* vol. 29, pp. 419-447, 2019.

[2] P. Murugeswari, A. Kabilan, M. Vaishnavi, and C. Divya, "Performance analysis of single-walled carbon nanotube and multi-walled carbon nanotube in 32nm technology for on-chip interconnect applications," in *Fifth International Conference on Computing, Communications and Networking Technologies (ICCCNT)*, 2014: IEEE, pp. 1-6.

[3] H. He, L. A. Pham-Huy, P. Dramou, D. Xiao, P. Zuo, and C. Pham-Huy, "Carbon nanotubes: applications in pharmacy and medicine," *BioMed research international,* vol. 2013, 2013.

[4] R. Maheswaran and B. P. Shanmugavel, "A critical review of the role of carbon nanotubes in the progress of next-generation electronic applications," *Journal of Electronic Materials,* vol. 51, no. 6, pp. 2786-2800, 2022.

[5] J. Pitroda, B. Jethwa, and S. Dave, "A critical review on carbon nanotubes," *Int. J. Constr. Res. Civ. Eng,* vol. 2, no. 5, pp. 36-42, 2016.

[6] V. N. Popov, "Carbon nanotubes: properties and application," *Materials Science and Engineering: R: Reports,* vol. 43, no. 3, pp. 61-102, 2004.

[7] A. Eatemadi *et al.*, "Carbon nanotubes: properties, synthesis, purification, and medical applications," *Nanoscale research letters,* vol. 9, pp. 1-13, 2014.

[8] A. Aqel, K. M. Abou El-Nour, R. A. Ammar, and A. Al-Warthan, "Carbon nanotubes, science and technology part (I) structure, synthesis and characterisation," *Arabian Journal of Chemistry,* vol. 5, no. 1, pp. 1-23, 2012.

[9] K. Donaldson *et al.*, "Carbon nanotubes: a review of their properties in relation to pulmonary toxicology and workplace safety," *Toxicological sciences,* vol. 92, no. 1, pp. 5-22, 2006.

[10] K. Varshney, "Carbon nanotubes: a review on synthesis, properties and applications," *International journal of engineering research and general science,* vol. 2, no. 4, pp. 660-677, 2014.

[11] E. Ganesh, "Single walled and multi walled carbon nanotube structure, synthesis and applications," *International Journal of Innovative Technology and Exploring Engineering,* vol. 2, no. 4, pp. 311-320, 2013.

[12] J. Prasek *et al.*, "Methods for carbon nanotubes synthesis," *Journal of Materials Chemistry,* vol. 21, no. 40, pp. 15872-15884, 2011.

[13] D. K. Patel, H.-B. Kim, S. D. Dutta, K. Ganguly, and K.-T. Lim, "Carbon nanotubes-based nanomaterials and their agricultural and biotechnological applications," *Materials,* vol. 13, no. 7, p. 1679, 2020.

[14] S. Iijima and T. Ichihashi, "Single-shell carbon nanotubes of 1-nm diameter," *nature,* vol. 363, no. 6430, pp. 603-605, 1993.
[15] D. S. Bethune *et al.*, "Cobalt-catalysed growth of carbon nanotubes with single-atomic-layer walls," *Nature,* vol. 363, no. 6430, pp. 605-607, 1993.
[16] C. D. Scott, S. Arepalli, P. Nikolaev, and R. E. Smalley, "Growth mechanisms for single-wall carbon nanotubes in a laser-ablation process," *Applied Physics A,* vol. 72, pp. 573-580, 2001.
[17] N. Yang, X. Chen, T. Ren, P. Zhang, and D. Yang, "Carbon nanotube based biosensors," *Sensors and Actuators B: Chemical,* vol. 207, pp. 690-715, 2015.
[18] N. Popovska, K. Danova, I. Jipa, and U. Zenneck, "Catalytic growth of carbon nanotubes on zeolite supported iron, ruthenium and iron/ruthenium nanoparticles by chemical vapor deposition in a fluidized bed reactor," *Powder technology,* vol. 207, no. 1-3, pp. 17-25, 2011.
[19] S. ChandraKishore and A. Pandurangan, "Electrophoretic deposition of cobalt catalyst layer over stainless steel for the high yield synthesis of carbon nanotubes," *Applied Surface Science,* vol. 258, no. 20, pp. 7936-7942, 2012.
[20] J. Sumfleth, K. Prehn, M. H. Wichmann, S. Wedekind, and K. Schulte, "A comparative study of the electrical and mechanical properties of epoxy nanocomposites reinforced by CVD-and arc-grown multi-wall carbon nanotubes," *Composites Science and Technology,* vol. 70, no. 1, pp. 173-180, 2010.
[21] J. Zhu, A. Holmen, and D. Chen, "Carbon nanomaterials in catalysis: proton affinity, chemical and electronic properties, and their catalytic consequences," *ChemCatChem,* vol. 5, no. 2, pp. 378-401, 2013.
[22] M. Karami, M. A. Bahabadi, S. Delfani, and A. Ghozatloo, "A new application of carbon nanotubes nanofluid as working fluid of low-temperature direct absorption solar collector," *Solar Energy Materials and Solar Cells,* vol. 121, pp. 114-118, 2014.
[23] M. H. Esfe, P. M. Behbahani, A. A. Arani, and M. R. Sarlak, "Thermal conductivity enhancement of SiO2–MWCNT (85: 15%)–EG hybrid nanofluids," *J Therm Anal Calorim,* vol. 128, no. 1, pp. 249-258, 2017.
[24] M. S. Mauter and M. Elimelech, "Environmental applications of carbon-based nanomaterials," *Environmental science & technology,* vol. 42, no. 16, pp. 5843-5859, 2008.
[25] V. Thirumal, A. Pandurangan, R. Jayavel, S. Krishnamoorthi, and R. Ilangovan, "Synthesis of nitrogen doped coiled double walled carbon nanotubes by chemical vapor deposition method for supercapacitor applications," *Current Applied Physics,* vol. 16, no. 8, pp. 816-825, 2016.
[26] S. J. Tans, A. R. Verschueren, and C. Dekker, "Room-temperature transistor based on a single carbon nanotube," *Nature,* vol. 393, no. 6680, pp. 49-52, 1998.

[27] P. Sharma and P. Ahuja, "Recent advances in carbon nanotube-based electronics," *Materials Research Bulletin,* vol. 43, no. 10, pp. 2517-2526, 2008.
[28] G. Rahman *et al.*, "An overview of the recent progress in the synthesis and applications of carbon nanotubes," *C,* vol. 5, no. 1, p. 3, 2019.
[29] M. J. Treacy, T. W. Ebbesen, and J. M. Gibson, "Exceptionally high Young's modulus observed for individual carbon nanotubes," *nature,* vol. 381, no. 6584, pp. 678-680, 1996.
[30] J.-P. Salvetat *et al.*, "Mechanical properties of carbon nanotubes," *Applied Physics A,* vol. 69, pp. 255-260, 1999.
[31] R. S. Jakati, K. B. Balavalad, and B. Sheeparamatti, "Comparative analysis of different micro-pressure sensors using comsol multiphysics," in *2016 International Conference on Electrical, Electronics, Communication, Computer and Optimization Techniques (ICEECCOT)*, 2016: IEEE, pp. 355-360.
[32] T. Dinh *et al.*, "Fabrication of a sensitive pressure sensor using carbon nanotube micro-yarns," in *2017 IEEE SENSORS*, 2017: IEEE, pp. 1-3.
[33] S. Pyo, E. Jo, D.-S. Kwon, W. Kim, W. Chang, and J. Kim, "Fabrication of carbon nanotube-coated fabric for highly sensitive pressure sensor," in *2017 19th International Conference on Solid-State Sensors, Actuators and Microsystems (TRANSDUCERS)*, 2017: IEEE, pp. 962-965.
[34] A. Sanli, R. Ramalingame, and O. Kanoun, "Piezoresistive pressure sensor based on carbon nanotubes/epoxy composite under cyclic loading," in *2018 IEEE International Instrumentation and Measurement Technology Conference (I2MTC)*, 2018: IEEE, pp. 1-5.
[35] K. B. Balavalad and B. Sheeparamatti, "Design, Simulation & Analysis of Si, SOI & Carbon Nanotube (CNT) based Micro Piezoresistive Pressure Sensor for a High Tmeperature & Pressure," in *2018 International Conference on Circuits and Systems in Digital Enterprise Technology (ICCSDET)*, 2018: IEEE, pp. 1-6.
[36] R. A. Shaik and E. Rufus, "Modelling and analysis of single node E-skin piezoresistive pressure sensor simulation results," in *2018 IEEE Electron Devices Kolkata Conference (EDKCON)*, 2018: IEEE, pp. 577-580.
[37] K. Park, P. Tran, N. Deaton, and J. P. Desai, "Multi-walled carbon nanotube (MWCNT)/PDMS-based flexible sensor for medical applications," in *2019 International Symposium on Medical Robotics (ISMR)*, 2019: IEEE, pp. 1-8.
[38] T. Kumpika *et al.*, "Stretchable and compressible strain sensors for gait monitoring constructed using carbon nanotube/graphene composite," *Materials Research Express,* vol. 7, no. 3, p. 035006, 2020.
[39] A. Sanchez-Soares, T. Kelly, G. Fagas, J. C. Greer, and E. Chen, "Top-Gated Carbon Nanotube FETs from Quantum Simulations: Comparison

with Experiments," in *2021 International Symposium on VLSI Technology, Systems and Applications (VLSI-TSA)*, 2021: IEEE, pp. 1-2.
[40] T. De Rijk, M. Cen-Puc, J. K. Piening, and W. Lang, "Single layer piezoresistive polyimide pressure sensor based on carbon nanotubes," in *2022 IEEE Sensors*, 2022: IEEE, pp. 1-4.
[41] M. A. Zamzami *et al.*, "Fabrication and characterization of field effect transistor based on single walled carbon nanotubes," *Journal of King Saud University-Science,* vol. 34, no. 6, p. 102137, 2022.
[42] G. Fedorov, R. Hafizi, V. Semenenko, and V. Perebeinos, "Metal Contact Induced Unconventional Field Effect in Metallic Carbon Nanotubes," *Nanomaterials,* vol. 13, no. 11, p. 1774, 2023.
[43] C. Wang *et al.*, "Ultra-sensitive and wide sensing-range flexible pressure sensors based on the carbon nanotube film/stress-induced square frustum structure," *ACS Applied Materials & Interfaces,* vol. 15, no. 6, pp. 8546-8554, 2023.
[44] C. Ma, R. Zhou, and L. Xie, "Recent advances in flexible pressure/strain sensors using carbon nanotubes," *International Journal of Agricultural and Biological Engineering,* vol. 15, no. 2, pp. 1-12, 2022.
[45] Z. Zand, M. Hayati, and G. Karimi, "Short-channel effects improvement of carbon nanotube field effect transistors," in *2020 28th Iranian Conference on Electrical Engineering (ICEE)*, 2020: IEEE, pp. 1-6.
[46] R. Chen *et al.*, "Carbon Nanotube SRAM in 5-nm Technology Node Design, Optimization, and Performance Evaluation—Part I: CNFET Transistor Optimization," *IEEE Transactions on Very Large Scale Integration (VLSI) Systems,* vol. 30, no. 4, pp. 432-439, 2022.
[47] Y. Fang *et al.*, "A Novel 3D Temperature Sensor Based On Buried-Gate Graphene Field Effect Transistors," in *2022 IEEE 35th International Conference on Micro Electro Mechanical Systems Conference (MEMS)*, 2022: IEEE, pp. 818-821.
[48] B. Singh *et al.*, "Carbon nanotubes. A novel drug delivery system," *International Journal of Research in Pharmacy and Chemistry,* vol. 2, no. 2, pp. 523-532, 2012.
[49] S. K. Sinha and S. Chaudhury, "Advantage of carbon nannotube field effect transistor (CNTFET) over double-gate MOSFET in nanometre regime," in *2012 NATIONAL CONFERENCE ON COMPUTING AND COMMUNICATION SYSTEMS*, 2012: IEEE, pp. 1-5.
[50] K. Mohana Sundaram, P. Prakash, D. Karthikeyan, and W. D. Mammo, "Improved Carbon Nanotube Field Effect Transistor for Designing a

Hearing Aid Filtering Application," *Journal of Nanomaterials,* vol. 2021, pp. 1-12, 2021.
[51] S. Wind, J. Appenzeller, and P. Avouris, "Lateral scaling in carbon-nanotube field-effect transistors," *Physical Review Letters,* vol. 91, no. 5, p. 058301, 2003.
[52] P. Avouris, "Molecular electronics with carbon nanotubes," *Accounts of chemical research,* vol. 35, no. 12, pp. 1026-1034, 2002.
[53] J. Appenzeller, "Carbon nanotubes for high-performance electronics—Progress and prospect," *Proceedings of the IEEE,* vol. 96, no. 2, pp. 201-211, 2008.
[54] S. Sharma, S. Mahajan, A. Rehalia, A. K. Pandit, S. Gupta, and A. Kumar, "Analysis of low power design techniques for GNRFET and CNTFET based devices," *J. Crit. Rev.,* vol. 7, no. 19, pp. 801-806, 2020.
[55] W. Mönch, "Mechanisms of Schottky-barrier formation in metal–semiconductor contacts," *Journal of Vacuum Science & Technology B: Microelectronics Processing and Phenomena,* vol. 6, no. 4, pp. 1270-1276, 1988.
[56] P. Avouris, "Carbon nanotube electronics and optoelectronics," *Mrs Bulletin,* vol. 29, no. 6, pp. 403-410, 2004.
[57] S. K. Sinha and S. Chaudhury, "Comparative study of leakage power in CNTFET over MOSFET device," *Journal of Semiconductors,* vol. 35, no. 11, p. 114002, 2014.
[58] K. Tserpes and P. Papanikos, "Finite element modeling of single-walled carbon nanotubes," *Composites Part B: Engineering,* vol. 36, no. 5, pp. 468-477, 2005.
[59] E. T. Thostenson, Z. Ren, and T.-W. Chou, "Advances in the science and technology of carbon nanotubes and their composites: a review," *Composites science and technology,* vol. 61, no. 13, pp. 1899-1912, 2001.
[60] E. Liu, Z. Cai, Y. Ye, M. Zhou, H. Liao, and Y. Yi, "An Overview of Flexible Sensors: Development, Application, and Challenges," *Sensors,* vol. 23, no. 2, p. 817, 2023.
[61] M. Zhou, Z. Wang, and X. Wang, "Carbon nanotubes for sensing applications," in *Industrial applications of carbon nanotubes*: Elsevier, 2017, pp. 129-150.
[62] N. Sinha and J.-W. Yeow, "Carbon nanotubes for biomedical applications," IEEE transactions on nanobioscience, vol. 4, no. 2, pp. 180-195, 2005.
[63] V. D. Bezzon et al., "Carbon nanostructure-based sensors: a brief review on recent advances," Advances in Materials Science and Engineering, vol. 2019, 2019.
[64] Y. Zang, F. Zhang, C.-a. Di, and D. Zhu, "Advances of flexible pressure sensors toward artificial intelligence and health care applications," *Materials Horizons,* vol. 2, no. 2, pp. 140-156, 2015.

[65] Y. Kanda, "Piezoresistance effect of silicon," *Sensors and Actuators A: Physical,* vol. 28, no. 2, pp. 83-91, 1991.
[66] S. Iijima, "Helical microtubules of graphitic carbon," *nature,* vol. 354, no. 6348, pp. 56-58, 1991.
[67] Z. Shi *et al.*, "Morphological engineering of sensing materials for flexible pressure sensors and artificial intelligence applications," *Nano-micro letters,* vol. 14, no. 1, p. 141, 2022.
[68] X. Shuai *et al.*, "Highly sensitive flexible pressure sensor based on silver nanowires-embedded polydimethylsiloxane electrode with microarray structure," *ACS applied materials & interfaces,* vol. 9, no. 31, pp. 26314-26324, 2017.
[69] X. Yang, Z. Zhou, Y. Wu, M. Xiao, Q. Luo, and C. Shao, "Measurement and simulation of carbon nanotube's piezoresistance property by a micro/nano combined structure," 2007.
[70] S. A. Selvin, S. A. Lovelin, N. B. Moorthy, A. Gupta, M. Alagappan, and V. Ramalingam, "Design and simulation of carbon nanotube based piezoresistive pressure sensor," in *Expert from the proceedings of the 2011 COMSOL Conference in Bangalore, Page*, 2011, no. 3.
[71] A. E. Bangera and S. M. Kulkarni, "Modeling and analysis of a SWCNT piezoresistive pressure sensor," in *2013 IEEE International Conference ON Emerging Trends in Computing, Communication and Nanotechnology (ICECCN)*, 2013: IEEE, pp. 466-471.
[72] V. Sydoruk, M. Petrychuk, A. Ural, G. Bosman, A. Offenhäusser, and S. Vitusevich, "Noise characterisation of transport properties in single wall carbon nanotube field-effect transistors," in *2011 21st International Conference on Noise and Fluctuations*, 2011: IEEE, pp. 238-241.
[73] B. Singh, B. Prasad, and D. Kumar, "DFT based estimation of CNT parameters and simulation-study of GAA CNTFET for nano scale applications," *Materials Research Express,* vol. 7, no. 1, p. 015916, 2020.
[74] K. R. Agrawal and R. Sonkusare, "PVT variations of a behaviorally modeled single walled carbon nanotube field-effect transistor (SW-CNTFET)," in *2015 International Conference on Nascent Technologies in the Engineering Field (ICNTE)*, 2015: IEEE, pp. 1-6
[75] A. Singh, M. Khosla, and B. Raj, "Comparative analysis of carbon nanotube field effect transistors," in *2015 IEEE 4th Global Conference on Consumer Electronics (GCCE)*, 2015: IEEE, pp. 552-555.
[76] A. Karimi and A. Rezai, "A design methodology to optimize the device performance in CNTFET," *ECS Journal of Solid State Science and Technology,* vol. 6, no. 8, p. M97, 2017.

[77] R. Marani and A. G. Perri, "Temperature Dependence of IV Characteristics in CNTFET Models: A Comparison," *International Journal of Nanoscience and Nanotechnology,* vol. 17, no. 1, pp. 33-39, 2021.

[78] A. Gafar, G. Atlam, and I. I. Mahmoud, "D2. Evaluation of carbon nanotube-based MEMS piezoresistive pressure sensors," in *2015 32nd National Radio Science Conference (NRSC)*, 2015: IEEE, pp. 329-339.

[79] A. Ali, A. Khan, K. S. Karimov, A. Ali, and A. Daud Khan, "Pressure sensitive sensors based on carbon nanotubes, graphene, and its composites," *Journal of Nanomaterials,* vol. 2018, pp. 1-12, 2018.

[80] A. C. Katageri and B. Sheeparamatti, "Sensitivity enhancement of piezoresistive pressure sensor using carbon nanotube as a piezoresistor," in *2019 Second International Conference on Advanced Computational and Communication Paradigms (ICACCP)*, 2019: IEEE, pp. 1-6.

الخلاصه

تحظى الانابيب النانويه الكاربونيه(CNTs) Carbon nanotube بأهميه كبيره بسبب خصائصها الالكترونيه والميكانيكيه. حيث تتمتع هذه المادة بموصلية كهربائية ممتازة يمكن استخدامها لانشاء ترانزستورات عاليه الأداء للأجهزه الالكترونيه, يمثل CNT ماده محتملة للأجهزة الالكترونيه الدقيقه المستقبلية. عززت هذه الرسالة تصميم ومحاكاة CNT باستخدام (COMSOL Multiphysics 6.0).

ونتيجه لعدم تضمين CNT في مكتبه الموادالخاصة ب (COMSOL 6.0) لذلك تم اضافة معاملات خصائص هذه المادة الكهربائيه والميكانيكيه بما في ذلك السماحيه النسبيه , فجوه النطاق, تقارب الالكترون, والكثافه الفعاله للحالات في نطاق التكافؤ والتوصيل, وتنقل الالكترون والفجوه, كثافه يونغ, ومعامل بواسون. تم عرض تصميم ومحاكاة ترانزستور التأثير الميداني المعتمد ع الانابيب النانويه الكاربونيه ذات الجدار الواحد مع البوابه الخلفيه وبأستخدم نموذج اللامركزية المتعرجة*(zig-zag)* للحصول على خصائص أشباه الموصلات لمادة CNTs. ويجب ان تؤخذ في نظر الاعتبار عدم التطابق عند تغير قطر *CNTs* حيث تتراوح قيم قطر CNTs من 1 نانومتر الى 4.5 نانومتر. كما تتأثر فجوه النطاق ل CNTs بتغير قطر CNTs وقد وجد ان زياده نطاق القطر يؤدي الى تقليل فجوه النطاق. بالاضافه الى ذلك, تمت دراسه تأثير اختلاف سمك السيلكون (سمك البوابه) على تيار التصريف ونتيجة لذلك, وجد أن تيار التصريف يقل مع زيادة سمك اكسيد البوابه , ان تردد الرنين الذي تم تحقيقه لترانزستور ال CNTs هو50 كيكاهرتز, وعرض النطاق الترددي يساوي 30 جيجا هرتز.

كما ناقش هذا البحث؛ تصميم ومحاكاة متحسس ضغط من نوع مستشعر المقاومة باستخدام CNTsأحادي الجدار ومتعدد الجدران حيث يعمل هذا المستشعر عن طريق استشعار التغير في المقاومة عبر الأنابيب بسبب الضغط المطبق. بالاضافه الى ذلك , تم مناقشة تأثير تغيير القطر على مقاومه CNTs *وفجوه* نطاق الطاقة حيث ان القطر في التصميم الحالي المختار يتراوح من 1 نانومتر إلى 4 نانومتر ووجد أن زيادة القطر يقلل من فجوة الطاقة و المقاومة. ومن ثم تم تحليل النموذج المقترح لمستشعر الضغط التجويفى من خلال حساب عدة عوامل ومنها انحراف الركيزة, التيار, تغيرات إجهاد فون ميزس , الحساسية , الاستجابة الزمنية , واستجابات التردد وباستخدام CNTs واحد ومجموعه من *CNTs*علاوة على ذلك تم حساب حساسيه CNTs احادي الجدار وCNTs متعدد الجدارعلى التوالي. ووجد ان حسياسيه CNTs احادي الجدار افضل من CNTs متعدد الجدار بسبب مساحه سطح CNT احاديه الجدار اعلى من مساحه سطح CNTs متعددة الجدار وكذلك يوثر طول وقطر CNTs على حساسيه المستشعر عاده ما تكون CNTs احاديه الجدار اطول واضيق من CNTs متعدده الجدار مما قد يعزز حساسيتها. تم تحديد الاستجابه الزمنيه للجهازعند نطاق ضغط من 100 كيلوباسكال الى 250 كيلوباسكال ووقت الارتفاع

المقابل هو 0.18 ثانيه الى 0.23 ثانيه حيث أظهرت هذه النتائج أنه تردد الاستجابه المحقق لمستشعر CNTs هو60 هرتزفي النطاق من 0 الى 200 هرتز وبالتالي فإن الخاصية الخطية للمستشعر تجعله واعدا للتطبيقات العمليه .

جمهورية العراق
وزارة التعليم العالي والبحث العلمي
جامعة بابل
كلية الهندسة / قسم الهندسة الكهربائية

توصيف الأنابيب النانويه الكاربونيه لتصميم أجهزه نانويه قابله للمط

رسالة

مقدمة الى كلية الهندسة في جامعة بابل

كجزء من متطلبات نيل درجة الماجستيرفي الهندسة

/الهندسه الكهربائية / الكترونيك

من قبل

زهراء عيسى محمد عيسى علوان

باشراف

الدكتور حيدر صاحب المؤمن

2023م 1445هـ